

**USE OF GEOSPATIAL AND MULTIVARIATE  
STATISTICAL ANALYSIS IN SUPPORT OF WATER  
QUALITY MONITORING OF HYDROELECTRIC  
RESERVOIRS**

**ISABEL LEIDIANY DE SOUSA BRANDÃO**



USE OF GEOSPATIAL AND MULTIVARIATE  
STATISTICAL ANALYSIS IN SUPPORT OF WATER  
QUALITY MONITORING OF HYDROELECTRIC  
RESERVOIRS

DISSERTATION

to obtain  
the degree of doctor at the University of Twente,  
on the authority of the rector magnificus,  
prof.dr. T.T.M. Palstra,  
on account of the decision of the Doctorate Board,  
to be publicly defended  
on Wednesday 20 March 2019 at 14:45 hrs

by

Isabel Leidiany de Sousa Brandão  
born on 28 August, 1984  
in Castanhal, Brazil

This thesis has been approved by:

**Dr.ir. C.M.M. Mannaerts** (supervisor)

**Prof.dr.ing. W. Verhoef** (supervisor)

ITC dissertation number 345

ITC, P.O. Box 217, 7500 AE Enschede, The Netherlands

ISBN 978-90-365-4735-2

DOI 10.3990/1.9789036547352

Cover designed by Marien Melisse

Printed by ITC Printing Department

Copyright © 2019 by Isabel Leidiany de Sousa Brandão



**UNIVERSITY OF TWENTE.**

**ITC** FACULTY OF GEO-INFORMATION SCIENCE AND EARTH OBSERVATION

Graduation committee:

**Chairman/Secretary**

Prof.dr.ir. A. Veldkamp

**Supervisors**

Associate Prof.dr.ir. C.M.M. Mannaerts      University of Twente

Prof.dr.ing. W. Verhoef      University of Twente

**Members**

Prof.dr. D. van der Wal      University of Twente

Dr.ir. D.C.M. Augustijn      University of Twente

Prof.dr. M. McClain      UN-IHE Delft

Prof.dr. E. Alcântara      UNESP (Sao Paulo, Brasil)

Dr. A. Saraiva      Belem, Brasil

Dr.ir. S. Salama      University of Twente

*Dedicated to my Brazilian and Dutch families,*

*To my boyfriend Marien Melisse....*

*...without you this dream would not be possible.*

---

## Acknowledgements

---

This PhD thesis was developed with the support of numerous people, without whom it would not have been possible to develop.

I would like to express my gratitude and appreciation to all of those whom have contributed to this dissertation.

First and foremost, I would like to express my deep gratitude to my promotors Prof. Dr. Chris Mannaerts and Prof. Dr. Wouter Verhoef for their valuable guidance, enthusiastic encouragement and valuable constructive suggestions to this research. My sincere gratitude to Prof. Dr. Rosildo dos Santos Paiva, who gave me the opportunity to learn about phytoplankton measurements and analysis. Without his assistance and guidance in identifying phytoplankton to the species level, this research would not be possible.

I would like to extend my thanks to Prof. Dr. Tundisi who provided the field equipment for phytoplankton data collection.

I would like to thank Dr. Augusto Saraiva and the staff of the Eletronorte in Tucuruí city, located in the North of Brazil, for helping with water limnology and greenhouse gases fieldwork surveys and laboratory analysis.

Last but not least, I express my deepest gratitude to the most valuable people in my life. I wish to thank my parents for their support and encouragement throughout this journey. To my boyfriend Marien Melisse who helped me to address all situations with positivity and tranquillity. He was the most supportive companion, in all steps of this journey.



---

## Table of Contents

Acknowledgements .....	i
Table of Contents .....	iii
List of figures .....	v
List of tables .....	vii
List of appendices .....	viii
List of abbreviations.....	x
<b>1 Introduction.....</b>	<b>1</b>
1.1 Research background and motivation .....	2
1.2 Reservoirs .....	2
1.3 Eutrophication in reservoirs.....	5
1.4 Greenhouse gases emission.....	6
1.5 Geospatial analysis for water management in reservoirs .....	7
1.6 Research objectives.....	11
1.7 Outline of this thesis.....	12
<b>2 Seasonal variation of phytoplankton indicates small impacts of anthropic activities in a Brazilian Amazonian reserve .....</b>	<b>15</b>
2.1 Introduction.....	17
2.2 Materials and methods .....	19
2.3 Material .....	22
2.4 Statistical analysis .....	23
2.5 Results .....	24
2.6 Discussion .....	30
2.7 Conclusions.....	32
<b>3 Using Synergy between Water Limnology and Satellite Imagery to Identify Algal Blooms Extent in a Brazilian Amazonian Reservoir ..</b>	<b>39</b>
3.1 Introduction.....	41
3.2 Materials and Methods .....	43
3.3 Results .....	50
3.4 Discussion .....	58
3.5 Conclusions.....	61
<b>4 Separation of hydrodynamic from biogeochemical factors affecting eutrophication in a tropical hydropower reservoir using Generalized Linear Models .....</b>	<b>71</b>
4.1 Introduction.....	73
4.2 Material and methods .....	75
4.3 Data analysis methodology.....	77
4.4 Results and discussion.....	80

4.5 Results of the data used in the models .....	81
4.6 Model results.....	86
4.7 Conclusions.....	91
<b>5 Conjunctive use of in situ gas sampling and chromatography with geospatial analysis to estimate greenhouse gas emissions of a large Amazonian hydroelectric reservoir.....</b>	<b>93</b>
5.1 Introduction.....	95
5.2 Methods.....	97
5.3 Results.....	104
5.4 Discussion .....	112
5.5 Conclusions.....	115
<b>6 Synthesis.....</b>	<b>127</b>
6.1 Introduction.....	128
6.2 Main results.....	129
6.3 Research contributions.....	137
6.4 Research recommendations.....	138
6.5 Future research paths: .....	139
<b>Bibliography.....</b>	<b>141</b>
<b>Summary .....</b>	<b>163</b>
<b>Samenvatting.....</b>	<b>167</b>

---

## List of figures

---

<b>Figure 1.1</b> Longitudinal zonation in reservoirs and factors controlling environmental conditions post impoundment. ....	4
<b>Figure 1.2</b> Comparison of relative spectral response between Landsat-8 and Landsat-5 bands. ....	11
<b>Figure 2.1</b> Study area .....	19
<b>Figure 2.3</b> Monthly accumulated rainfall and the water level of the Tucuruí reservoir along the year of 2014. ....	21
<b>Figure 2.2</b> Deforestation at SDR Alcobaça from 2000-2015 .....	21
<b>Figure 2.4</b> Boxplot of the abiotic factors in the dry and rainy seasons. ....	25
<b>Figure 2.5</b> Phytoplankton biomass in the rainy season (upper panel) and dry season (lower panel) at Caraiapé 1- Alcobaça SDR.....	26
<b>Figure 2.6</b> Seasonal variation of phytoplankton species richness and Margalef diversity index of Caraiapé 1 considering absolute numbers or densities. ....	28
<b>Figure 2.7</b> Canonical correspondence analysis (CCA) between abiotic explanatory variables and the most frequent phytoplankton functional group in the rainy season (left side) and in the dry season (right side). The explanatory variables are represented by lines with arrows and phytoplankton functional groups by blue color (M, MP, Lo, S1, H1, P, Na, J, A).....	29
<b>Figure 3.1</b> Study area with sample sites location.....	43
<b>Figure 3.2</b> Monthly rainfall from January 2014 to December 2016 at the study area. ....	44
<b>Figure 3.3</b> Contribution of algae groups to the total biovolume in relative percentage. (a) Study sites (April); (b) Study sites (July). ....	52
<b>Figure 3.4</b> Rayleigh corrected reflectance ( $\rho_{\lambda}$ ) collected in (a) April and (b) July, 2016.....	54
<b>Figure 3.5</b> Locations where the SARED-NIR algorithm was applied: (a) M1 site; (b) MR; (c) M3 site with algal bloom indication. The scene is LC82240632016112LGN01 (April 2016) in natural color (R = 665 nm, G = 561 nm, B = 483 nm); (d–f) are SARED-NIR classifications. ....	55
<b>Figure 3.6</b> Location where the SARED-NIR algorithm was applied: (c) M3 site with algal bloom indication and other sites (a, b, d and e) without bloom indication. The scene is LC82240632016208LGN01 (July 2016) in natural color (R = 665 nm, G = 561 nm, B = 483 nm); (f) SARED-NIR classification.....	56
<b>Figure 3.7</b> Chl-a estimated with the Ocean Biology Processing Group (OBPG) algorithm. ....	57
<b>Figure 3.8</b> Maps of Chl-a concentrations ( $\text{mg m}^{-3}$ ) estimated using the OLI sensor and the OBPG algorithm for (a) April 21, and (b) July 26 of 2016, respectively. ....	58
<b>Figure 4.1</b> Tucuruí HPP study area and sampling sites located throughout the reservoir, Pará, Brazil. ....	76
<b>Figure 4.2</b> Chl-a ( $\text{mg m}^{-3}$ ) concentration per zone (A) and cycle B), and Secchi depth per zone (C) and cycle (D).....	84
<b>Figure 4.3</b> Histograms for Chlorophyll-a concentration and transparency S (m).....	87

<b>Figure 4.4</b> Diagnostic charts for the concentration of Chlorophyll-a: leverage, Cook's distance and linear prediction with Range model. ....	88
<b>Figure 4.5</b> Diagnostic diagrams for transparency: (a) leverage, (b) Cook distance and (c) linear predictor of the inverse normal model.....	90
<b>Figure 4.6</b> Normal probability plot of deviance component standardized with envelope generated for the model (Range for Chl-a and Normal inverse for transparency (Secchi)).	91
<b>Figure 5.1</b> Accumulated monthly precipitation and typical water levels in the THR (upstream and downstream of the dam) during the four fieldwork campaigns .....	98
<b>Figure 5.2</b> Study area at (a) South America, (b) Tucuruí dam, and (c) sampling sites upstream (U) and downstream (D) locations at the THR reservoir.....	99
<b>Figure 5.3</b> Diffusive flux of CO <sub>2</sub> and CH <sub>4</sub> at each sampled site of the THR. Letters U and D stand for sites location upstream and downstream of the THR dam, respectively. ....	104
<b>Figure 5.4</b> Spatial and temporal distribution of CH <sub>4</sub> fluxes in the entire THR system (including river upstream and downstream) corresponding to: (a) June; (b) September; and (c) December of 2011; (d) March of 2012. ....	108
<b>Figure 5.5</b> Spatial and temporal distribution of CO <sub>2</sub> in the entire THR system (including river upstream and downstream) corresponding to: a) June-2011; b) September-2011; c) December -2011; and d) March of 2012. ....	110

---

## List of tables

---

<b>Table 1.1</b> Characteristics of each zone formed after impoundment, Tundisi et al. (2012)....	5
<b>Table 1.2</b> Performance characteristics of the Landsat-8/OLI and Landsat-5/Thematic mapper.....	10
<b>Table 2.1</b> Main general features of the Tucuruí reservoir.....	20
<b>Table 2.2</b> Summary statistics for the first two axes of CCA on the phytoplankton functional groups and abiotic variables in the rainy season. ....	29
<b>Table 2.3</b> Summary statistics for the first two axes of CCA on the phytoplankton functional groups and abiotic variables.....	30
<b>Table 3.1</b> L8/ Operational Land Imager (OLI) bands with wavelength and ground sampling distance (GSD). ....	47
<b>Table 3.2</b> Main characteristics of algal blooms according to Ogashawara et al. (2017). ....	49
<b>Table 3.3</b> Summary of error analysis used in this study.....	50
<b>Table 3.4</b> Environmental characteristics of the sample sites of the study area. ....	51
<b>Table 3.5</b> Descriptive statistics of the water quality parameters measured in (a) April and (b) July, 2016. Statistical metrics include: minimum value (Min), maximum value (Max), average, standard deviation (SD) and coefficient of variation (CV) in percentages (%) .....	53
<b>Table 3.6</b> Error analysis results. ....	58
<b>Table 4.1</b> Distribution of water samples by zone and hydrological cycle of the reservoir given by the cluster analysis.....	81
<b>Table 4.2</b> Summary of the limnological parameter statistics from 2005-2016 during the different hydrological cycles at the Tucuruí reservoir. ....	83
<b>Table 4.3</b> Model parameter estimates for Chlorophyll-a. ....	88
<b>Table 4.4</b> Model parameter estimates for the inverse normal model transparency. References: Cycle: Dry and Zone: Lacustrine. Bold values are significant considering $\alpha = 5\%$ . ....	90
<b>Table 5.1</b> Correlation between GHG fluxes and water environmental and biogeochemical variables. Variables included water temperature (wt), total suspended solids (TSS), total phosphorus (TP), nitrate (NO <sub>3</sub> <sup>-</sup> ), Chlorophyll- <i>a</i> (Chl- <i>a</i> ), electrical conductivity (EC), pH, dissolved oxygen (DO), turbidity (Turb), ion ammonium (NH <sub>4</sub> <sup>+</sup> ) and orthophosphate (PO <sub>4</sub> <sup>3-</sup> ).....	106
<b>Table 5.2</b> Geostatistical parameters for CH <sub>4</sub> and CO <sub>2</sub> fluxes in the THR.....	107
<b>Table 5.3</b> Calculation of CH <sub>4</sub> emissions over the entire THR system during the monitoring period.....	111
<b>Table 5.4</b> Calculation of CO <sub>2</sub> emissions over the entire THR system during the monitoring period.....	112

---

## List of appendices

---

<b>Appendix 2.1</b> List of species that contributed with biomass $\geq 5\%$ , and their respective phytoplankton functional groups.....	35
<b>Appendix 2.2</b> Phytoplankton functional groups found at Caraipé site, adapted from Reynolds et al. (2002) and Padisák et al. (2009). .....	37
<b>Appendix 2.3</b> Inter-set correlations between environmental variables and phytoplankton functional groups, during the rainy season. ....	38
<b>Appendix 2.4</b> Inter-set correlations between environmental variables and phytoplankton functional groups, during dry season.....	38
<b>Appendix 3.1</b> OLI processing flow applied to the imagery of this study.....	63
<b>Appendix 3.2</b> Chl-a Algorithm Processing Steps .....	64
<b>Appendix 3.3</b> Rayleigh Corrected Reflectance.....	65
<b>Appendix 3.4</b> Maps of Chl-a concentration (mg m <sup>-3</sup> ) estimated from OLI sensor using the OBP algorithm for 16 June, 18 July and 03 August of 2013, respectively. ....	65
<b>Appendix 3.5</b> Time series of Chl-a in the Tucuruí hydroelectric reservoir from 2014 to 2016. ....	66
<b>Appendix 3.6</b> Time series of turbidity in the Tucuruí hydroelectric reservoir from 2014 to 2016. ....	66
<b>Appendix 3.7</b> Time series of Secchi disc in the Tucuruí hydroelectric reservoir from 2014 to 2016. ....	67
<b>Appendix 3.8</b> Time series of color in the Tucuruí hydroelectric reservoir from 2014 to 2016. ....	67
<b>Appendix 3.9</b> Cyanobacteria taxa and biovolume in percentage in April 2016.....	68
<b>Appendix 3.10</b> Cyanobacteria taxa and biovolume in percentage in July 2016. ....	69
<b>Appendix 5.1</b> Linearity results of CH <sub>4</sub> .....	117
<b>Appendix 5.2</b> Linearity results of CO <sub>2</sub> .....	117
<b>Appendix 5.3</b> Residuals from CH <sub>4</sub> linearity. ....	117
<b>Appendix 5.4</b> Residuals from CO <sub>2</sub> linearity .....	117
<b>Appendix 5.5</b> Detection and quantification limits obtained from gas chromatography of CH <sub>4</sub> .....	118
<b>Appendix 5.6</b> Detection and quantification limits obtained from gas chromatography of CO <sub>2</sub> .....	118
<b>Appendix 5.7</b> Repeatability for CH <sub>4</sub> . ....	119
<b>Appendix 5.8</b> Repeatability for CO <sub>2</sub> . ....	119
<b>Appendix 5.9</b> Intermediate precision of CH <sub>4</sub> . ....	120
<b>Appendix 5.10</b> Intermediate precision of CO <sub>2</sub> . ....	120
<b>Appendix 5.11</b> Accuracy for CH <sub>4</sub> . ....	121
<b>Appendix 5.12</b> Accuracy for CO <sub>2</sub> . ....	121
<b>Appendix 5.13</b> Methane – Field 1 (Jun/2011): data transformed with square root.....	122
<b>Appendix 5.14</b> Methane – Field 2 (Sep/2011): data not transformed.....	122

<b>Appendix 5.15</b> Methane – Field 3 (Dec/2011): data transformed with square root. ....	122
<b>Appendix 5.16</b> Methane – Field 4 (Mar/2012): data not transformed. ....	122
<b>Appendix 5.17</b> Geospatial analysis and semivariograms details. ....	123
<b>Appendix 5.18</b> Semivariograms for methane. ....	124
<b>Appendix 5.19</b> Semivariograms for carbon dioxide. ....	125

---

## List of abbreviations

---

### General abbreviations

THR	Tucuruí Hydroelectric Reservoir
GHGs	Greenhouse gases
OACs	Optically active components
IOPs	Inherent optical properties
VNIR	Visible near infrared
SWIR	Shortwave infrared
OLI	Operational Land Imager
TM	Thematic Mapper
SDR	Sustainable Development Reserve
INMET	National Brazilian meteorological institute
ANA	National Brazilian water agency
SM	Standard methods
USEPA	United States Environmental Protection Agency
ANOVA	Analysis of Variance
HSD	Tukey's honest significance difference test
CCA	Canonical correspondence analysis
WT	Water temperature
COD	Chemical oxygen demand
TP	Total phosphorus
EC	Electrical conductivity

SS	Suspended solids
OBPG	Ocean Biology Processing Group
CHABs	Cyanobacteria harmful algal blooms
USGS	United States Geological Survey
LPGS	Level 1 Product generation System
UTM	Universal Transversal Mercator
MSE	Mean Square Error
MAE	Mean Absolute Error
MAPE	Mean Absolute Percentage Error
RMSE	Root Square error
MNB	mean normalized bias
R <sup>2</sup>	determination coefficient
GLMs	Generalized Linear models
HHP	Hydroelectric Power Plant
SDR	Sustainable Development Reserve
EPA	Environmental Protection Area
SM	Standard Methods
DO	Dissolved Oxygen
TSS	Total suspended solids
FID	Flame ionization detector
SAR	Synthetic Aperture Radar
TCD	Thermal conductivity detector
Chl- <i>a</i>	Chlorophyll- <i>a</i>

**Specific  
abbreviations**

N	Nitrogen
P	Phosphorus
CO <sub>2</sub>	Carbon dioxide
CH <sub>4</sub>	Methane
DOC	Dissolved organic carbon
DIC	Dissolved inorganic carbon
O <sub>2</sub>	oxygen
nm	nanometer
m	meter
Km <sup>2</sup>	Square kilometer
Km <sup>3</sup>	Cubic kilometer
S	South
W	West
L	Liter
mL	milliliter
μg	microgram
mm <sup>3</sup>	cubic milliliter
m <sup>3</sup>	Cubic meter



## ***1.1 Research background and motivation***

This thesis explores the potential of combining *in situ* monitoring with remote sensing and geospatial analysis to monitor and assess the water quality in hydropower reservoirs. The monitoring together with the identification of critical pollution sources supports the planning, management and conservation in surrounding areas of reservoirs. Management of reservoirs using geospatial information derived from remote sensors and *in situ* sampling monitoring is important to improve knowledge of key factors controlling and responding to trophic levels in reservoirs. Thus, these tools can help to guide decision makers in the selection of the more appropriate tasks to improve water quality monitoring within these ecosystems.

## ***1.2 Reservoirs***

Hydropower reservoirs are man-made artificial aquatic ecosystems that present a high dynamic and complexity in space and time, with interactions between its structural (dam), physical-chemical and biological components (Tundisi et al., 2012). They are important not only for their electrical power generation, but also for other functions such as water supply (e.g. irrigation, drinking and industry water), flood control, fisheries, as ecological wetland, for leisure activities and navigation (Chapman, 2016). However, their construction cause diverse impacts to terrestrial and aquatic systems. In aquatic systems they interfere with the physical and chemical conditions of the water quality due to alterations of the hydrological regime of the dammed river, and with the functioning mechanisms and succession of phytoplankton communities (Tundisi et al., 2008). Terrestrial impacts include loss of fauna and flora, dislocation of population in areas which will be flooded and increase of endemic diseases (Tundisi et al., 2006a).

Among these impacts, the alteration of a lotic into a lentic environment, affecting the local hydrological characteristics is a concern because of changes in the water residence time (Timpe and Kaplan, 2017). The increase in residence time affects nutrients availability in the water, and may consequently, induce water eutrophication (Esteves, 2011). In addition to this, reservoirs with dendritic pattern form several compartments, which introduces spatial heterogeneity within these water bodies.

The degree of spatial (horizontal and vertical) heterogeneity within a reservoir is influenced by its morphometry, flow and stratification conditions. The organization

of a reservoir and its spatial features are described in Figure 1.1 (Straskraba and Tundisi, 2013):

The size and spatial heterogeneity of reservoirs depend on their morphometry, retention time, thermal stratification, season, and geographical location (Tundisi et al., 2012). The longitudinal distribution of biogeochemical variables depends on the extent of individual zones (Roberto et al., 2009) and due to nutrient inputs and optimal light availability, the maximum development of chlorophyll is located in the transitional zone (Wetzel, 2001).

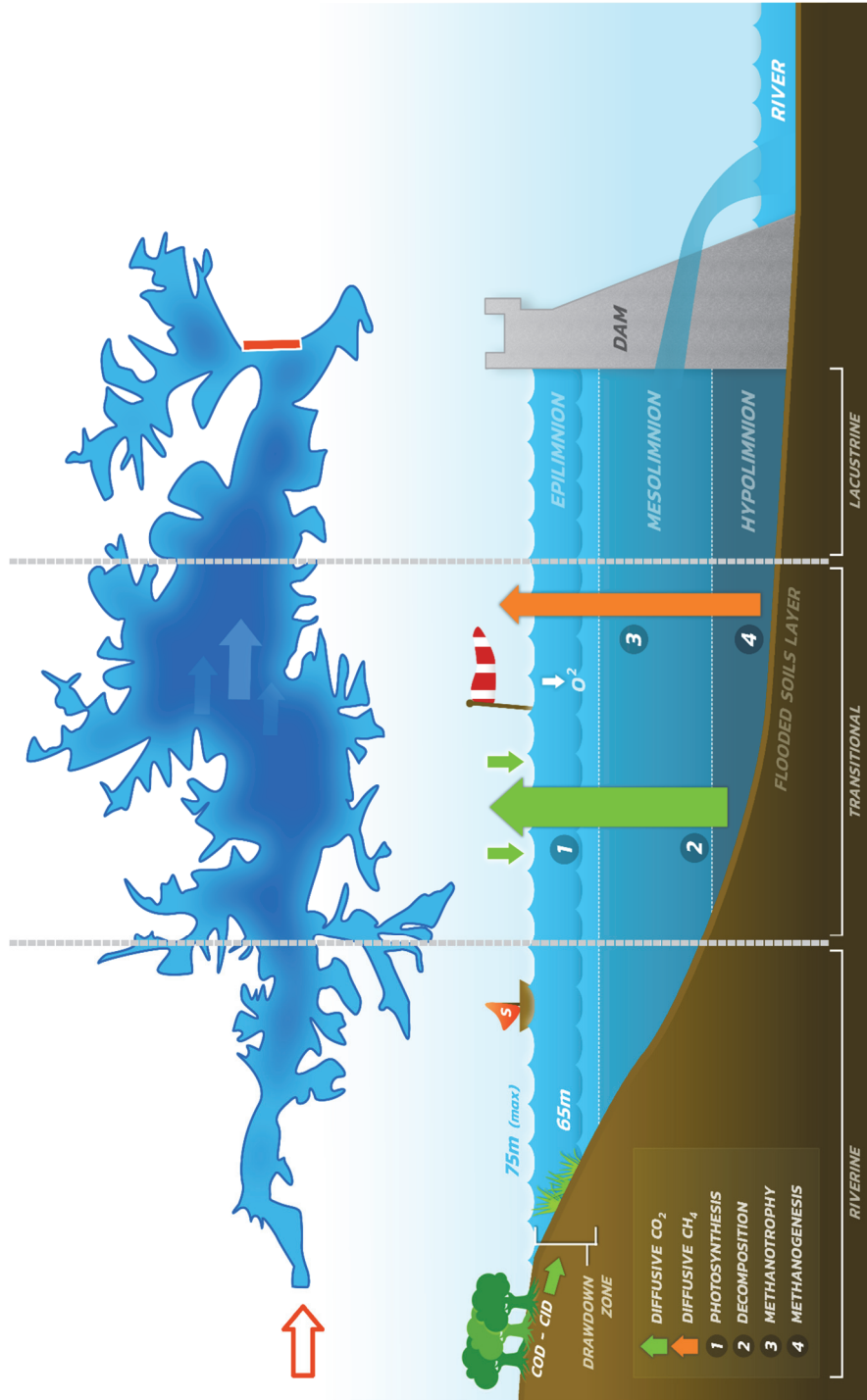


Figure 1.1 Longitudinal zonation in reservoirs and factors controlling environmental conditions post impoundment.

**Table 1.1** Characteristics of each zone formed after impoundment, Tundisi et al. (2012)

<b>Riverine</b>	<b>Transitional</b>	<b>Lacustrine</b>
<ul style="list-style-type: none"> <li>• Narrow, channelized basin</li> <li>• Relatively high flow</li> <li>• High suspended solids, turbidity, nutrients</li> <li>• Organic matter &gt; allochthonous</li> <li>• More eutrophic</li> </ul>	<ul style="list-style-type: none"> <li>• Broader, deeper basin</li> <li>• Reduced flow</li> <li>• Reduced suspended solids, less turbid, increased light availability</li> <li>• Intermediate organic matter</li> <li>• Less eutrophic</li> </ul>	<ul style="list-style-type: none"> <li>• Broad, deep, lake-like basin</li> <li>• Little flow</li> <li>• Relatively clear water</li> <li>• Organic matter &gt; autochthonous</li> <li>• More oligotrophic</li> </ul>

### **1.3 Eutrophication in reservoirs**

Eutrophication of water bodies, characterized by intense phytoplankton growth can be harmful to human health, and can have a drastic effect on the water quality and availability for multiple uses (Wagner and Erickson, 2017). This process is usually attributed to human induced activities in water bodies and it is characterized by the over-enrichment of waters with nutrients, such as phosphorus (P) and nitrogen (N), originating from point and non-point pollution sources (Watanabe et al., 2015). These nutrients (N and P) initially cause an increase in the primary production of the ecosystem and, only at a later stage, there are significant changes in sedimentation rate, oxygen dynamics, changes and growth of phytoplankton communities and in the reduction of the water quality for economic and leisure purposes (Esteves, 2011). Phytoplankton has an important role in aquatic ecosystems as biomass indicator and it is due to the presence of a photosynthetic pigment (Chl-*a*), in their cells. Moreover, they are responsible for the ocean being considered as carbon sink because they use CO<sub>2</sub> dissolved in the water, for photosynthesis process, therefore they play an important role in the global carbon cycle (Daggers et al., 2018). Eutrophication and harmful algae blooms (HABs) have also been linked to other processes such as food web disruptions and zooplankton grazing (Scheffer et al 1999).

In the Amazon, the construction of reservoirs has generated discussions due to the changes of the environmental characteristics at local scale, consequently affecting its biodiversity (Lees et al., 2016). Among the several Amazonian reservoirs, the Tucuruí Hydroelectric Reservoir (THR) stands out, currently being the largest artificial reservoir in operation (Manyari and de Carvalho, 2007). With the increasing use of continental waters for energy and water supply, pertaining information on the trophic status of large ecosystems, such as reservoirs, is essential for decision makers in the selection of strategies to manage these environments in an ecologically sustainable way (Straskraba and Tundisi, 2013).

The trophic status of a water body is a fundamental limnological parameter and it is characterized by the level of primary productivity (Hollister et al., 2016), which is often connected to the increasing of pigments or algal biomass concentrations, as well as the concentration of certain nutrients such as nitrogen and phosphorus (Schröder, 1991). Trophic conditions are often associated with water quality and it has a large impact on the water uses (Tundisi et al., 2008).

The knowledge on water quality in reservoirs is essential for the sustainability within these environments as well as for many organisms inhabiting there. Parameters such as phytoplankton biomass, chlorophyll-*a*, physical-chemical parameters play an important ecological function in these ecosystems and, depending on their concentrations, are considered water quality indicators (Juanes et al., 2008). Assessment of the degradation of water quality in reservoirs requires that these water bodies are managed by careful research and management strategies (Chapman, 2016).

One of the major challenges for the water management in reservoirs is to understand that they are complex ecosystems, with own dynamic pattern, physics, chemistry and biology, and that these characteristics are due to changes within the impoundment area over time (Tundisi et al., 2007).

#### ***1.4 Greenhouse gases emission***

Globally changes are connected to a variety of causes such as the increase of the human population growth, excessive use of natural resources, technological progress and intensification of globalization. One of these global changes of great interest to water management in freshwater reservoirs is climate change (Straskraba and Tundisi, 2013).

Climate change has become one of the most relevant issues in the world in recent decades (Patz et al., 2005; Sahoo and Schladow, 2008; Tranvik Lars et al., 2009). Inland aquatic ecosystem, despite occupying a small area of the planet's surface (about 3%) (Nelson Mello thesis, citing Downing et al 2006) has a key role in the continental carbon balance. If in one hand, these ecosystems are considered as a sink of carbon, due to the organic carbon stock in the sediment, in other hand they are significant sources of greenhouse gases (GHG), such as carbon dioxide (CO<sub>2</sub>) and methane (CH<sub>4</sub>) to the atmosphere due to both aerobic and anaerobic microbial degradation processes (Bastviken et al., 2011; Cole et al., 2007; Mello et al., 2018; Tranvik Lars et al., 2009).

With all these impacts caused by hydropower reservoirs, a question has been raised between scientists and water managers about hydropower's viability for multiple purposes and influence in the climate change.

Besides the already cited impacts of eutrophication, the increase inputs of organic matter and nutrients availability in these water bodies also favour the greenhouse gases emission into the atmosphere (Deemer et al., 2016). High discharge from both point and nonpoint sources from surrounding areas are responsible to increase carbon, nitrogen and phosphorus concentrations and all this together increases autochthonous biomass available in the water column (Tundisi et al., 2012).

Recent studies show that reservoirs are potential sources of greenhouse gas emissions even, when, presenting high phytoplankton concentrations, which in this case should be acting as sinkers (Mendonça et al., 2012). Phytoplankton are carbon sinkers because they partly absorb CO<sub>2</sub> through photosynthesis, and many autotrophic species can also utilize carbon dioxide and or bicarbonate as a carbon source (Verspagen et al., 2014). Therefore, the assimilation of inorganic carbon by dense phytoplankton in blooms conditions leads to low concentrations of dissolved CO<sub>2</sub> (Gu et al., 2011). Depletion in CO<sub>2</sub> has been reported to increase pH levels (Sandrini et al., 2016; Verspagen et al., 2014). Several studies in Brazilian hydropower reservoirs showed that GHG were emitted by these aquatic systems due to high eutrophication levels (Davidson Thomas et al., 2015). Indeed the combination of high pH values and CO<sub>2</sub> depletion in freshwaters is often associated with cyanobacterial blooms, which in turn is a consequence of the eutrophication (Sandrini et al., 2016).

### ***1.5 Geospatial analysis for water management in reservoirs***

The increased nutrient loads into reservoirs is usually attributed to the intensification of agricultural production and human population growth, and the use of chemical fertilizers for agriculture in surrounding areas (Lee et al., 2009). These factors together with precipitation result in inputs of autochthonous and allochthonous organic matter, which are responsible for the release of nutrients such as carbon, phosphate, and nitrogen in the water column and deeper layers (Tranvik Lars et al., 2009). With accumulation of the organic matter in the sediments, there will be a cycling of nutrients by microorganisms that results in the production, accumulation and consequently, the emission of GHG (Straskraba and Tundisi, 2013). According to Tundisi et al. (2012) the action of changes in climatological forcing (precipitation, wind and solar radiation) are closely related to the operational mechanisms of dams (retention time and outflow). These, together with the system's morphometry,

produce differences in the horizontal and vertical circulation throughout a temporal and spatial scales in reservoirs (Becker et al., 2010).

In addition to various impacts caused by reservoirs, this thesis discusses two main environmental issues occurring in reservoirs, which are eutrophication and greenhouse gases emission and these are presented in the following paragraphs.

The input of nutrients in a reservoir via its tributaries is a factor to be considered when studying eutrophication in these water bodies (Novotny, 2011). Waters from tributaries become diluted toward the main axis, and the many secondary water sources along the hydrographic basin that flow into the reservoir and contribute not only to the eutrophication of the system but also to the formation of compartments with different environmental conditions (Chapman, 2016). Potential impacts resulting from eutrophication include phytoplankton blooms, oxygen-depletion in deep layers, emission of greenhouse gases and water quality deterioration for multiple uses (Cooke et al., 2016).

One of the visible problems within reservoirs generated by eutrophication is the "*bloom*" of algae that not only cause aesthetic degradation of water quality resulting in the formation of foam on the water surface, but also cause unpleasant taste and odour in drinking water, and poses additional threats human health due to the presence of toxins in harmful algae (Qin et al., 2015).

Generally, the monitoring of aquatic ecosystems requires *in situ* sampling, which in most cases is costly and time consuming. Due to the complexity associated with the field collection of water samples and subsequent laboratory analysis, scientists and researchers have been using remote sensing techniques to obtain information on the quality of these water bodies (Bonansea et al., 2015; Curtarelli et al., 2015; Gholizadeh et al., 2016; Lim and Choi, 2015; Palmer et al., 2015).

The feasibility of the use of optical remote sensing data for monitoring and management of these water bodies has been widely evaluated, since some components used in the water quality assessment interact with electromagnetic radiation in the visible and near infrared region by changing the colour of the water (Kirk, 2010). Thus, the water colour is directly related to the presence and the different concentrations of these constituents in the water column, which in turn cause differences in the underwater optical characteristics (IOCGG, 2000).

In synergy with *in situ* measurements, remote sensing of water is an important tool for monitoring the trophic status of inland waters, such as reservoirs. In addition, it provides information to support new strategies for sustainable management of these water bodies (Brivio et al., 2001; Gurlin et al., 2011). The combination of remote sensing data and limnological studies was already reported in the past by (Dekker, 1993b) as possibility to evaluate large areas and to relate the spectral response of water with *in situ* limnological data, supporting *in situ* monitoring programs with the indication of the best sampling locations.

A major interest in the use of remote sensing data in aquatic environments is to ascertain the spatial and temporal variation of the water composition and to investigate the origin and displacement of specific suspended or dissolved components. Suspended solids, dissolved organic matter, water molecules and phytoplankton are called optically active components (OACs) and these are the main factors controlling the inherent optical properties (IOPs) of the water (Mobley, 1994).

Chlorophyll-*a* is the main pigment found in all phytoplankton, with amounts varying per taxonomic groups (Bellinger and Sigee, 2015; Reynolds, 2006) and it is widely used as proxy in the determination of phytoplankton biomass and primary productivity studies (Boyer et al., 2009; Oliveira et al., 2016; Tan et al., 2017). The estimation of Chl-*a* concentrations from satellite imagery requires the development of algorithms with maximum sensitivity for the concentration of this pigment and minimum sensitivity to the concentration of other components present in the water (Bukata et al., 1995; Dall’Olmo and Gitelson, 2005; Moses et al., 2009; Szeto et al., 2011). Thus, estimating this Chl-*a* for Case 2 waters using remote sensing is challenging since the optical properties of these types of water are significantly influenced by mineral particles, sediments, and organisms associated with phytoplankton (Dowell and Platt, 2009).

As phytoplankton is the basis of the food web in aquatic ecosystems and are accountable for 50% of the global primary production (Finkel et al., 2009), and is responding very fast to environmental change (Häder and Gao, 2017), it is important to monitor the ongoing effects of climate change and eutrophication on the phytoplankton community in hydropower reservoirs.

In this study, we use an integrated approach including field observations, laboratory experimentation and satellite data to provide important information for sustainable water management in hydropower reservoirs. The usefulness of remote sensing

techniques is that it can help overcome the limited spatial dimension of traditional in situ methods, as it permits to acquire information at different spatial and temporal scales. Therefore it allows a more broad view of these water bodies, because it provides analysis in synoptic order.

This research uses medium high resolution sensor, Landsat 8 OLI, data and Landsat 5 as images source. Landsat 5 is used to retrieve water extent described in chapter 5 and Landsat 8 to monitor the spatial distribution of algal blooms in chapter 3.

The OLI sensor onboard of Landsat 8 is composed of nine spectral bands with four bands in the visible range of the electromagnetic spectrum. The spatial resolution of the images are 30m (OLI sensor) and 100 m (TIRS), and the radiometric resolution is 16 bits. Differences between Landsat 5 and 8 characteristics are given in table 1.1.2.

**Table 1.2** Performance characteristics of the Landsat-8/OLI and Landsat-5/Thematic mapper

Satellite/sensor	Subsystem	Band name	Band number	Spectral range (µm)	Spatial resolution (m)
Landsat-8/OLI	VNIR	Coastal aerosol	1	0.43 – 0.45	30
		Blue	2	0.45 – 0.51	
		Green	3	0.53 – 0.59	
		Red	4	0.64 – 0.67	
		Near Infrared	5	0.85 – 0.88	
	SWIR	Shortwave Infrared 1	6	1.57 – 1.65	
		Shortwave infrared 2	7	2.11 – 2.29	
	VNIR	Panchromatic	8	0.5 – 0.68	15
		Cirrus	9	1.36 – 1.38	30
Landsat-5/TM	VNIR	Blue	1	0.45 – 0.52	30
		Green	2	0.52 – 0.60	
		Red	3	0.63 – 0.69	
		Near Infrared	4	0.77 – 0.90	
	SWIR	Shortwave Infrared	5	1.55 – 1.75	
		Shortwave infrared	7	2.09 – 2.35	

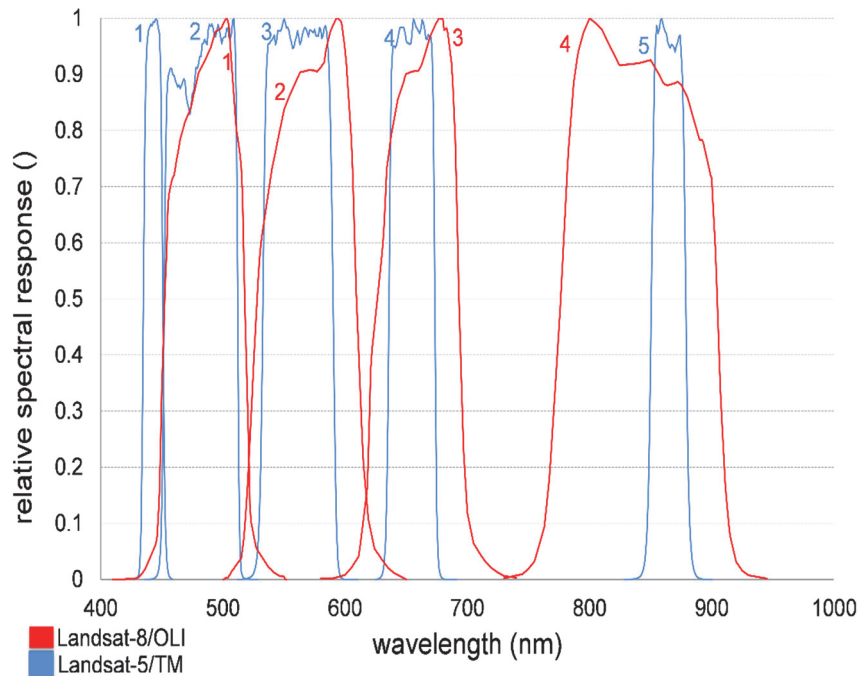


**Figure 1.2** Comparison of relative spectral response between Landsat-8 and Landsat-5 bands.

### 1.6 Research objectives

The main objective of this thesis is to integrate geospatial information with *in situ* water quality monitoring to improve on the cost efficiency of environmental management schemes of hydropower reservoirs in the Amazon region. To achieve the main objective, four specific objectives were proposed and these are specified below.

- 1 To analyze the effect of seasonal phytoplankton groups dynamic on the retrieval of Chl-*a* concentration (algal pigment) by optical remote sensors from tropical water bodies.
- 2 To assess the feasibility of using medium high resolution sensors, such as Landsat-8 OLI sensor in monitoring the spatial distribution and frequency of algal blooms in the Tucuuruí reservoir.
- 3 To identify key environmental factors influencing eutrophication and associated harmful algae bloom occurrences in the Tucuuruí hydropower, e.g. human influences and climate forcing (deforestation, human settlements, aquaculture, reservoir hydrological operation cycles and management, climate variations).

- 4 To estimate the GHG emissions in the THR in temporal and spatial scales using geospatial analysis and to assess if emissions are related to the eutrophication process due to anthropic activities or climate forcings.

### ***1.7 Outline of this thesis***

The research described in this dissertation is organized in six chapters. The **first chapter**, the introduction, consists of a research motivation, problem and objectives and its main goal is to give a general understanding about the topic discussed here. The main subjects dealt with in this thesis are described in **chapters 2 to 5**, which are assigned to achieve the research objectives.

**The chapter 2** deals with the seasonal phytoplankton ecology in a hydropower. The objective of this chapter is to investigate phytoplankton response to environmental disturbance in a Sustainable reserve located within the Tucuruí hydroelectric reservoir. The main hypothesis of this chapter is that there is a correlation between the diurnal and seasonal variations in vertical distribution of phytoplankton with nutrient loads and human interferences within this sustainable reserve.

**Chapter 3** deals with algal blooms in hydropower reservoirs. The objective of this chapter is to investigate if the combination between water limnology and satellite imagery is a suitable approach to identify harmful algal bloom extent in reservoirs.

The **chapters 4 and 5** investigate the key environmental impacts caused by the construction of hydroelectric reservoirs: eutrophication and the emission of greenhouse gases.

**Chapter 4** explores the occurrence of eutrophication processes in hydropower reservoirs using generalized linear models, which were applied to identify relationships between the hydrological operating cycle of an Amazon reservoir and the water quality in its limnological zones with respect to factors influencing eutrophication processes.

**In chapter 5**, greenhouse gases emissions by reservoirs are discussed. The objective of this chapter is to assess an approach, which is based on a combination of *in situ* sampling with laboratory chemical analysis, geostatistics and remote sensing data to model the spatial and temporal variations in greenhouse gases.

Finally, **Chapter 6** is a synthesis of the results obtained in this dissertation. It contains main conclusions of this research and provides suggestions in developing future research in this field.



---

**Seasonal variation of phytoplankton  
indicates small impacts of anthropic  
activities in a Brazilian Amazonian reserve**

---

2



### ***Abstract***<sup>1</sup>

Knowledge about phytoplankton community structure helps in assessing the quality of a water body. However, variables related to it are not routinely surveyed in most of the water quality monitoring programs. Our approach included studying the diversity of these organisms, in a large tropical reservoir in a Brazilian Amazonian reserve. The research was carried out in the rainy and dry season when measurements were performed every three hours and at five different depths. A total of 40 water samples were collected to assess temporal variations of abiotic and biotic factors. Physico-chemical parameters were analysed to characterize the ecosystem and relationships between these variables and phytoplankton functional groups were statistically tested. The data were examined using analysis of variance and canonical correspondence analysis. We identified 9 functional groups in both seasons. The functional group M, which represents organisms with developed adaptations to high insolation and stable environments, had a higher relative percentage of contribution to the total biomass in the rainy season. Group P, which tends to be present in the more eutrophic lakes and is tolerant to carbon deficiency, had a higher relative percentage of contribution to the total biomass in the dry season. This study indicated that the fluctuations of the water level reflected in seasonal changes of phytoplankton biomass and environmental variables. Additionally, this experiment permitted to advise on sampling strategies for monitoring phytoplankton in lakes and reservoirs.

---

<sup>1</sup> This chapter is based on: **Brandão**, I.L.S, Mannaerts, C.M., Saraiva, A.C.F. *Seasonal variation of phytoplankton indicates small impacts of anthropic activities in a Brazilian Amazonian reserve* (2017). *Ecologyhydrology & Hydrobiology* Volume 17, Issue 3, 2017, Pages 217-226.

## **2.1 Introduction**

The main rivers of the Brazilian amazon rainforest are being exploited for purposes of hydroelectric generation. Extensive constructions of reservoirs produced huge impacts to the aquatic ecosystems of the watershed in the last years (Tundisi et al., 2006a).

Uncontrolled land occupation and use by populations living along reservoir areas are a negative impact, which favours the increase of pollution sources to the water body. Sources of pollution in aquatic ecosystems are mainly from the discharge of sewage, pesticides from agricultural and reforestation uses. These factors contribute to the increase of nutrients (N and P) in the water body, consequently favouring eutrophication (Straskraba and Tundisi, 2013).

Studies on the functional roles and structural adaptations of planktonic organisms are a subject of very interest by researchers' worldwide (Reynolds et al., 2002). The study of planktonic organisms is of great ecological importance because phytoplankton produce organic matter by photosynthesis and so represent the base of the food chain (Lee, 2008). Moreover, they are considered as a good indicator of the physical and chemical conditions of water in reservoirs due to their diversity index assessment (Costa et al., 2009). The diversity of planktonic organisms and their various compositions may signal the deterioration of a water body as they grow excessively under water-rich nutrient conditions (Bilous et al., 2016; Tundisi and Tundisi, 2012).

Phytoplankton are autotrophic organisms that are present in most freshwater basins. These organisms have the tendency to perform vertical migration as a result of any significant change that occurs in the water environment (Mellard et al., 2011b). This ability to regulate in a vertical position is related to their intrinsic features (such as flagella, walls, and mucilages, plastids, etc.) and extrinsic features related to the water movements and changes in variables such as temperature, nutrient loading and light availability as described by Xu et al. (2011); Carl et al. (2004). Furthermore, when in functional group association, phytoplankton provide a better understanding of the ecosystem dynamics and species selection (Okogwu and Ugwumba, 2012).

Artificial ecosystems such as hydroelectric reservoirs are lakes which are continually manipulated by human activities. They are intermediate ecosystems between lotic and lentic environments (Margalef, 1983). In addition, reservoirs are important not only for electrical power generation but also for their multiple roles such as water

supply, flood control, and navigation. However, human activities such as fisheries and recreation in these artificial lakes have been reported as the main cause for eutrophication occurrence (Straskraba and Tundisi, 2013).

Eutrophication of water bodies is characterized by excessive production of phytoplankton biomass, which is usually associated with increasing of nutrients concentration, such as phosphorus and nitrogen (Ansari et al., 2011). High phytoplankton biomass is known as “*algae blooms*” and these can be harmful to human health having a drastic effect on the quality and availability of water for various purposes (Tundisi et al., 2004). Harmful algae “*blooms*” cause aesthetic degradation of lakes and reservoirs resulting in the formation of foam on the water surface, unpleasant taste and odor in drinking water and health effects from the toxins present in some of these algae (H. and Schindler, 2009; Smith and Schindler; Smith and Schindler, 2009).

In this work, the main goal was to investigate phytoplankton response to the effect of the nutrient load at the surrounding areas of a Brazilian Amazonian reserve. Thus, as phytoplankton perform vertical migration as a result of any change in the environment, we proposed to take measurements in temporal and vertical scales. According to Mellard et al. (2011b), the vertical dimension is the major axis responsible for explaining phytoplankton heterogeneity due to its effect on primary production as well as energy transfer to high trophic levels (Lampert et al., 2003). In addition, we hypothesized that there is a correlation between the diurnal and seasonal variations in vertical distribution of phytoplankton with nutrient loads likely caused by human activities, such as fish-farming and recreation.

## 2.2 Materials and methods

### 2.2.1 Description of study site

The study area was the Alcobaça Sustainable Development Reserve (SDR) which is located in the Tucuruí reservoir, the second largest in Brazilian territory (Espíndola et al., 2000). This SDR extends from 3° 50' 32, 8" S 49° 40' 38, 8" W to 4° 3' 49, 6" S to 49° 55' 36, 1" W and occupies 36.128,00 ha of the protected areas around the Tucuruí reservoir (Figure 2.1).

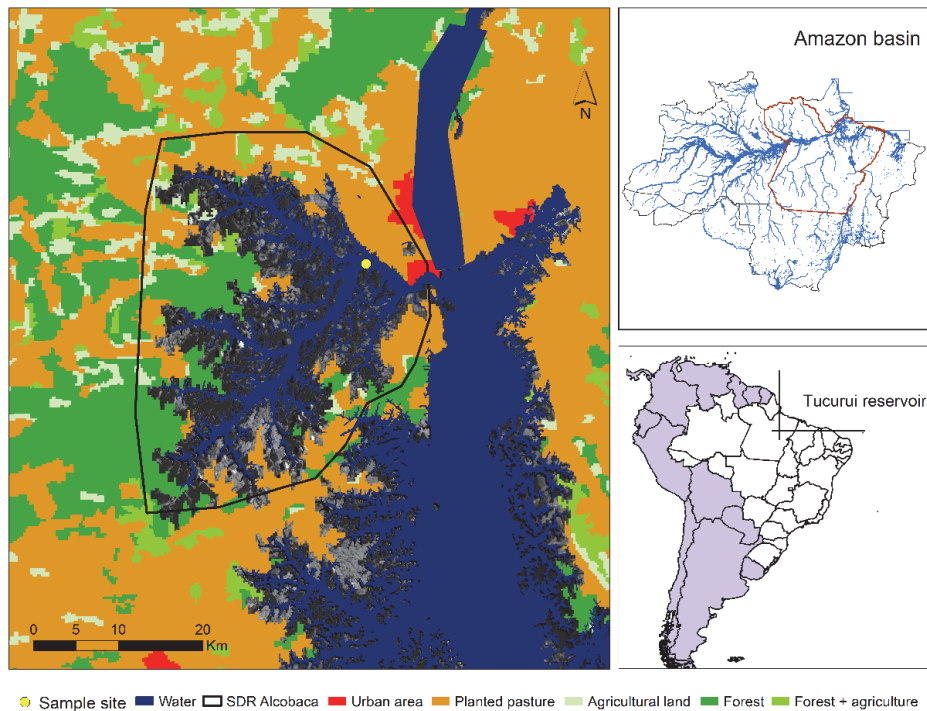


**Figure 2.1** Study area

The Alcobaça SDR is part of a mosaic of protected areas dedicated to biodiversity conservation. The main characteristic of this reserve is the presence of several islands, which were formed by the Tucuruí dam. According to Barata (2011), the environmental characteristics of this RDS remain with little changes and huge biodiversity. In spite of the legislation prohibits any predatory exploitation of the natural resources, the RDS has been occupied without planning. This issue directly affects forestry resources, which has to be cut-off for land occupation.

This Amazonian SDR has faced problems related to deforestation along the last decade but it is decreasing as shown in Figure 2.2 (INPE, 2017b). This process has serious

consequences such as soil erosion, leaching, disturbance of the water, oxygen, and carbon dioxide cycles. The leaching of soil, during rainfall periods and high waters, loads organic matter into the aquatic environment, thereby increasing nutrient levels, total solids, and decreasing water transparency. These consequences directly affect the reservoir ecosystem, which has a varying water level throughout the year. The water level in Tucuuruí reservoir is characterized by four distinct periods: rising (December to February); high (March to May); falling (June to August) and low (September to November) (Eletronorte, 2016). Main characteristics of the Tucuuruí reservoir are in Table 2.1 and the water level along 2014 in Figure 2.3.

**Table 2.1** Main general features of the Tucuuruí reservoir.

<b>Technical characteristics</b>	
Basin's drainage area (km <sup>2</sup> ) <sup>a</sup>	758.000
Surface area (km <sup>2</sup> ) <sup>a</sup>	2430
Max. depth (m) <sup>a</sup>	75
Mean depth (m) <sup>a</sup>	18.9
Volume (km <sup>3</sup> ) <sup>c</sup>	45.5
Water retention time (days) <sup>a,b</sup>	46
Main use <sup>d</sup>	electricity
Secondary uses <sup>d</sup>	fish-farming, recreation

a = (Espíndola et al., 2000), b= (Deus et al., 2013), c=(Tundisi et al., 2006a), d= (Ideflor-bio, 2017)

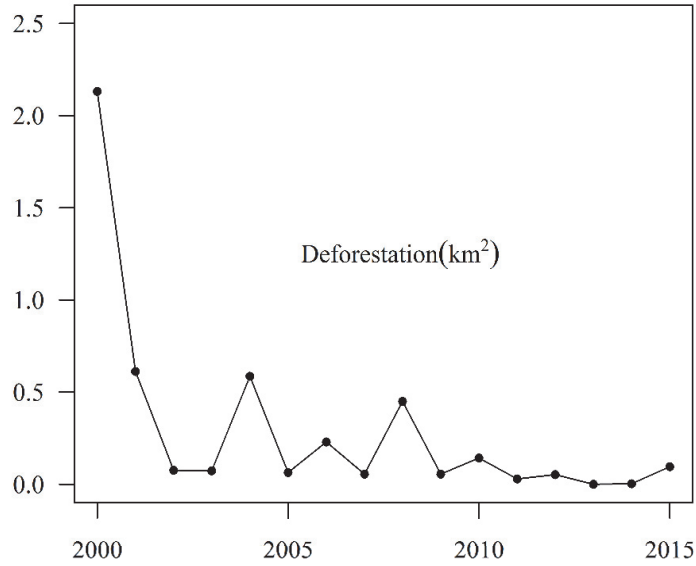


Figure 2.3 Deforestation at SDR Alcobaça from 2000-2015

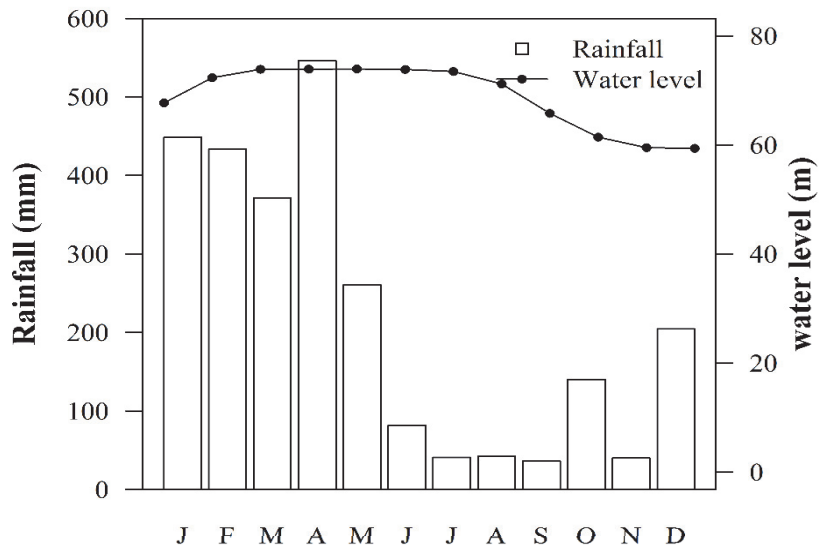


Figure 2.3 Monthly accumulated rainfall and the water level of the Tucuruí reservoir along the year of 2014.

We conducted the experiment at a single site (Caraipé 1) in one day each season. The Caraipé 1 is located at the main water mouth of the Amazonian SDR (03° 50' 03.4" S e 49° 42' 32.10" W). It is characterized by shallower waters and longer residence time comparing to the whole reserve and reservoir due to its dendritic morphology. Furthermore, dendritic edges and several islands around Caraipé 1 contribute to the increase of organic matter production due to water level fluctuation (Espíndola et al., 2000). Ecosystems with long residence time usually present high density and diversity of phytoplankton (Esteves, 2011).

### **2.3 Material**

Samplings were performed during two seasonal periods: rainy (June 2014 – the falling phase of the Tucuruí reservoir) and dry (September 2014 – low water) at a single station and in one day each season. The monthly rainfall for the year of 2014 was acquired from the Brazilian Meteorological Institute (INMET) (INMET, 2017) and the Tucuruí water level from ANA (2017).

Abiotic and biotic variables were collected from the water column on the surface, 3m, 6m, 10m and 15m, and at four different times: 10 am, 1 pm, 3 pm, and 6 pm. Depths were estimated according to the light penetration, calculated by Secchi disk and the photic zone was determined multiplying Secchi disk by three (Tyler, 1968). A total of 40 water samples (20 samples in the rainy season and 20 in the dry season) were collected to analyze temporal variations of abiotic and biotic variables.

The following variables were measured *in situ*: water temperature (digital thermometer, *SM 2550*), conductivity (Hatch device, *SM 2510*) and pH (PHTEK device, *NBR 9896/1993*). Dissolved oxygen (*SM 4500-OC*), turbidity (nephelometric method, *SM 2130B*), ion ammonium (*SM 4500-NH<sub>3</sub>C*), total phosphorus (ascorbic acid method USEPA (1978)), Chl-a was estimated using the extraction by acetone method (Gotterman et al., 1978), total suspended solids (*SM 2540-D*), color (spectrophotometer, *SM 2120B*) and alkalinity (*SM 2320*) were measured in the laboratory.

Water samples (12 L) for phytoplankton analysis were collected with a bucket at the surface and with a Van Dorn bottle in the other depths and passed through a mesh plankton net with 20 µm. Samples were fixed with 4% Lugol's solution and concentrated to approximately 150 mL. Then the phytoplankton samples were stored in plastic bottles and transported to the laboratory for further processing and analysis.

### 2.3.1 Methods

Phytoplankton analysis was done with the aim to identify taxonomic composition and population structures in the water column. Quantitative analysis was performed under an inverted microscope (Zeiss135) using the sedimentation method proposed by Utermöhl (Utermöhl, 1958b) and samples were set up in different chamber sizes ranging from 2 to 6 mL. The minimum sedimentation time was 24 hours for all samples (Ollrik et al., 1998). Counting was performed for one transect of the sedimentation chamber at different magnifications (of 100x, 200x, and 400x) for different taxa, depending on their respective size. Unicellular organisms, filaments, trichomes, colonies, and coenobium were considered as a single organism. Taxonomic identification was based on Bicudo and Bicudo (1970); Bicudo and Menezes (2006); Komárek et al. (1983); Sant'Anna and Azevedo (2000) and organisms were separated into the divisions *Cyanophyta*, *Chlorophyta*, *Charophyta*, *Dinophyta*, *Ochromophyta* and *Euglenophyta* (Hoek et al., 1995) and functional groups.

Phytoplankton biomass was estimated based on the cell or colony dimensions and cell numbers. Biovolume was calculated using formulae proposed by Hillebrand et al. (1999) and expressed into biomass [ $\mu\text{g}$  (fresh weight  $\text{L}^{-1}$ )], where  $1\text{mm}^3 \text{L} = \text{mg} \text{L}^{-1} = 1 \mu\text{g} \text{L}^{-1}$  as described by Wetzel and Likens (2000).

Phytoplankton diversity was calculated using Margalef index (Gamito, 2010; Margalef, 1983) and their associations were established according to Reynolds et al. (2002) and Padisák et al. (2009). Functional groups of phytoplankton were determined from species contributing equal or more than 5% to the biovolume of each observation.

Classification of the phytoplankton through their functional attributes is a way to better understand, describe and forecast their behaviour due to any change in the ecosystem. Reynolds et al. (2002), proposed a list of functional groups, which is based on survival strategies such as tolerance and sensibility to different environmental conditions. This list includes 31 groups of species (assigned as codons and represented by letters), belonging to different classes, but with similar characteristics to prevail in specific environmental conditions.

### 2.4 Statistical analysis

In order to enable comparisons between time and depths in both seasons and the validation of the results, normality tests of Lilliefors and Jarque-Bera were performed with a significance level of 5%. Since the abiotic variables presented a

different scale of measurements, they were standardized for z-score and biotic variables were the fourth root transformed.

In addition, we investigated if a multiple depths and time sampling approaches were needed to estimate the phytoplankton biomass in the reservoir, due environmental changes. Thus, to test the significance of the sampling strategy of this experiment, the phytoplankton biomass was subjected to a two-way analysis of variance (ANOVA) and Tukey's honest significant difference (HSD) with a significance level of 5%. Depth and time were considered as factors and the test was performed for both the dry and rainy seasons.

Canonical correspondence analysis (CCA) was performed using phytoplankton functional groups and abiotic variables to assess possible associations between them during both seasons. The functional groups used in this analysis were selected from the species which had relative contribution equal or greater than 5% to the total biovolume of at least one sample. Statistical analyses were performed using the program R version 3.3.1 (R Development Core Team, 2008).

## **2.5 Results**

### **2.5.1 Environmental variables**

The rainy season was characterized by lower temperatures ( $33.35 \pm 0.81$  °C) and higher accumulated precipitation levels ( $81.9 \pm 7.83$  mm) and the dry season by higher temperatures ( $34.07 \pm 0.86$  °C) and lower accumulated precipitation levels ( $36.2 \pm 5.97$  mm). The water level in the reservoir reached values of 73.84 m in June and 65.77 m in September. The Figure 2.3 (in the study are section) shows the rainfall and the water level distributed along the year of 2014.

The water temperature did not reveal extreme changes in a temporal scale. In the rainy season the average was 30.2°C and in the dry season, 29.7°C. The average conductivity was  $36.39 (\pm 0.6)$   $\mu\text{S cm}^{-1}$  in the rainy season and  $31.89 (\pm 0.07)$   $\mu\text{S cm}^{-1}$  in the dry season. Higher values of dissolved oxygen were recorded in the rainy season, with an average of  $5.57 (\pm 1.83)$   $\text{mg L}^{-1}$  (Figure 2.4).

The total phosphorus average was  $12.24 (\pm 2.6)$   $\mu\text{g L}^{-1}$  in the rainy season and  $11.85 (\pm 1.47)$   $\mu\text{g L}^{-1}$  in the dry season. Ion ammonium  $28.37 (\pm 3.93)$   $\mu\text{g L}^{-1}$  in the rainy season, and  $47.05 (\pm 7.54)$   $\mu\text{g L}^{-1}$  in the dry season. Both variables revealed variation in vertical and temporal scales.

Most of abiotic variables revealed significant variation between seasons (ANOVA and THD tests;  $p > 0.05$  (Figure 2.4). However, TP and Chl-*a* concentrations were not significantly different. Significant variations in depth were observed for water

temperature ( $F=10.32$ ;  $p<0.001$ ), DO ( $F=13.65$ ;  $p<0.001$ ), pH ( $F=4.15$ ;  $p<0.01$ ), EC ( $F=5.53$ ;  $p<0.01$ ), Chl-*a* ( $F=4.37$ ;  $p<0.01$ ), and color ( $F=3.41$ ;  $p<0.05$ ), whereas over time significant variations were observed for water temperature ( $F=3.94$ ;  $p<0.05$ ), ion ammonium ( $F=3.74$ ;  $p<0.05$ ), TP ( $F=4.49$ ;  $p<0.01$ ) and color ( $F=3.42$ ;  $p<0.05$ ) Figure 2.4.

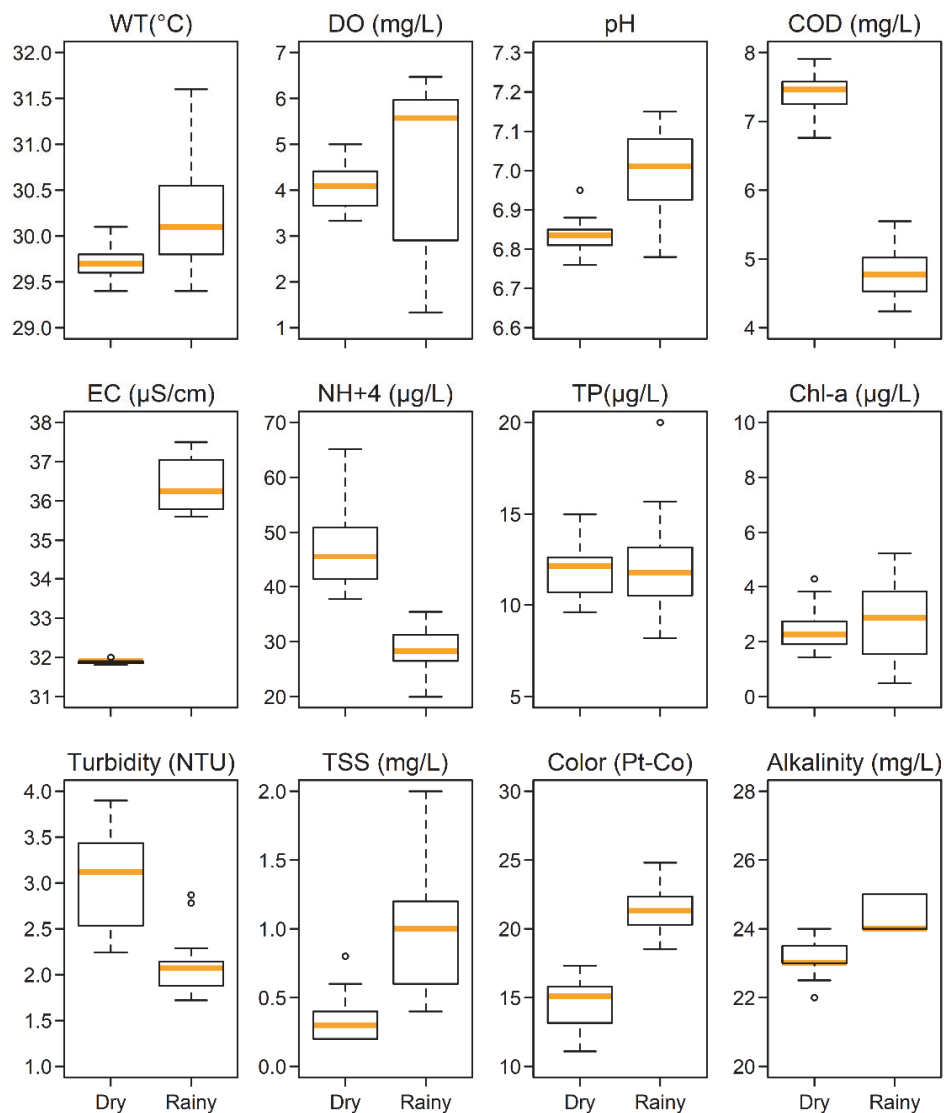


**Figure 2.4** Boxplot of the abiotic factors in the dry and rainy seasons.

## 2.5.2 Phytoplankton community

### 2.5.2.1 Qualitative analysis

The phytoplankton composition of the Caraipé 1 site in Alcobaça SDR was classified into five divisions. These were *Cyanophyta* (69), *Chlorophyta* (50), *Charophyta* (48), *Dinophyta* (1), and *Bacillariophyta* (20) cumulating into 188 taxa for both seasons. Figure 2.5 - upper panel shows phytoplankton biomass for rainy and lower panel for dry seasons, respectively.

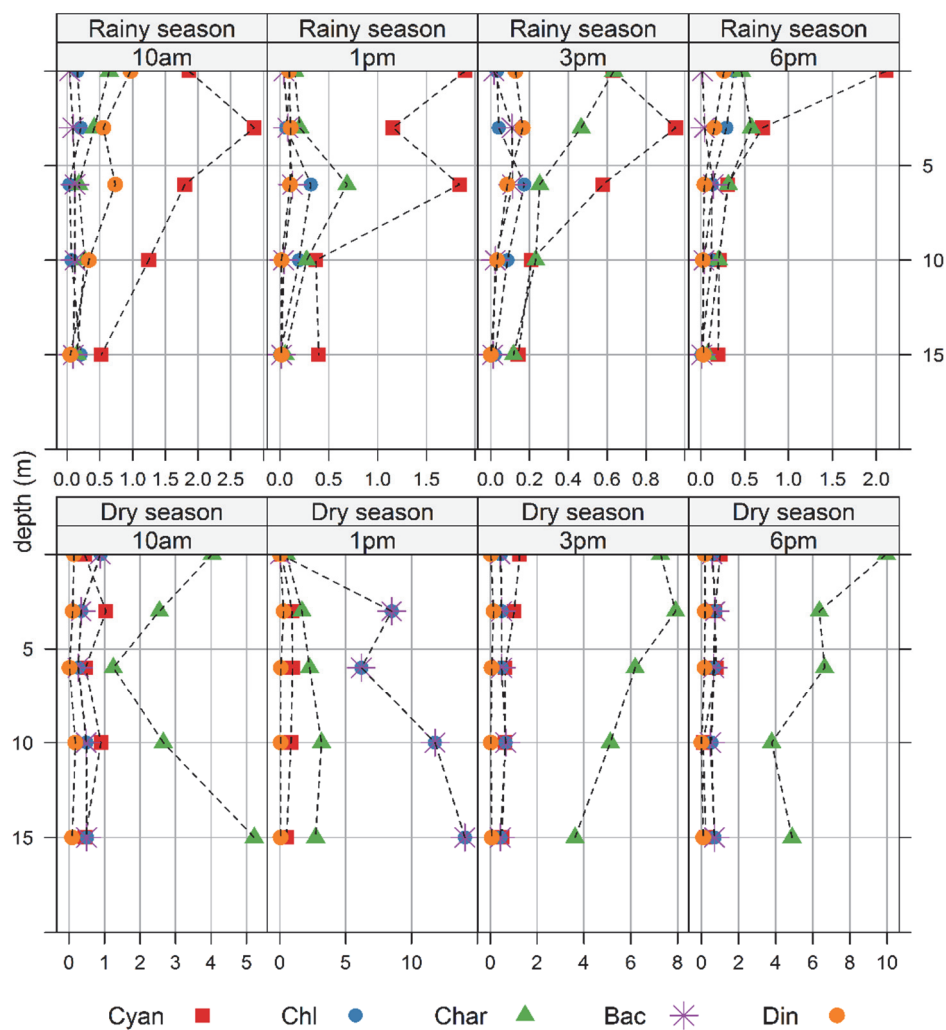


**Figure 2.5** Phytoplankton biomass in the rainy season (upper panel) and dry season (lower panel) at Caraipé 1- Alcobaça SDR.

### 2.5.2.2 Biomass

The highest phytoplankton biomass was recorded at 1 pm in 15 m in the dry season (Figure 2.5, lower panel). In the rainy season, the mean biomass was  $1.80 (\pm 1.15) \mu\text{g L}^{-1}$  and in the dry season  $7.95 (\pm 4.58) \mu\text{g L}^{-1}$ . Although the dry season exhibited a significant higher phytoplankton biomass, diversity indices were lower compared to the rainy season.

In the rainy season, *Cyanophyta* was the most important division with mean biomass of  $0.99 (\pm 0.8) \mu\text{g L}^{-1}$  and 83.1% of relative contribution in the biomass at 1 pm at the surface water (Figure 2.5, upper panel). In the dry season, *Charophyta* was the most abundant division recording 84.2% of the relative contribution of the total biomass (Figure 2.5, lower panel). However, in the dry season, *Bacillariophyta* and *Chlorophyta* divisions presented peaks at 1 pm.

The main species of *Cyanophyta* and *Charophyta*, which contributed to increase the biomass in Alcobaça SDR were *Microcystis sp.* and *Anabaena sp.*, in the rainy season, while *Aulacoseira granulata*, *Staurastrum sp.*, and *Staurodesmus sp.*, in the dry season. *Bacillariophyta* represented by *Rhizosolenia sp.* showed peaks of biomass in the dry season. More details on species contribution to the total biomass are available in the appendix 2.1.

### 2.5.2.3 Functional groups of phytoplankton

Functional groups of phytoplankton varied significantly on temporal and vertical scales in the rainy season and in temporal scale in the dry season (ANOVA;  $p > 0.05$ ). Taxa were grouped in 9 associations (codons) according to Reynolds et al. (2002). These associations considered only species which contributed with 5% or greater to the total biomass of one observation. The *Cyanophyta* division presented a higher number of associations with 4 (**H1**, **Lo**, **M**, and **S1**), *Chlorophyta* had 1 association (**J**), *Bacillariophyta* had 2 associations (**P**, **A**) and *Charophyte* had 2 associations (**Na**, **P**), and *Dinophyta* 1 association (**Lo**). A table with the functional groups and their main characteristics found in this work is available in the appendix 2.2.

### 2.5.3 Diversity indexes

Species richness (S) during the rainy season was higher than those recorded during the dry season. Although the dry season was characterized by the dominance of the *Charophyta* division on the vertical profile, our results show a tendency toward a

homogenous distribution of the assemblages, considering both temporal and spatial scales.

The Margalef's diversity index ranged from 7.03 to 11.76 in the rainy season (Figure 2.6) but 6.93 to 9.96 in the dry season. Higher values, for the rainy season, were recorded at 10 am and 3 pm in surface water. In the dry season, high values were recorded at 3 pm at 10 m.

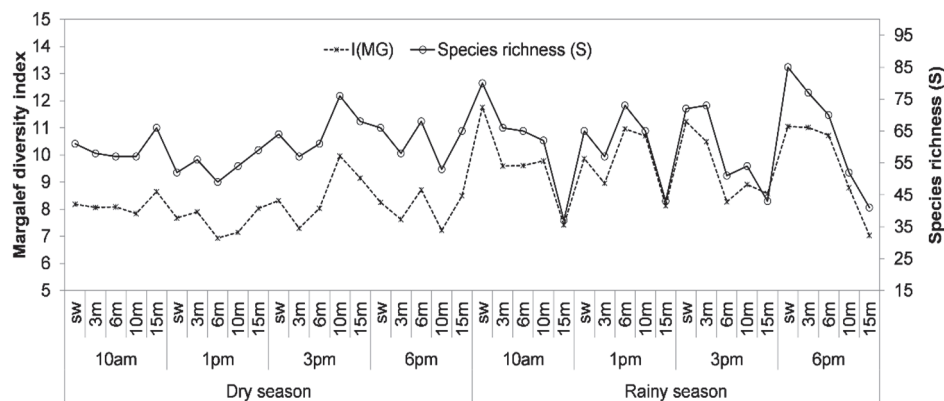


Figure 2.6 Seasonal variation of phytoplankton species richness and Margalef diversity index of Caraipé 1 considering absolute numbers or densities.

### 2.5.4 Sample strategies

During the rainy season, significant differences between phytoplankton biomass and sampling times ( $F=7.56 < F_{cr}=3.49$  and  $p=0.004$ ) and depth ( $F=16.71 < F_{cr}=3.26$  and  $p<0.001$ ) were observed at a 0.05 confidence interval. The time of sampling during the day (between 10 am and 6 pm) showed significant during the rainy season. For the dry season, no significant differences between water depth and sampling times were found with a two-way analysis of variance at the 5% confidence level. For depth we obtained ( $F=0.20 < F_{cr}= 3.26$  and  $p=0.93$ ) and for sampling time ( $F=1.20 < F_{cr}= 3.49$  and  $p=0.35$ ).

### 2.5.5 Canonical correspondence analysis

Canonical correspondence analysis (CCA) was performed to investigate any association between phytoplankton functional groups and abiotic variables. Figure 2.7 contains a result of the CCA analysis and tables 2.2 and 2.3 present the summary statistics for axis 1 and 2 of the CCA and significance test for rainy and dry seasons, respectively. Permutation test (nperm=999) confirmed linear relationship between phytoplankton functional groups and abiotic variables ( $p < 0.05$ ) in both seasons.

In the rainy season, CCA analysis (Figure 2.7. left side) reveals that the first two axes of the abiotic variables explained 70% of the variance in phytoplankton functional groups. The test of significance showed significant results for both axes (Table 2.2). Higher contributions to axis 1 were from the loading of water transparency (-0.56), total phosphorus (0.33) and ion ammonium (-0.25). Higher contributions to axis 2 were from the loading of turbidity (0.41), alkalinity (0.39), water temperature (-0.36) and ammoniacal nitrogen (-0.25) as shown in the appendix 2.3.

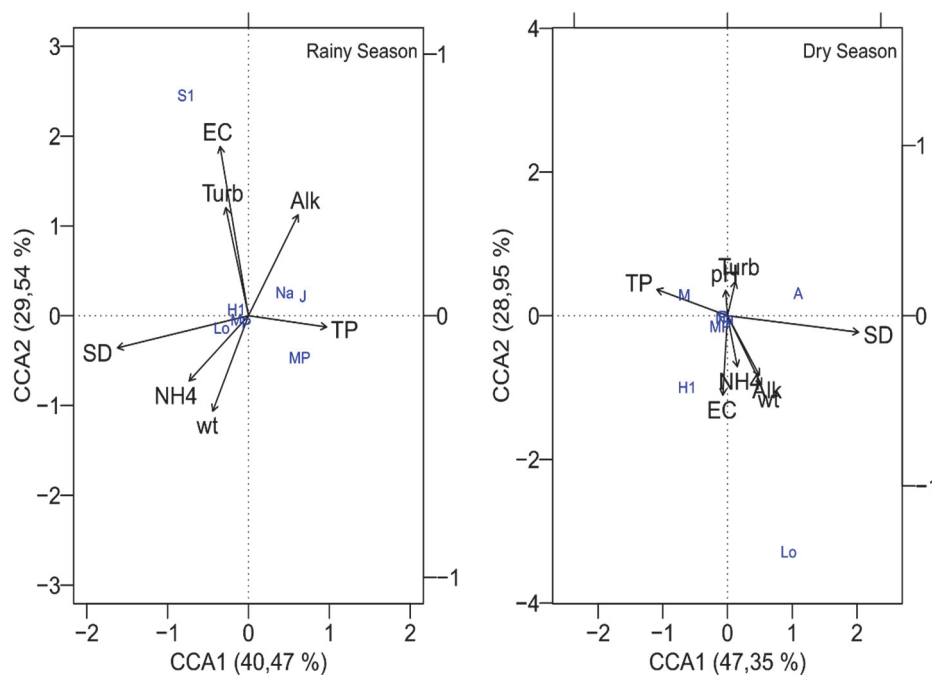


**Figure 2.7** Canonical correspondence analysis (CCA) between abiotic explanatory variables and the most frequent phytoplankton functional group in the rainy season (left side) and in the dry season (right side). The explanatory variables are represented by lines with arrows and phytoplankton functional groups by blue color (M, MP, Lo, S1, H1, P, Na, J, A)

**Table 2.2** Summary statistics for the first two axes of CCA on the phytoplankton functional groups and abiotic variables in the rainy season.

	Axis 1	Axis 2
Eigenvalues	0.10	0.08
Proportion explained variance (%)	40.47	29.54
Test of significance of first canonical axis (Chi-square)	F = 3.38 p = 0.013	F = 2.47 p = 0.028

Phytoplankton functional groups **Na** and **J** were more associated to alkalinity and total phosphorus, whereas, **MP** was more related to total phosphorus and water temperature. Group **S1**, was more related to conductivity (EC) and turbidity when the accumulated precipitation was high. Groups **Lo**, **M**, **P**, and **H1** were related to water temperature, ion ammonium ( $\text{NH}_4^+$ ) and water transparency.

In the dry season, CCA analysis (Figure 2.7, right side) shows that the first two axes of the abiotic variables explained 76% of the variance in phytoplankton functional groups. The test of significance showed significant results for both axes (table 3). Abiotic variables responsible for predicting the spatial and temporal distribution of phytoplankton functional groups in the dry season were from water transparency (0.85), total phosphorus (-0.46), water temperature (0.22), alkalinity (0.21), conductivity (-0.47), and ion ammonium (-0.30).

**Table 2.3** Summary statistics for the first two axes of CCA on the phytoplankton functional groups and abiotic variables

	Axis 1	Axis 2
Eigenvalues	0.19	0.12
Proportion explained variance (%)	47.35	28.95
Test of significance of first canonical axis (Chi-square)	F = 4.74 p = 0.002	F = 2.89 p = 0.033

Phytoplankton functional groups **A** was close associated to turbidity and water transparency while group **M** was high associated to total phosphorus. Group **S1**, was more related to conductivity (EC). Groups **Na**, **P**, and **MP** were related ion ammonium ( $\text{NH}_4^+$ ), total phosphorus, and conductivity. More about inter-set correlations in the dry season is available in the appendix 2.4.

## **2.6 Discussion**

The main goal of this study was to investigate phytoplankton response to environmental changes in a Brazilian Amazonian reserve. Thus, we investigated their vertical migration on a temporal scale. The main hypothesis was that the phytoplankton vertical and temporal distribution would correlate with nutrient loads likely caused by human activities in the surrounding areas of this reserve.

The fieldwork of this research included the period of the high water level of the Tucuruí reservoir (June/2014) and low water level (September). Variations in the

water levels increase resuspension and accelerate nutrient cycling, increasing suspended solids and dissolved nutrients concentrations (Straskraba and Tundisi, 2013). Thus, when the water level increases, the water from the flooded areas of the reservoir transport nutrients affecting biogeochemical cycles, and consequently the phytoplankton biomass (Tundisi and Tundisi, 2012).

Additionally, factors such as weather, thermic stability, and geographic distribution are important to explain phytoplankton dynamics in aquatic environments (Tundisi et al., 2007). In the rainy season, the accumulated precipitation and the reservoir water level contributed to the dominance of Cyanophyta division. Cyanobacteria dominance is related to eutrophication conditions, which concerns water management due to their potential impact on health (through its toxins), ecology, and environment (Chien et al., 2013). However, high values of diversity index were also recorded in the rainy season. High values of diversity index indicate an improvement of the physico-chemical quality of the water as defended by Tyokumbur and Okorie (2013).

The phytoplankton functional groups showed to be varying between the rainy and dry season. In the rainy season, precipitation and water level favored the dominance of *Cyanophyta*, which recorded a higher biomass than other divisions. The group **M** was dominant indicating that higher temperatures and the stability of the water level might contribute to increase *Microcystis aeruginosa* biomass in this season. *Cyanophyta* division has been reported as the dominant division in several Brazilian ecosystems (Gomes et al., 2009) and it is due to their wide variety of morphological and metabolic adaptations to a diverse ecosystem (Sant'Anna and Azevedo, 2000).

In the dry season, the temporal and vertical distribution of the phytoplankton biomass was dominated by group **P** with high contribution of *Staurastrum* sp., and *Staurodesmus* sp., in all depths and times and peaks of *Rizhbosolenia* sp., at 1 pm. Additionally, due to the low accumulated precipitation levels and high concentrations of ion ammonium, phytoplankton biomass increased and low diversity index was recorded. Ion ammonium is the inorganic nitrogen form, which is easier assimilated than nitrate by phytoplankton (Rückert and Giani, 2004) whereas, low diversity index indicates eutrophic conditions (Tyokumbur and Okorie, 2013).

In aquatic systems, pH variations affect phytoplankton metabolism and nutrient solubility (Esteves, 2011). A water surface showing low pH is characterized by low phytoplankton diversity, not necessary low biomass (Straskraba and Tundisi, 2013).

Hence, some species of the *Desmids* order, increase biomass in  $\text{pH} < 7$  (Coesel, 1982). Therefore, the dominance of group **P** is explained by low pH levels in the dry season.

According to Reynolds et al. (2002), species associated with the group **P** are able to live in more eutrophic waters and tolerate low light availability. Low water levels in the dry season mixed the water column bringing to the upper layer other species such as *Staurastrum sp.*, *Stauroidesmus sp.* and *Rhizosolenia sp.* genus.

Results from Deus et al. (2013) described that the Tucuruí reservoir hydrodynamic affects phytoplankton growth. Thus, when the reservoir is falling, phytoplankton growth is limited by incoming water flow and short residence time. With reservoirs, residence time is an important regulating factor to the biomass levels and species succession (Tundisi and Tundisi, 2012). Therefore, we suggest that the residence time, which may be higher than at other locations in the reservoir, contributed the increasing of phytoplankton biomass. The hypothesis of longer resident time attributed to the Caraipé site is due to this be a dendritic area. Authors such as Espíndola et al. (2000); Straskraba and Tundisi (2013), and Nybakken and Bertness (2005) reinforced this idea by reporting that when the residence time is long, the phytoplankton biomass increases due to nutrient loaded from the drainage basin.

CCA analysis revealed that the main environmental variables responsible for explaining the variation in phytoplankton functional groups in the rainy season were water temperature, conductivity, turbidity, water transparency, and nutrients. High temperature, water column stability, and nutrients availability result in decreasing of *Chlorophyta* and increasing of *Cyanophyta* due to the *Cyanophyta* capability to migrate in the water column by regulating cell density (Chien et al., 2013).

CCA analysis for dry season revealed that the main environmental variables explaining the phytoplankton functional groups variation were water transparency, nutrients, and conductivity. Group **M** showed a preference for total phosphorus and group **A** for water transparency. Group **M** is represented by cyanobacteria colonies, organisms with preferential adaptations for eutrophic to hypereutrophic ecosystems whereas, **A** association is represented by organisms which have affinities for clear water with phosphorus deficiency (Reynolds et al., 2002).

## ***2.7 Conclusions***

We investigated the phytoplankton functional groups response to the effect of the nutrient load at the surrounding areas of a Brazilian Amazonian reserve. To

accomplish this goal we studied phytoplankton in vertical and temporal scales, as well as relating them to environmental variables.

In general, the phytoplankton biomass was driven by seasonal changes in the water level of the reservoir and was most influenced by abiotic variables such as water temperature, pH, water transparency and nutrient loads.

Our results indicate that the water level in this reserve is the main factor causing changes in phytoplankton structure and composition and not human interference as hypothesized. Low water levels favored *Desmids* and *Bacillariophyta*, indicating a mixed water column while high water levels favored *Cyanophyta*. Even though there are not reported harmful algae blooms in the waters of this Brazilian Amazonian reserve, the dominance of *Cyanophyta* raises concern to the water management due to its potential impact on human health and aesthetic degradation of aquatic ecosystems.

Interestingly, our results revealed that in the dry season, with less accumulated precipitation and low water level, turbidity concentration increased, whereas, suspended solids decreased. The increasing on phytoplankton biomass may be contributed to increasing turbidity concentrations, which is high in the euphotic layer decreasing towards the metalimnion and increasing in the hypolimnion. Due to the lack of measurements deeper than 15 m, our results are not able to explain that this tendency appears after 10 m where low levels of turbidity are detected increasing towards the bottom layer.

Regardless of phytoplankton biomass increased from rainy to dry season, Chl-*a* concentration diminished. This may be due to *Bacillariophyta* division presents low Chl-*a* pigment percentage and the method used for Chlorophyll estimation (extraction by acetone) did not include absorbance of spectra for fucoxanthin, the major pigment of this division.

Additionally, this study verified the importance of the sampling strategy (number of sampling depths and repetitions in time during a day) to obtain a total phytoplankton biomass for reservoirs or lakes with medium deep (e.g. > 10m) water columns. Here, seasonal differences were observed, and multiple depth samplings of this reservoir can be highly recommended in the rainy season and the morning times are very indicated due to high diversity indices. The differences in total phytoplankton biomass were explained by variations in its behavior throughout the seasons as a response to seasonal changes in environmental factors such as weather and reservoir hydrodynamics. The main advantage of sampling phytoplankton in vertical and

temporal scales is the ability to identify species response to the environmental changes.

**Appendix 2.1** List of species that contributed with biomass  $\geq 5\%$ , and their respective phytoplankton functional groups.

Observation/Taxa	Biomass (%)					
	10am – rainy season					
	FG	surface	3m	6m	10m	15m
<i>Microcystis aeruginosa</i>	M	18.2	23.9	20.3	28.6	14.7
<i>Microcystis nesebergii</i>	M	5.1		7.3	7.7	7.0
<i>Anabaena circinalis</i>	H1	5.1	6.1			
<i>Anabaena sp.</i>	H1	8.2	19.2	14.2	5.6	11.9
<i>Peridinium</i>	Lo	26.5	13.4	25.7	16.4	4.9
<i>Staurastrum sp.</i>	P	14.7	7.6		6.6	7.3
<i>Anuloseira granulata</i>	P				5.0	6.2
<i>Staurodesmus triangularis</i>	Na				4.7	
<i>Monactinus simplex</i>	J					19.4
1 pm – rainy season						
<i>Microcystis aeruginosa</i>	M	64.3	58.8	45.8	32.3	68.6
<i>Microcystis nesebergii</i>	M	4.9				
<i>Microcystis robusta</i>	M					4.8
<i>Anabaena sp.</i>	H1	5.3				
<i>Peridinium</i>	Lo		6.7			
<i>Staurastrum sp.</i>	P		9.3	9.5	13.5	6.3
<i>Closterium macilentum</i>	P			5.2		
<i>Monactinus simplex</i>	J			8.0	16.6	
<i>Closterium juncidum</i>	P				4.7	
<i>Staurodesmus triangularis</i>	Na				11.7	
3 pm – rainy season						
<i>Microcystis aeruginosa</i>	M	29.80	39.79	35.13	17.95	28.19
<i>Anabaena fertilissima</i>	H1	5.32				
<i>Anabaena sp.</i>	H1		4.80		6.76	4.80
<i>Oscillatoria sp.</i>	MP			5.69		14.74
<i>Peridinium</i>	Lo	8.78	9.50	7.06	5.65	
<i>Closterium setaceum</i>	P	22.11				
<i>Staurastrum sp.</i>	P	15.37	18.18	14.17	21.46	21.57
<i>Eunotia</i>	MP		5.38	7.77		
<i>Staurodesmus triangularis</i>	Na		5.51		7.44	
<i>Monactinus simplex</i>	J			12.35	8.48	
<i>Closterium juncidum</i>	P				8.97	18.04
<i>Pediastrum duplex</i>	J				4.95	
6 pm – rainy season						
<i>Microcystis aeruginosa</i>	M	33.53	10.86	20.30	18.37	37.03
<i>Microcystis botrys</i>	M					11.85
<i>Anabaena fertilissima</i>	H1	9.96	4.92			
<i>Anabaena planktonica</i>	H1	5.0				
<i>Anabaena sp.</i>	H1	13.09	15.91		5.31	5.92
<i>Peridinium</i>	Lo	8.09	8.78	4.54		10.14

*Seasonal variation of phytoplankton indicates small impacts of anthropic activities*

<i>Staurastrum sp.</i>	P	8.06	15.40	20.36	14.23	13.09
<i>Staurodesmus sp.</i>	Na		12.26	6.64	6.48	
<i>Monactinus simplex</i>	J	10.61	13.96	10.59	16.54	
<i>Eunotia</i>	MP			8.56		
<i>Closterium juncidum</i>	P				11.37	9.66
10 am – dry season						
<i>Microcystis aeruginosa</i>	M	4.56	9.68	7.39	10.96	4.75
<i>Oscillatoria limosa</i>	MP		7.40	12.55	6.96	
<i>Anabaena circinalis</i>	H1		5.51			
<i>Aulacoseira granulata</i>	P	6.19	5.95	7.92	5.72	5.25
<i>Rhizosolenia</i>	A	9.10				
<i>Staurastrum sp.</i>	P	45.00	38.05	46.52	42.85	69.72
<i>Staurodesmus sp.</i>	Na	25.78	23.24	15.50	19.00	12.79
1 pm – dry season						
<i>Chroococcus turgidus</i>	Lo	9.76				
<i>Staurastrum sp.</i>	P	42.59	13.17	20.66	17.99	14.66
<i>Staurodesmus sp.</i>	Na	31.79	9.78	12.73	8.80	5.95
<i>Rhizosolenia</i>	A		65.14	53.79	64.38	74.05
<i>Oscillatoria limosa</i>	MP			5.11		
3 pm – dry season						
<i>Microcystis aeruginosa</i>	M	6.70		5.26	4.86	6.17
<i>Oscillatoria limosa</i>	MP	5.20	5.39			
<i>Staurastrum sp.</i>	P	41.78	39.01	45.79	45.97	44.20
<i>Staurodesmus sp.</i>	Na	38.33	43.29	37.67	27.15	32.75
<i>Closterium (archerianum)</i>	P				5.56	
<i>Aulacoseira granulata</i>	P				4.91	5.98
6 pm – dry season						
<i>Oscillatoria limosa</i>	MP	4.91	6.60	7.05		
<i>Staurastrum sp.</i>	P	40.18	41.13	49.88	47.90	74.47
<i>Staurodesmus sp.</i>	Na	43.62	37.28	29.52	34.94	32.72
<i>Aulacoseira granulata</i>	P				7.16	8.03

**Appendix 2.2** Phytoplankton functional groups found at Caraipé site, adapted from Reynolds et al. (2002) and Padisák et al. (2009).

Codon	Habitat template	Representatives	Tolerances	Sensitivities
H1	Eutrophic, both stratified and shallow lakes with low nitrogen content	<i>Anabaena circinalis</i> <i>Anabaena planctonica</i> <i>Anabaena spp.</i>	Low-nitrogen and carbon	Mixing and poor light, low phosphorus
Lo	Deep and shallow, oligotrophic to eutrophic, medium to large lakes	<i>Peridinium spp.</i> , <i>Merismopedia glauca</i> , <i>M. minima</i> , <i>M. punctata</i> , <i>M. tenuissima</i> , <i>Merismopedia spp.</i>	Segregated nutrients	Prolonged or deep mixing
M	Eutrophic to hypertrophic, small to medium sized water bodies	<i>Microcystis</i> species	High insolation	Flushing, low total light
S1	Turbid mixed environments.	<i>Pseudoanabaena limnetica</i> , <i>Pseudoanabaena sp.</i> , <i>Planktolyngbya limnetica</i> , <i>Lynngbya sp.</i>	High light deficient conditions	flushing
J	Shallow, mixed, highly enriched systems	<i>Pediastrum spp.</i> , <i>Scenedesmus spp.</i> , <i>Coelastrum spp.</i>	-----	Settling into low light
P	Eutrophic epilimnia	<i>Aulacoseira granulata</i> , <i>A. granulata var. angustissima</i> , <i>Staurastrum gracile</i> , <i>Staurastrum sp.</i>	Mild light and carbon deficiency	Stratification Silica depletion
A	Clear, deep, base poor lakes, with species sensitive to pH rise.	<i>Urosolenia spp.</i> , <i>Rhizosolenia spp.</i>	Nutrient deficiency	pH rise
Na	Oligo-mesotrophic environments	<i>Cosmarium</i> , <i>Staurodesmus</i> , <i>Staurastrum</i>		destratification

**Appendix 2.3** Inter-set correlations between environmental variables and phytoplankton functional groups, during the rainy season.

<b>Variables</b>	<b>Axis1</b>	<b>Axis 2</b>
Water temperature (°C)	-0.15	-0.36
Secchi disk (m)	-0.56	-0.12
Conductivity	-0.12	-0.25
NH+4	-0.25	-0.25
Total phosphorus	0.33	-0.04
Turbidity	-0.10	0.41
Alkalinity	0.21	0.39
<b>Phytoplankton groups score</b>	<b>Axis1</b>	<b>Axis 2</b>
M	0.15	-0.05
S1	-0.77	2.45
H1	-0.15	0.07
Lo	-0.33	-0.14
P	-0.02	-0.09
Na	0.45	0.26
J	0.67	0.22

**Appendix 2.4** Inter-set correlations between environmental variables and phytoplankton functional groups, during dry season.

<b>Variables</b>	<b>Axis1</b>	<b>Axis 2</b>
Water temperature (°C)	0.22	-0.41
Secchi disk (m)	0.85	-0.10
Conductivity	-0.03	-0.47
NH+4	0.06	-0.30
Total phosphorus	-0.46	0.15
Turbidity	0.05	0.20
Alkalinity	0.21	-0.35
pH	-0.01	0.15
<b>Species score</b>	<b>Axis1</b>	<b>Axis 2</b>
M	-0.67	0.28
H1	-0.63	-0.99
Lo	0.95	-3.28
P	-0.07	-0.01
Na	-0.04	-0.03
A	1.09	0.31

---

**Using Synergy between Water Limnology and  
Satellite Imagery to Identify Algal Blooms Extent** 3  
**in a Brazilian Amazonian Reservoir**

---



## ***Abstract***<sup>2</sup>

Monitoring algal blooms from space is a very challenging task, which becomes particularly difficult when dealing with cyanobacteria blooms. Cyanobacteria are strategic organisms adapted to a wide variety of environmental conditions. In high concentrations, they form scum on the water surface, which is a concern for public health due to the production of toxins, as well as being a nuisance. Knowledge of the ecological role of these organisms is, therefore, essential when trying to estimate their extent from satellite-based data. We present a multidisciplinary approach, based on both the ecological and the optical perspective. This approach is applied in a Brazilian Amazonian reservoir using spatial and temporal scales. The ACOLITE processor is employed to perform atmospheric correction. Extent of the algal bloom is mapped with outputs such as Rayleigh reflectance atmospheric corrected images. Chlorophyll-*a* estimation is accomplished using a blue-green edge algorithm from the Ocean Biology Processing Group (OBPG), and shows reasonable results ( $R^2 = 0.95$ ; RMSE = 0.40). The  $SA_{\text{red-NIR}}$  slope algorithm identifies the extent of the algal bloom at both the spatial and temporal scale. Unfortunately, the performance of these algorithms is most likely affected by weather conditions and glint effects. Therefore, this study recommends that cyanobacteria or phytoplankton studies in this area ensure that their ecological functioning is carefully considered when attempting to map occurrence using limited satellite imagery.

---

<sup>2</sup> This chapter is based on: **Brandão**, I.L.S., Mannaerts, C.M., Verhoef, W., Saraiva, A.C.F., Paiva, R.S., Silva, E.V. *Using Synergy between Water Limnology and Satellite Imagery to Identify Algal Blooms Extent in a Brazilian Amazonian Reservoir* (2017). Sustainability, 9(12), [2194].

### **3.1 Introduction**

Eutrophication in man-made reservoirs has received considerable attention over time due to its harmful effects on the aquatic environment and on human and animal health (Johnson et al., 2001; Tundisi and Tundisi, 2012). The increased probability of algal blooms occurring is of major concern, especially where these blooms are due to (toxic) cyanobacteria species. Under natural conditions in aquatic ecosystems, a balance exists between cyanobacteria and other phytoplankton groups (Mur et al., 1999). However, specific characteristics may allow cyanobacteria to become prevalent. These characteristics are determined by a range of features, including cellular physiology (gas vesicles within cells allow regulation of buoyancy) and physiological response (light and nutrient utilization, for example), cell size, cell structure, and general morphology (Lee, 2008). The predominance of cyanobacteria over other species occurs under specific environmental conditions, including optimal light intensity and water temperature, nutrient availability and stability in the water column (Tundisi and Tundisi, 2012).

Cyanobacteria harmful algal blooms (CHABs) form an increasing problem globally in all types of water bodies due to mounting eutrophication (Chorus, 2012; Figueiredo et al., 2004; Repavich et al., 1990; Sivonen et al., 1989). Moreover, they are responsible for a variety of impacts on environmental, economic and social scales (Waxter, 2014). They greatly impact on zooplankton and fish populations in aquatic ecosystems (Havens, 2008). The presence or absence of particular cyanobacteria species may signal the ecological status of a water body; the dominance of cyanobacteria has been particularly useful as an indicator for a high nutrient status (Chorus and Bartram, 1999). Thus, monitoring of cyanobacteria blooms in drinking water and reservoirs with secondary uses is necessary (Randolph et al., 2008). However, estimating the occurrence of CHABs hot spots in unmeasured locations using traditional sampling methods is very difficult (Backer, 2002; Pitois et al., 2000; Randolph et al., 2008).

Satellite remote sensing techniques offer suitable tools to integrate large-scale water quality monitoring data (Giardino et al., 2001; Koponen et al., 2002) and have been widely used to estimate Chlorophyll-*a* (Kallio et al., 2001; Koponen et al., 2007; Koponen et al., 2002; Strömbeck and Pierson, 2001; Thiemann and Kaufmann, 2002) and phycocyanin (Dekker, 1993a; Hunter et al., 2010; Hunter et al., 2008; Hunter et al., 2009; Qi et al., 2014; Schalles and Yacobi, 2000; Simis et al., 2005; Sun et al., 2015; Vincent et al., 2004). Cyanobacteria blooms have been studied using the bio-optical approach based on retrieval algorithms for phycocyanin, a specific

pigment of cyanobacteria. Very few methods use multispectral data, such as Landsat, to estimate cyanobacteria density from atmospherically corrected surface reflectance values, as proposed by Ogashawara et al. (2017), Woźniak et al. (2016) and Potes et al. (2011). The main challenge is still the low availability of sensors with suitable spectral bands to retrieve cyanobacteria data using field-based approaches (Ogashawara et al., 2014).

The Operational Land Imager (OLI) sensor onboard the Landsat-8 satellite has shown potential regarding application in studies on aquatic environments (Pahlevan et al., 2014). OLI images were used by Torbick and Corbiere (2015) to estimate cyanobacteria density by means of empirical models and Huang (2016a) emphasized the value of OLI images based on the blue to green spectral region for assessing waters with a low to medium amount of biomass of blue-green algae.

The study of CHABs in the Tucuruí hydroelectric reservoir (THR) in Brazil is of great importance, due to the multiple uses of its water by the local population. However, the reservoir has only been mentioned in a few studies (Cunha, 2013; Tavares, 2011) concerning phytoplankton density and never specifically regarding CHABs. Monitoring cyanobacteria density with satellite images has not been undertaken at all. Here we propose a multidisciplinary approach that aims to assess algal bloom extent and which includes ecological and optical studies, in a spatial and temporal context as supported by IOCCG (2012). The first approach was based on the water limnology of the THR, consisting of physico-chemical parameters and phytoplankton studies. The latter was based on the categorization of phytoplankton according to their species' survival strategy regarding different environmental changes. This categorization consists of a list of 31 functional phytoplankton groups, represented by alphanumeric terms, established by Reynolds et al. (2002). The use of this classification has as main objective to detect patterns in the phytoplankton dynamic and distribution, as well as relate them to environmental changes. The second approach was based on the algal bloom extent and Chlorophyll-*a* estimated from OLI data.

The main goal of this study was to investigate if the combination between water limnology and satellite imagery is a suitable approach to identify CHAB extent in the Tucuruí hydroelectric reservoir. This motivation was based on the characteristics of the THR water conditions (with low/medium Chlorophyll-*a*) and using the literature of Ogashawara et al. (2017) and Huang (2016a). The application of satellite remote sensing techniques may help to compensate for the limited spatial dimension of traditional *in situ* methods. It permits acquisition of necessary information at

different spatial and temporal scales, allowing a more complete analysis of aquatic ecosystems, and it is a functional analysis in synoptic order. We also aim to map Chlorophyll-*a* on a spatial and temporal scale, as it is closely related to cyanobacteria occurrence. The outcomes of this study aim to support water management regarding CHABs impact in the Tucuruí hydroelectric reservoir.

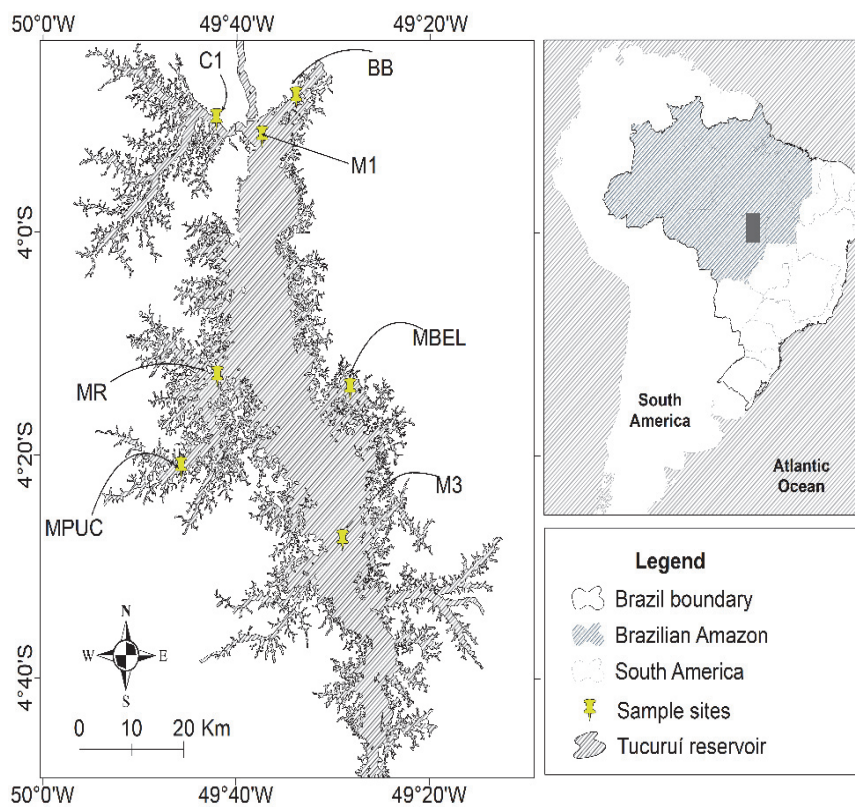


Figure 3.1 Study area with sample sites location

## 3.2 Materials and Methods

### 3.2.1 Study Area

The Tucuruí hydroelectric reservoir (THR) is located in the Tocantins watershed (Amazon region) between 3°39' S 50°6' W and 4°45' S 49°23' W, Pará State, in Brazil. It is one of the largest hydroelectric reservoirs of the Amazon region with a surface area ranging between 2800 and 3000 km<sup>2</sup> during the year and a storage capacity of 45.5 km<sup>3</sup>. The reservoir's length is approximately 170 km and its average width is 14 km. Study sites included 16 sampling points for Chlorophyll-*a*, and 7 sampling sites



Although these secondary uses require lower water quality standards than necessary for drinking water, the Brazilian legislation (CONAMA) has established certain criteria for secondary uses. These include maximum values for Chl-*a* (10 mg m<sup>-3</sup>), cyanobacteria density (20.000 cells mL<sup>-1</sup>) or biovolume (2 mm<sup>3</sup> L<sup>-1</sup>), turbidity (100 NTU), and color (75 mg Pt Co L<sup>-1</sup>).

### 3.2.2 Field Survey Methodology

Two field surveys were conducted at two different water level phases of the THR, which is full from February to May, and emptying from July to August. The first field survey was conducted in April, and the second in July of 2016. The field survey times were chosen in order to show the cyanobacteria spatial and temporal variability between full and dry reservoir phases and to coincide, where possible, with Landsat-8 satellite overpasses during cloud-free periods. As the Amazon region is covered in cloud most months, it was difficult to study periods of high rainfall (Figure 3.2).

#### 3.2.2.1 Phytoplankton Sampling and Analysis

Samples displaying physico-chemical and biological parameters were collected at 7 sites during the four fieldwork campaigns and analyzed using standard methods described in Brandao et al. (2017). The following variables were measured: dissolved oxygen (SM 4500-OC); temperature (digital thermometer, SM 2550); pH (PHTEK device, NBR 9896/1993); suspended solids (SM 2540-D; transparency (Secchi disk); nitrite (SM 4500-NO<sub>2</sub>-B); nitrate (SM 4500-NO<sub>3</sub>-B); ion ammonium (SM 4500NH<sub>3</sub>C); phosphate (SM4500-PC), and Chlorophyll-*a* (extraction by acetone (Golterman et al., 1978)). Phytoplankton was sampled in the morning using plankton netting of 20 µm, fixed in the water at a depth of one meter with the boat moving at low-speed for about three minutes at each sampling site. These samples were collected in 250 mL bottles and used for qualitative analysis. For quantitative analysis, samples were collected from the water surface with 500 mL bottles. Samples were fixed with 4% Lugol's solution at a proportion of 0.5 mL to each 100 mL.

The density of phytoplankton (cell L<sup>-1</sup>) was determined by the sedimentation method and analyzed under an inverted microscope (Zeiss135) using a maximum magnification of 400× as described in (Utermöhl, 1958a) and different chamber sizes ranging from 2 mL to 6 mL. Qualitative analyses were performed using non-permanent slides with 1 mL subsamples. Approximately 10 to 15 counts were conducted per slide until the first 100 individuals of the same species were observed. This analysis was realized using a binocular microscope with 40× and 100× lenses (Leica). The species were identified to the lowest possible taxonomic level, based on

Desikachary (1959). Phytoplankton biomass and biovolume were estimated based on the cell or colony linear dimensions according to Hillebrand et al. (1999) using the same inverted microscope as we used to measure phytoplankton density, and expressed in [mg (fresh weight  $m^{-3}$ )], where  $1\text{ mm}^3 = 1\text{ mg m}^{-3}$ , and in percentage (%) as described in Wetzel and Likens (2000).

Descriptive statistics and correlation tests were performed to evaluate the dataset obtained in this survey. Descriptive statistics were accomplished through determination of the minimum, maximum and average values as well as standard deviation and coefficient of variation. Analysis of variance was performed through a Kruskal-Wallis test to investigate differences between spatial and temporal scales of limnology parameters with  $p < 0.05$  significance. Correlation tests were assessed through the Pearson coefficient with  $p < 0.05$ . Statistical analyses were performed using the program RStudio version 1.0.153 (RStudio, Boston, MA, USA)(R Development Core Team, 2010).

### **3.2.2.2 Water Sampling and Analysis**

The limnological measurements were made available by the Centre of Environmental Protection of Eletrobras-Eletronorte (the company responsible for monitoring the water quality in the THR). Water samples were measured every two months (from 2014 to 2016) at 16 locations and filtered through a Whatman GF/52-C glass fiber filter, 47 mm in diameter and with a  $1.2\text{ }\mu\text{m}$  pore size, to estimate the Chl-*a* concentration in the laboratory. The filter was frozen and kept in the dark until further analysis was undertaken. The Chl-*a* concentration was estimated using the extraction-by-acetone method through spectrophotometric analysis and a time-series is shown in the appendix 3.5.

### **3.2.2.3 Remote Sensing Data Processing**

In this study, we tested five scenes (on path 224, row 63) acquired between June 2013 and September 2016 by the OLI multispectral sensor onboard of Landsat-8. Of the selected scenes, only the data of those presenting clear skies and cloud-free conditions over the Chlorophyll-*a* sample sites were considered. The free availability of data from the United States Geological Survey (USGS) (<http://earthexplorer.usgs.gov/>), as well as the temporal resolution of 16 days of the OLI sensor, provide certain advantages over other sensors. Orthorectified and terrain corrected Level1 OLI imagery was obtained. Imagery of the USGS website is processed by the Level 1 Product generation System (LPGS) and is provided in GeoTIFF format with UTM projection and WGS84 datum. The fieldwork data were

collected approximately three days before and/or after the overpass of the OLI sensor for all scenes. The main characteristics of the OLI sensor are summarized in Table 3.1.

**Table 3.1** L8/ Operational Land Imager (OLI) bands with wavelength and ground sampling distance (GSD).

Band	Wavelength (nm) Range	GSD (m)
1 (Coastal/aerosol)	433–453	30
2 (Blue)	450–515	30
3 (Green)	525–600	30
4 (Red)	630–680	30
5 (NIR)	845–885	30
6 (SWIR 1)	1560–1660	30
7 (SWIR 2)	2100–2300	30
8 (PAN)	500–680	15
9 (CIRRUS)	1360–1390	30

According to Kutser et al. (2005), the atmospheric correction of satellite measurements in aquatic ecosystems is very important for the reason that a large part of radiation detected by the sensor is backscatter from the atmosphere. Thus, to properly identify the pixel content in an image in terms of water quality, the atmospheric correction presents a critical step in data processing of satellite images (Perkins et al., 2012).

The atmospheric correction was performed using the ACOLITE - a binary processor for atmospheric correction developed by the Royal Belgium Institute of Natural Science (RBINS), which uses the Gordon and Wang approach (Gordon and Wang, 1994). The ACOLITE allows for a robust and easy atmospheric correction. This process is fully described in Vanhellemont and Ruddick (2014); Vanhellemont and Ruddick (2015). Basically, the processor performs an atmospheric correction in two steps: (1) a Rayleigh correction for scattering by air molecules, using a Look-Up Table generated using 6SV (Vermote et al., 2006); and (2) an aerosol correction based on the short wavelength infrared (SWIR) band. Output of ACOLITE is the water-leaving radiance reflectance (referred as  $\rho_w$ ), remote sensing reflectance ( $R_{rs}$ ), among others, which can be used to compute multiple other parameters, such as Chl-*a* and turbidity (Vanhellemont and Ruddick, 2016). A summary of the atmospheric correction flow used in this study is shown in the appendix 3.1.

Moreover, this processor allows for the creation of an image subset to separate water (the area of interest) from land and cloud. To apply image processing procedures on the water covered areas, an image masking procedure was thus applied. In the masking process, the SWIR 1 band (1609 nm) was used with a 2.15% threshold.

### **3.2.2.4 Chlorophyll-*a* Algorithm**

The ACOLITE processor allows for a specification of outputs per wavelength. In this study, we specified outputs such as remote sensing reflectance ( $R_{rs}(sr^{-1})$ ), Chlorophyll-*a* using an algorithm developed by the Ocean Biology Processing Group (OBPG) (<http://oceancolor.gsfc.nasa.gov/>), and the atmospheric correction applied here is fully described in Vanhellemont and Ruddick (2014) and a summary is described in the appendix 3.2. The OLI sensor has appropriate bands to retrieve Chl-*a* concentrations using the blue-green ratio (Equation (3.1)) according to Vanhellemont and Ruddick (2016).

$$\text{Chl-}a \text{ (mg m}^{-3}\text{)} = 10^{(a_0 + a_1 \times R + a_2 \times R^2 + a_3 \times R^3 + a_4 \times R^4)}, \quad (3.1)$$

where,  $R$  is the logarithm of the ratio of maximum blue to green reflectance, and  $a_0$  to  $a_4$  are 0.2412,  $-2.0546$ ,  $1.1776$ ,  $-0.5538$  and  $-0.4570$ , respectively. This algorithm has been calibrated for the OLI sensor by Franz et al. (2015) in the three band configuration ( $\sim 440$ ,  $\sim 490$ , and  $\sim 560$  nm).

A group of 21 sample matches-up and five scenes were used to assess the Chlorophyll-*a* concentration. All sampling matches were buffered to create a  $3 \times 3$  pixel window corresponding to the spatial scale (pixel size) of the OLI sensor as described in Torbick and Corbiere (2015). The median value for the  $3 \times 3$  window was extracted from all scenes generated by the Chl-*a* algorithm. After extraction of each sampling point, we proceeded with the statistical analysis to compare the measured in situ Chl-*a* with the values estimated by the Chl-*a* algorithm. Pixel extraction and map layouts were performed using the latest version of SeaDAS (version 7.4, NASA, Washington, DC, USA) available on <https://seadas.gsfc.nasa.gov/> and ArcMap (version 10.5.1, ESRI, Redlands, CA, USA), respectively.

### **3.2.2.5 Algal Blooms Extent**

To assess the extent of algal blooms in the THR, we used a simple slope algorithm approach (referred as  $SA_{red-NIR}$ ) developed by Ogashawara et al. (2017) for inland waters, using OLI and TM sensors of the Landsat imagery and Equation (3.2):

$$SA_{\text{red-NIR}} = \left( \frac{\rho_{\text{c(red)}} - \rho_{\text{c(NIR)}}}{\lambda_{\text{red}} - \lambda_{\text{NIR}}} \right) \times 1000 \quad (3.2)$$

where, red stands for 665 nm, NIR for 865 nm and  $\rho_c$  for Rayleigh corrected reflectance. A summary of the processing steps to obtain  $\rho_c$  is described in appendix 3.3. This algorithm allows the identification of different classes of algal bloom, including severe and moderate bloom, which are summarized in Table 3.2. High probability of severe bloom of cyanobacteria occurs when  $SA_{\text{red-NIR}}$  results are greater than the factor of 0.15 and when Chl-*a* concentration is higher than 50 ( $\mu\text{g L}^{-1}$ ). Moderated bloom is probable to occur when the results of the  $SA_{\text{red-NIR}}$  is in the range of  $-0.05$  to  $0.15$  and Chl-*a* 5 to 10 ( $\mu\text{g L}^{-1}$ ). Additionally, severe bloom is characterized by positive slope between band 4 (665 nm) and 5 (865 nm), and it is more neutral for moderated bloom and negative for non-bloom conditions according to Ogashawara et al. (2017).

**Table 3.2** Main characteristics of algal blooms according to Ogashawara et al. (2017).

Characteristics	Severe Bloom (SB)	Moderate Bloom (MB)
Water surface layer	Characterized by a thick scum of algae	No scums but is visible in the surface layer
Cyanobacteria counts ( $\text{cell L}^{-1}$ )	$\geq 100,000$	10,000–100,000
Toxins	Presence of cyanotoxin	
Biovolume ( $\text{mm}^3 \text{L}^{-1}$ )	$\geq 10$	1–10
Chl- <i>a</i> ( $\mu\text{g L}^{-1}$ )	$\geq 50$	5–10
$SA_{\text{red-NIR}}$	$> 0.15$	$-0.05$ – $0.15$

The advantages of the  $SA_{\text{red-NIR}}$  algorithm are its ability to identify algal blooms in the presence of thin cloud (a frequent issue in inland waters, mainly in the Amazon region) and it uses the OLI sensor products, which are freely available from the United States Geological Survey (USGS, 2017). Moreover, input to the  $SA_{\text{red-NIR}}$  algorithm in this study is level 1 data, first corrected by removing the molecular scattering effects and converted to Rayleigh corrected reflectance as described by Hu (2009); Vanhellefont and Ruddick (2014) and summarized in appendix 3.3.

### 3.2.3 Performance Assessment

Results of the Chlorophyll-*a* algorithm performance was assessed using error metrics such as Mean Square Error (MSE), Mean Absolute Error (MAE), Mean Absolute

Percentage Error (MAPE), Root Square error (RMSE), bias, mean normalized bias (MNB), and determination coefficient (R<sup>2</sup>), which are described in Table 3.3.

**Table 3.3** Summary of error analysis used in this study.

Estimator	Equations
MSE	$\frac{1}{n} \sum_{i=1}^n (x_i^{estimated} - x_i^{measured})^2$
MAPE	$\left\{ \text{mean} \left( \frac{1}{n} \sum_{i=1}^n \left  \frac{x_i^{estimated} - x_i^{measured}}{x_i^{measured}} \right  \right) \right\} \times 100\%$
RMSE	$\text{RMSE} = \sqrt{\text{MSE}}$
bias	$\frac{1}{n} \sum_{i=1}^n (x_i^{estimated} - x_i^{measured})$
MNB	$\frac{100}{n} \sum_{i=1}^n \left  \frac{x_i^{estimated} - x_i^{measured}}{x_i^{measured}} \right $

### 3.3 Results

#### 3.3.1 Ecological, Spatial and Temporal Approaches

The ecological data, both spatial and temporal, are summarized in Table 3.4, which presents the main environmental characteristics of the sampling sites. Each site was characterized based on work by Espíndola et al. (2000) and according to the phytoplankton functional group classification described in Reynolds et al. (2002).

**Table 3.4** Environmental characteristics of the sample sites of the study area.

Sites (Spatial Perspective)	Local Characteristics	Functional Groups (Ecological Perspective)
		April to July
M3	River zone	<b>P</b> → <b>B</b>
MPUC	Transition zone	<b>M</b> → <b>B</b>
MBEL	Transition zone	<b>G</b> → <b>NA</b>
MR	Transition zone	<b>M</b>
M1	Lake	<b>M</b> → <b>F</b>
BB	Lake	<b>P</b> → <b>B</b>
C1	Lake	<b>H1</b> → <b>MP</b>

Our results on Table 3.4 showed that at the sites MPUC, MBEL, and M1 the seasonal progression passes through a sequence leading from eutrophic to mesotrophic waters. M3, however, depicts an oligotrophic to mesotrophic classification at a temporal scale. These sites are characterized by species of the **M** and **P** associations in April and the **B**, **NA**, and **F** associations in July.

Phytoplankton organisms of the **M** and **P** associations are typical of the turbid waters, with mixed layers, and major representatives are cyanobacteria species. Those of the **B**, **NA**, and **F** associations mostly represented by *Chlorophyta* and *Zygnematophyta*, are organisms thriving in clear, deeply mixed oligo to mesotrophic and meso to eutrophic waters. The sites that are situated at the dendritic regions of the reservoir (C1 and BB) (Figure 3.1) are characterized in April by species adapted to eutrophic waters with low nitrogen content, and in July by species adapted to nutrient-rich, warm and mixed water columns.

Figure 3.3a,b present the algae groups contribution to the total biovolume in percentage for April and July of 2016, respectively. Our results show dominance of cyanobacteria in April, while in July there is an increase of green algae and diatoms. In April, the average cyanobacteria dominance is 63.10% ( $\pm 9.18$ ) with maximum contribution of the *Microcystis aeruginosa* specie (27.71%) to total biovolume, while in July, cyanobacteria average is 21.95% ( $\pm 6.73$ ) with maximum contribution of the *Raphidiopsis curvata* specie (30.16%).

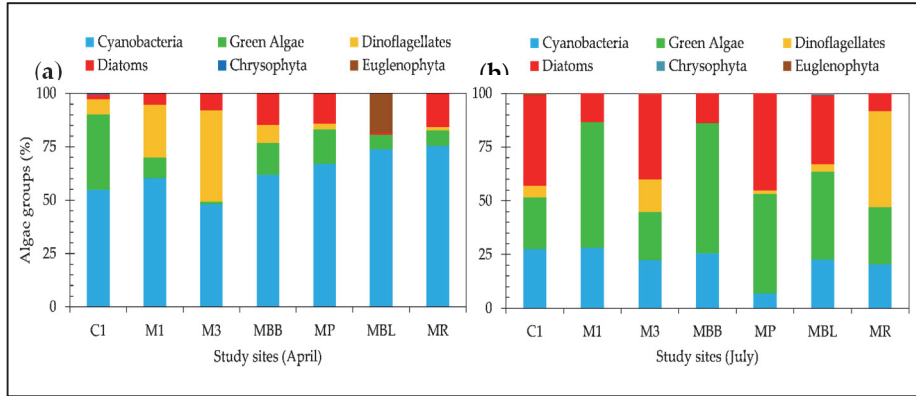


**Figure 3.3** Contribution of algae groups to the total biovolume in relative percentage. (a) Study sites (April); (b) Study sites (July).

The average Chl-*a* concentration was  $5.90 (\pm 2.22) \text{ mg m}^{-3}$  in April, and  $2.85 (\pm 1.07) \text{ mg m}^{-3}$  in July (Table 3.5) with significant variation only in temporal scale ( $p < 0.01$ ). Cyanobacteria density decreased from April to July at all sites with significant variation in temporal scale ( $p < 0.01$ ) and was negatively correlated with Chl-*a* in April ( $-0.81; p < 0.05$ ) and in July ( $-0.83; p < 0.05$ ). The decreasing in cyanobacteria density and reduction of the water pH, may have favored conditions to other phytoplankton species to prevail in July. The water pH showed significant variation in temporal scale ( $p < 0.01$ ). In April, Chl-*a* was correlated with dissolved oxygen ( $0.93; p < 0.02$ ), transparency ( $0.98; p < 0.01$ ), and nutrients, such as nitrate ( $0.98; p < 0.01$ ), ion ammonium ( $0.99; p < 0.01$ ) and phosphate ( $0.99; p < 0.01$ ). In July, Chl-*a* was correlated with phosphate ( $0.87; p < 0.05$ ), ion ammonium ( $0.99; p < 0.01$ ), and nitrate ( $0.99; p < 0.01$ ).

**Table 3.5** Descriptive statistics of the water quality parameters measured in (a) April and (b) July, 2016. Statistical metrics include: minimum value (Min), maximum value (Max), average, standard deviation (SD) and coefficient of variation (CV) in percentages (%)

<b>a. Dataset Measured on April 2016 at 7 Sites</b>					
<b>Parameter</b>	<b>Min</b>	<b>Max</b>	<b>Average</b>	<b>SD</b>	<b>CV (%)</b>
DO (mg L <sup>-1</sup> )	4.24	6.22	5.53	0.52	9.35
Temperature (°C)	29.28	30.91	29.73	0.52	1.75
pH	7.55	8.67	7.87	0.30	3.77
Suspended solids (mg L <sup>-1</sup> )	0.20	3.00	1.43	1.00	69.80
Transparency (m)	1.10	3.10	1.86	0.67	36.30
EC (µs/s)	36.30	40.60	37.65	1.41	3.74
Nitrate (mg L <sup>-1</sup> )	0.00	0.05	0.02	0.02	82.02
Ion ammonium (mg L <sup>-1</sup> )	0.02	0.29	0.11	0.12	107.25
Phosphate (µg L <sup>-1</sup> )	0.00	0.01	0.01	0.00	58.37
Silicate (mg L <sup>-1</sup> )	1.90	5.01	4.04	1.08	26.79
Chl- <i>a</i> (mg m <sup>-3</sup> )	2.34	58.54	13.44	14.78	110.00
<b>b. Dataset Measured on July 2016 at 7 Sites</b>					
<b>Parameter</b>	<b>Min</b>	<b>Max</b>	<b>Average</b>	<b>SD</b>	<b>CV (%)</b>
DO (mg L <sup>-1</sup> )	4.62	7.14	5.57	0.82	14.78
Temperature (°C)	29.54	31.60	30.55	0.68	2.22
pH	6.97	7.20	7.07	0.07	1.04
Suspended solids (mg L <sup>-1</sup> )	0.20	1.10	0.59	0.32	53.74
Transparency (m)	1.60	4.50	2.50	0.85	33.81
EC (µs/s)	13.00	41.30	26.26	10.12	38.54
Nitrate (mg L <sup>-1</sup> )	0.01	0.44	0.16	0.15	90.49
Ion ammonium (mg L <sup>-1</sup> )	0.02	0.47	0.16	0.13	77.26
Phosphate (mg L <sup>-1</sup> )	0.00	0.06	0.01	0.02	132.64
Silicate (mg L <sup>-1</sup> )	7.04	8.16	7.77	0.38	4.92
Chl- <i>a</i> (mg m <sup>-3</sup> )	0.89	8.50	2.59	2.47	95.64

Table 3.5 contains descriptive statistics of the water quality parameter results. Higher values of dissolved oxygen were measured in April with an average of 5.55 ( $\pm 0.69$ ) mg L<sup>-1</sup>. Nutrients such as nitrite, nitrate, and phosphate were more abundant in July than in April with averages of 0.49 ( $\pm 0.24$ ) µg L<sup>-1</sup>, 0.22 ( $\pm 0.09$ ) mg L<sup>-1</sup>, and 11.08 ( $\pm 2.96$ ) µg L<sup>-1</sup>, respectively. The mineral silicate presented maximum concentrations in July with an average of 7.58 ( $\pm 0.30$ ) mg L<sup>-1</sup> and significant variation in temporal scale ( $p < 0.01$ ). Water transparency, which is the combination of effects of color, turbidity and algae, increased from April to July, however this parameter did not

present significant spatial and temporal variation. The average color in the time series analysis (Appendix 3.8) was 29.82 ( $\pm 27.76$ ) Pt-Co and this parameter varied significantly in spatial and temporal scales ( $p < 0.05$ ).

### 3.3.2 Optical, Spatial and Temporal Approaches

Figure 3.4 shows the spectral Rayleigh corrected reflectance values at sampling sites with less weather interference (i.e., a cloudless sky and the absence of haze) acquired from the OLI sensor in (Figure 3.4a) April and (Figure 3.4b) July, 2016. This Figure indicates that the spectral reflectance characteristics, which are associated with the algal bloom intensity, of the sample sites are similar in April, differing only in magnitude. The slope between band 4 (665 nm) and 5 (865 nm) is positive for severe bloom conditions due to the high absorption of Chl-*a* in the red region of the spectrum and high scattering of algal cells in the NIR region. The MR and M1 sites showed higher cyanobacteria relative percentage than the M3 site (see Figure 3.3a). On the other hand, in July the slope at the NIR region is less evident than in April, indicating high absorption of water, low scattering in the NIR region, corroborating with low Chl-*a* concentrations in these sites.

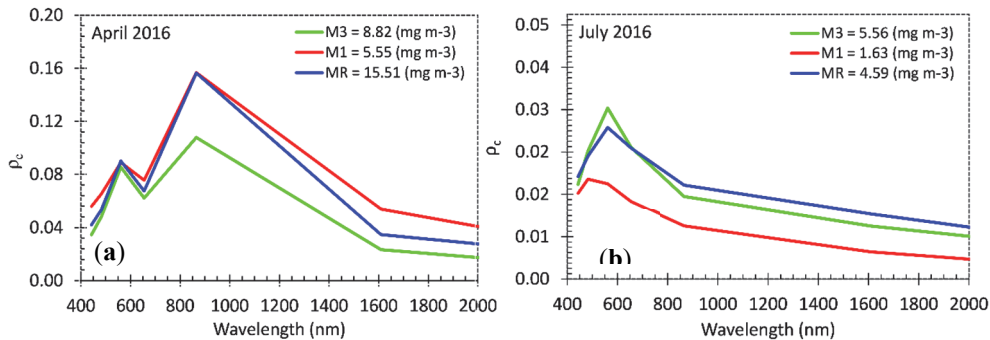
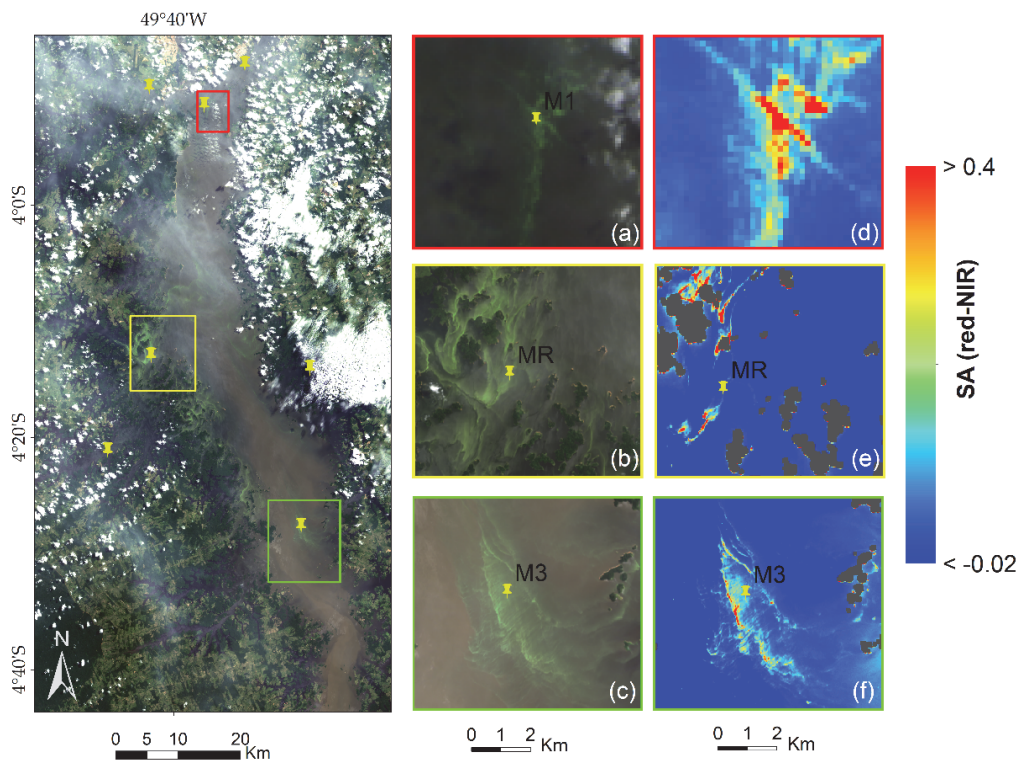


Figure 3.4 Rayleigh corrected reflectance ( $\rho_e$ ) collected in (a) April and (b) July, 2016.

In addition, Figure 3.4 shows that sites can be distinguished according to the difference in Chl-*a* concentration in the visible spectral region. The MR and M1 sites will very likely see an increase in Chl-*a* concentration in April (Appendix 3.5), contributing to the increase in magnitude of their spectral features. Features associated with phycocyanin absorption (near 630 nm) and reflectance by Chl-*a* (near 720) do not occur. However, the high reflectance in the green region and low absorption in the blue region are associated with Chl-*a* presence (Kirk, 1994).

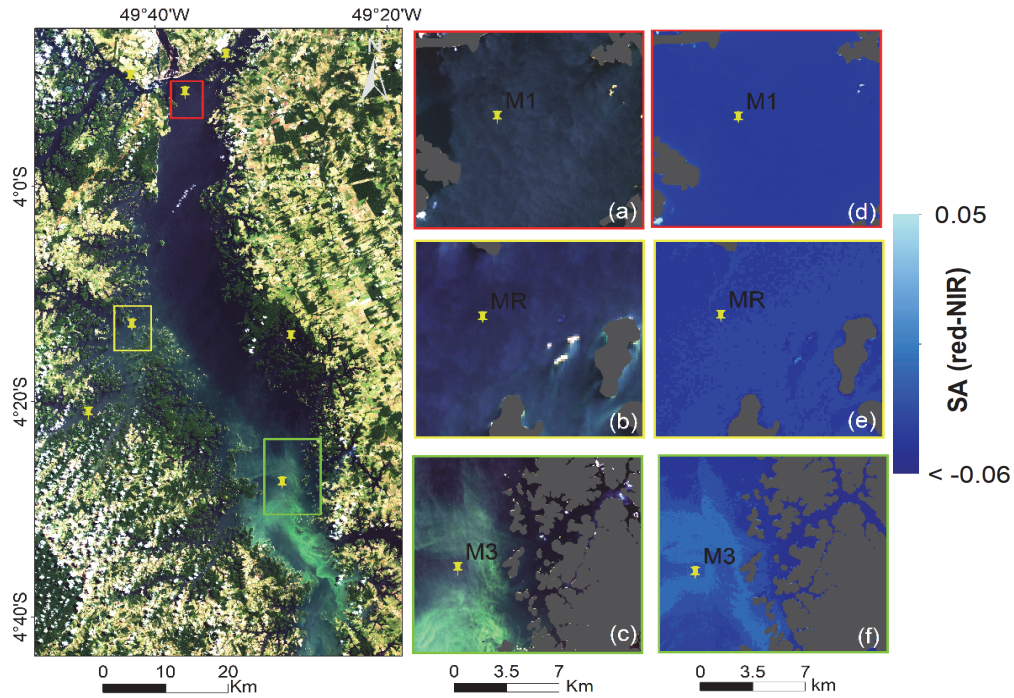
Figure 3.5 shows the results of the SA<sub>red-NIR</sub> algorithm applied to the Rayleigh corrected reflectances in April 2016 in the false color composition (R = 665 nm, G = 561 nm, B = 483 nm). Three sites indicated the presence of algal bloom

corroborating with our results in Figure 3.3a,b. These three sites are very likely to display severe algal blooms in April, decreasing to moderate or no bloom in July. In addition, our Chl-*a* results show higher concentrations in April than in July. This would classify this reservoir to eutrophic conditions while in the emptying phase, it is categorized as oligotrophic to mesotrophic due to its low Chlorophyll-*a* concentration.



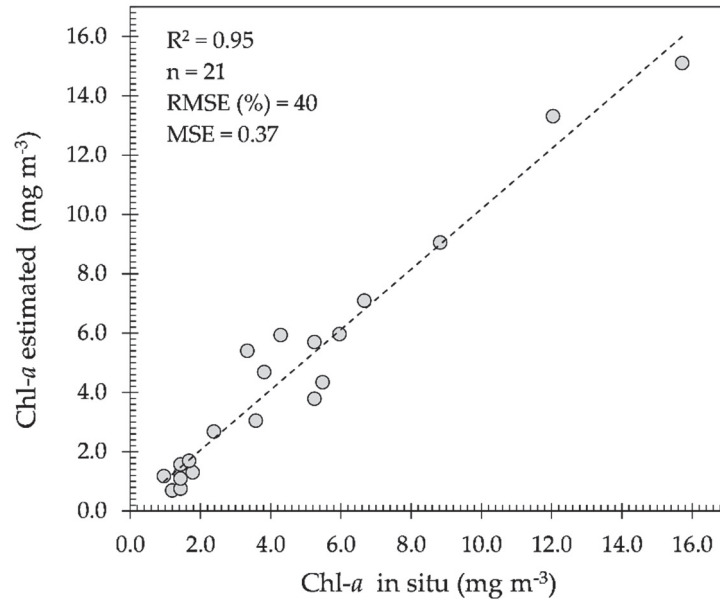
**Figure 3.5** Locations where the Sared-NIR algorithm was applied: (a) M1 site; (b) MR; (c) M3 site with algal bloom indication. The scene is LC82240632016112LGN01 (April 2016) in natural color (R = 665 nm, G = 561 nm, B = 483 nm); (d–f) are Sared-NIR classifications.

Figure 3.6 shows the results of the  $SA_{red-NIR}$  algorithm applied to the Rayleigh corrected reflectances of July, 2016. In this month, the THR is very likely to exhibit low Chl-*a* concentrations and oligo to mesotrophic waters. However, M3 site showed an indication of a moderate bloom and  $SA_{red-NIR}$  varying from  $-0.06$  to  $0.05$ .



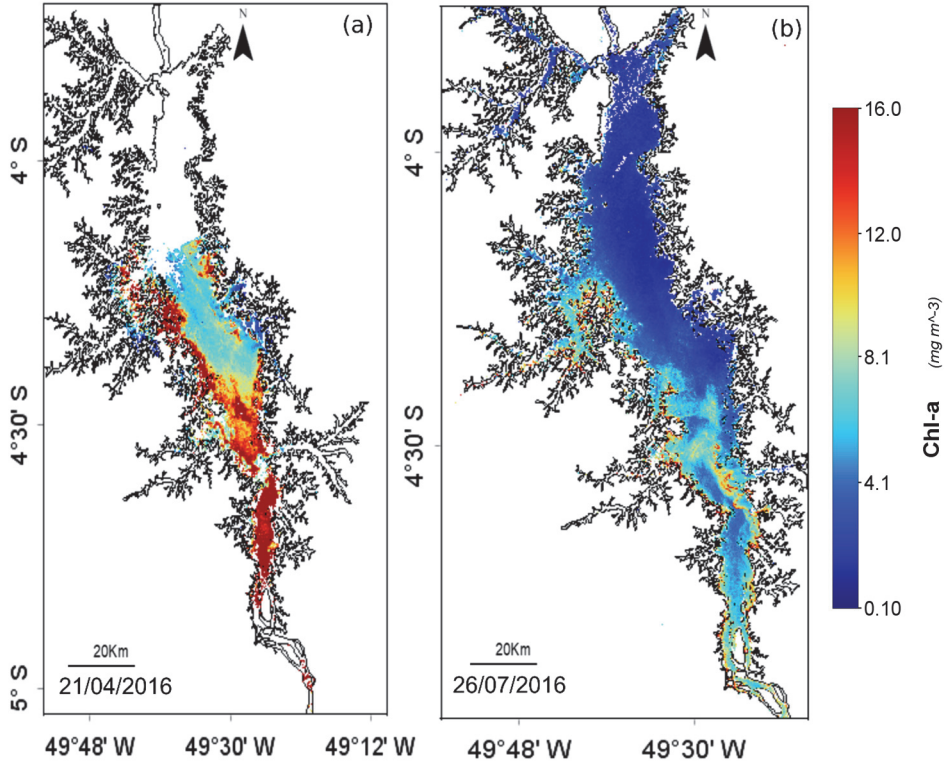
**Figure 3.6** Location where the Sared-NIR algorithm was applied: (c) M3 site with algal bloom indication and other sites (a, b, d and e) without bloom indication. The scene is LC82240632016208LGN01 (July 2016) in natural color (R = 665 nm, G = 561 nm, B = 483 nm); (f) Sared-NIR classification

Figure 3.7 shows a plot of measured and estimated values of Chl-*a*. Chlorophyll-*a* is estimated using the OBPG algorithm and it is an output of the ACOLITE processor.



**Figure 3.7** Chl-*a* estimated with the Ocean Biology Processing Group (OBPG) algorithm.

Figure 3.8 shows the map of Chl-*a* concentrations estimated by the OBPG algorithm using the coastal aerosol (443 nm), blue (483 nm) and green (561 nm) bands and the dataset of Chl-*a* time series. Many pixels with cloud cover and aerosol effects were not retrieved through remote sensing reflectance, resulting in such areas emerging without pixel value (i.e., white in color). For the depicted results from 2016 (spatial and temporal variation), we only used sites unaffected by weather conditions to assess the goodness of the fit between measured and estimated values (Figure 3.7).



**Figure 3.8** Maps of Chl-a concentrations ( $\text{mg m}^{-3}$ ) estimated using the OLI sensor and the OBPG algorithm for (a) April 21, and (b) July 26 of 2016, respectively.

Performance assessment revealed good agreement between measured and estimated Chl-a as described in Table 3.6.

**Table 3.6** Error analysis results.

Parameter	RMSE (%)	MAPE (%)	Bias	MNB (%)
Chl-a ( $\text{mg m}^{-3}$ )	40	31.97	0.37	13.46

### 3.4 Discussion

Water quality monitoring in reservoirs is an important approach to understanding the complexity of this environment. These environments are classified as ecosystems with permanent disturbance on a vertical and horizontal scale (Tundisi et al., 2007) and their water quality is greatly influenced by human interference.

In the case of the THR, little human interference affects its water quality, due to minimal occupation near its edges and insignificant changes in land use and cover, as is described by (Curtarelli et al., 2016). When the THR is full, the main source of nutrient loading is rainfall, while in the emptying phase it is the water level, which releases nutrients from the bottom (Pettersson and Pozdnyakov, 2012). The THR is characterized by areas with different limnological patterns as a result of its morphometry, and areas which were not deforested prior to the flooding (Espíndola et al., 2000; Tundisi et al., 2014).

This study proposes a multidisciplinary approach to assess the feasibility for the OLI sensor to monitor algal blooms in the THR. To this effect, an ecological and optical approach in both spatial and temporal scale is applied. An understanding of the ecological characteristics of reservoirs, including bio-physical and chemical features, is important for their water management. Biological studies are important to assess uses of water in reservoirs due to their close relation to the effects of algal blooms. Enhanced phytoplankton growth is a major concern for policy and management particularly when the reservoir is used for recreation, aquaculture or potable supplies (Chapman, 2016).

Our results show that Chl-*a* concentrations were higher in April (full reservoir and at the river zone) at  $15.51 \text{ mg m}^{-3}$  than in July at  $4.10 \text{ mg m}^{-3}$ . Significant variation ( $p < 0.05$ ) of Chl-*a* concentration was found between months but not in spatial scale. In the full phase of the reservoir, Chl-*a* tends to increase at certain sites near dendritic and edge areas. In April, Chl-*a* concentrations in the water were in the range of eutrophic, while in July the range reached oligotrophic to mesotrophic values. Lobato et al. (2015) showed similar results in the emptying phase of the reservoir (June to August), classifying this reservoir as mesotrophic with few oligotrophic sites. Low trophic levels in this reservoir could be related to its stabilization process, which is a positive factor for the maintenance of the phytoplankton diversity and biomass (Tundisi and Tundisi, 2012).

The OBPG algorithm applied to this study area showed to be able to represent the spatial dynamic of the THR in favorable weather conditions for Chl-*a*. The  $SA_{\text{red-NIR}}$  algorithm could identify the algal bloom extent even in thin cloud conditions (Figure 3.5d). The algorithm attached higher values of  $SA_{\text{red-NIR}}$  to areas with higher nutrients in calm weather conditions, as preferred by cyanobacteria (Chorus and Bartram, 1999).

We observed a negative correlation between Chl-*a* and cyanobacteria density; a result that was also observed by Tavares (2011) in earlier years. In developing a trophic state index for tropical/subtropical reservoirs, Cunha et al. (2013b) noted poor correlation between Chl-*a* concentration and phytoplankton abundance. The main reason for such a poor correlation between Chl-*a* and phytoplankton abundance is a shift occurring between phytoplankton groups, which contributes to the total Chlorophyll-*a* content. This shift was reported by Li et al. (2009) studying algae in the Arctic, where authors reported an increase in small phytoplankton cells over larger cells, while Chl-*a* concentrations did not change.

We also observed an increase in phytoplankton abundance in the lake zone (sites M1, C1 and BB), although the Chl-*a* concentration did not show significant variation between sites. Kasprzak et al. (2008) reported shifts within the phytoplankton community related to the nutrient load during eutrophication periods. They reported a replacement of small flagellates by green algae. This may be caused by different requirements among phytoplankton species for nutrients. Due to this shifting in the phytoplankton group, caution is necessary when using Chl-*a* as an estimator of phytoplankton biomass (Felip and Catalan, 2000). Dinoflagellates and some cyanobacteria species can actually have relatively low Chlorophyll-*a* content per cell biovolume (Cunha et al., 2013a; Vargas, 2012). Certain cyanobacteria species, such as *Dolichospermum circinalis* and *Microcystis aeruginosa*, present protoplasm that reflects in the green region; and sometimes these species appear to be dark or brown in color with their gas-filled vesicles scattering light in the blue region (Chorus, 2012).

Our results show an increase in density of the *Nostocales* order represented by the *Raphidiopsis curvata* species in the cyanobacteria group from April to July of 2016 (see appendices 3.9 and 3.10). We also observed an increase in nutrients such as phosphate between April and July, accompanied by an increase in silicate. Species of the *Nostocales* order favor turbid waters with a high phosphorus concentration (Chorus and Bartram, 2002). They are able to fix atmospheric nitrogen in low, combined inorganic sources, opening up opportunities for them to grow in low Chl-*a* waters classified as oligotrophic (Sukenik et al., 2012). The increase in turbidity in the THR during its emptying phase is due to the increase in diatoms, which could explain the high silicate values in July (Brandao et al., 2017).

In spite of this study area being located in a cloudy region and investigated in the wet season (Figure 3.8a), the OBPG algorithm made a fair estimation of the Chl-*a* concentrations during the cloud-free period with low glint effect, corroborated with field measurements as shown in Figure 3.7. However, when the glint effect is high

(August to September), the estimation becomes very poor. In appendix 3.4, the OBPG algorithm is seen to be applied in cloud-free and low glint conditions. In this case, it is evident that the THR seasonally alternates between being classified as eutrophic (in April Figure 3.8a—full reservoir) and as meso-oligotrophic (in July Figure 3.8b; appendix 3.4 — emptying reservoir).

In April, M1, MR and M3 were classified as severe bloom areas based on the  $SA_{red-NIR}$  algorithm. The main causes were significant variation on pH levels and changes in weather conditions in temporal scale (Tundisi and Tundisi, 2012). The pH level, in many aquatic systems, plays an important role regulating algal abundance and distribution as showed by Chenl (1994). Moreover, a decrease in cyanobacteria under acidified water conditions has been showed by Eichner et al. (2014) and Yamamoto and Nakahara (2005). We believe that it is very unlikely that the OLI sensor is capable of monitoring algal bloom in July (emptying phase) in this study area on a temporal scale. The main reason being the turbulent environment, which favors diatom biomass increase, consequently increasing turbidity and benefitting species adapted to high turbidity, such as those of the *Nostocales* order. Additionally, filamentous cyanobacteria, as the *Notocales*, may be abundant but rarely form scums in turbulent waters (Reynolds, 2006). Turbidity increase is due to the increase in phytoplankton biomass. Scum is conductive to high reflectance in the red and NIR bands as outlined by Pettersson and Pozdnyakov (2012) and it allows for flagging of the algal bloom extent; however, if no scum is formed, algal bloom will not be detectable using the OLI sensor.

### 3.5 Conclusions

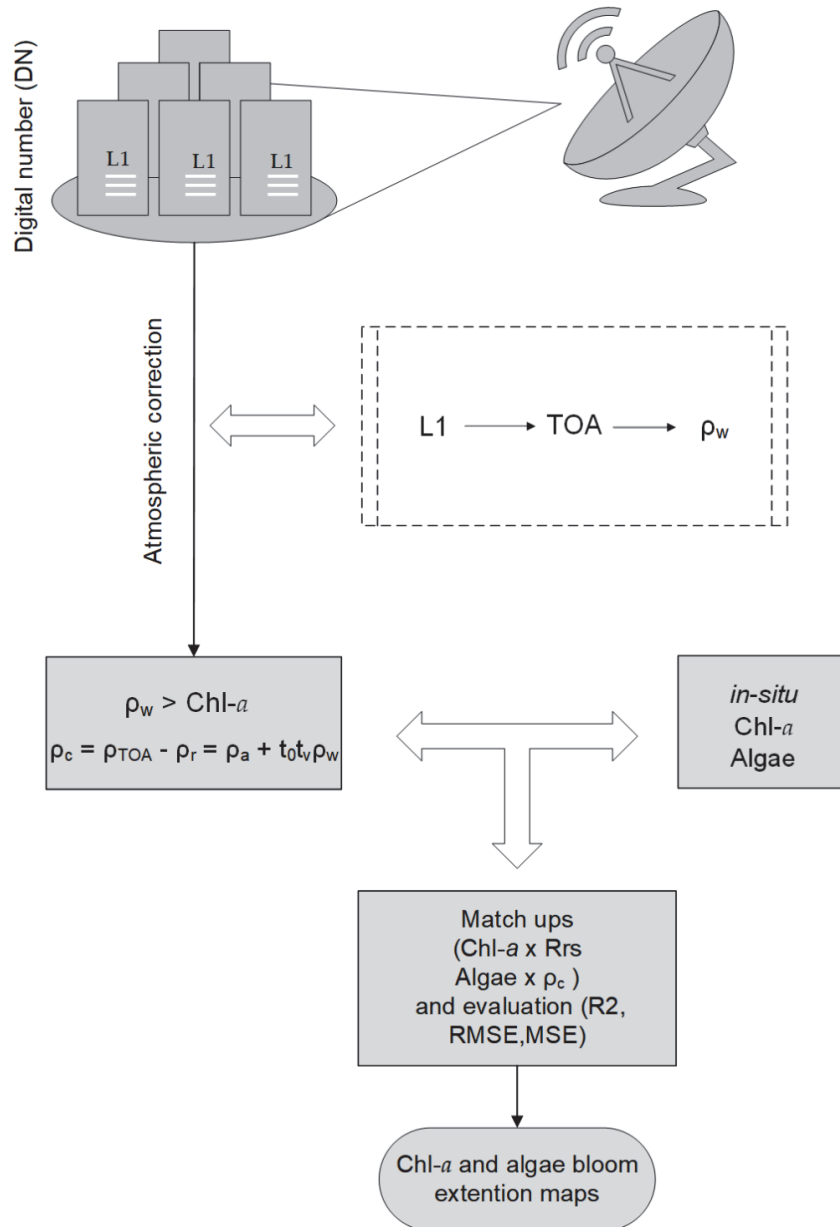
We used ecological and optical approaches in spatial and temporal contexts to map algal bloom extent in the Tucuruí hydroelectric reservoir (THR). Our main objective was to investigate whether the combination between water limnology and satellite imagery is a suitable approach for monitoring spatial distribution and temporal frequency of algal blooms and establish their potential toxicity in the THR. Despite the fact that the ecological and optical approaches showed both drawbacks and advantages, the overall conclusion is that the OBPG algorithm is suitable for estimating the spatial and temporal variability in Chl-*a* concentrations. Thus, this algorithm may be applied to this study area, using L8-OLI imagery in the periods of little cloud cover on a temporal scale and with good understanding of its water limnology.

Interestingly, the OBPG algorithm showed a fair result for this study area, which was not expected due to the use of the blue green ratio. However, the explanation

for such a result might be that the oligotrophic to mesotrophic classification between July and September yielded  $R_{rs}$  towards the blue-green region. Additionally, this study area presents low turbidity and color concentrations from July to September as shown in the supplementary material (Appendices 3.6 and 3.8).

Despite the limitations of the  $SA_{red-NIR}$  algorithm, it showed that it is possible to flag algal bloom occurrence with some a priori knowledge of the study area and availability of limnological and remote sensing data. As the main drawback of this study was using a reduced number of satellite images, we recommend that cyanobacteria or phytoplankton studies in this area ensure that their ecological functioning is carefully considered when attempting to map occurrence using limited satellite imagery. Moreover, the goal of this study was not to quantify algal blooms directly. Instead, this approach meant to search for patterns in space and time based on their ecological preferences for conditions (such as physical, chemical and biological) that would favor algal blooms. Therefore, generated maps based on their probable occurrence would help water management decisions.

In conclusion, further study on the bio-optical properties of Amazonian reservoir waters would be beneficial to local water management in order to understand the water quality issues in these areas.



**Appendix 3.1** OLI processing flow applied to the imagery of this study.

In this appendix 3.1 a flowchart is included which shows the processing steps of the atmospheric correction, from the OLI imagery to the final maps in this study.

L8-OLI imagery at L1 was obtained from Earth Explorer website (USGS, 2017) and used as input to the ACOLITE processor. In ACOLITE, atmospheric correction is performed through the advanced settings section. This section includes aerosol and Rayleigh correction options. For scenes of this study, we used NIR atmospheric correction because our samples showed turbidities lower than 30 NTU. The default is to use the SWIR band when water is moderately to extremely turbid (>30 NTU).

### **Appendix 3.2 Chl-*a* Algorithm Processing Steps**

To achieve the Chl-*a* algorithm results, level 1 images were first converted from Digital Numbers (DN) to Top Of Atmosphere radiances (TOA):

$$L_{TOA} = M_L \times DN + A_L \quad (\text{Eq 3.2.1})$$

where,  $M_L$  (multiplicative factor, gain) and  $A_L$  (additive factor, offset) are values provided in the metadata file. TOA reflectances ( $Q_{TOA}$ ) were computed according to the Equation (2):

$$\rho_{TOA} = \frac{\pi \times L_{TOA} \times d^2}{F_0 \times \cos\theta_0} \quad (\text{Eq 3.2.2})$$

where,  $F_0$  stands for extraterrestrial solar irradiance,  $d$  for sun-earth distance in Astronomical Units, and  $\theta_0$  the sun zenith angle.  $Q_{TOA}$  is assumed to be the sum of aerosol reflectance ( $Q_a$ ), Rayleigh reflectance ( $Q_r$ ) and the water-leaving radiance reflectance just above the surface ( $Q_w^{0+}$ ):

$$Q_{TOA} = Q_a + Q_r + t \times \rho_w^{0+} \quad (\text{Eq 3.2.3})$$

$$Q_w^{0+} = \frac{\pi \times L_w^{0+}}{E_d^{0+}} \quad (\text{Eq 3.2.4})$$

where,  $E_w^{0+}$  is the water-leaving radiance, and  $E_d^{0+}$  the down-welling irradiance, both above the water surface. The superscript from  $Q_w^{0+}$  is dropped and water-leaving radiance reflectance is referred as  $Q_w$  which was divided by  $\pi$  to convert into remote sensing reflectance ( $R_{rs}$ ). More details on atmospheric correction of Landsat 8 imagery using ACOLITE is given in Ruddick et al. (2006); Vanhellemont and Ruddick (2014); Vanhellemont and Ruddick (2015); Vanhellemont and Ruddick (2016).

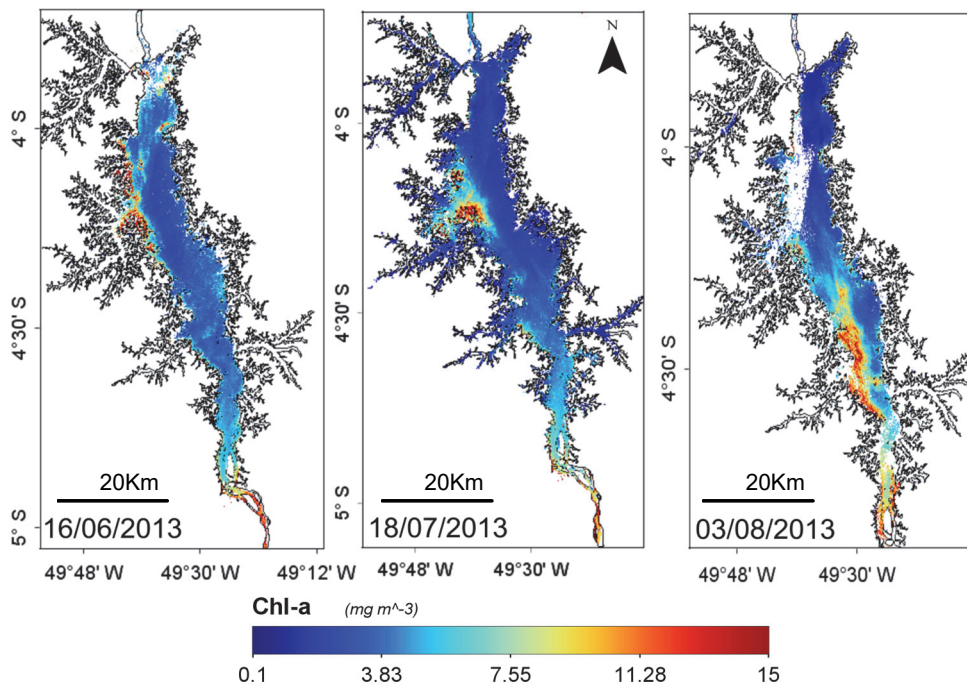
### Appendix 3.3 Rayleigh Corrected Reflectance

Rayleigh corrected reflectance ( $\rho_c$ ) products used as input to the  $SA_{\text{red-NIR}}$  were obtained from Rayleigh reflectance ( $\rho_r$ ), which uses sun and sensor geometry. Input atmospheric conditions were atmospheric pressure (1004 hPa); Rayleigh scale factor (0.99), and site elevation (70 m). Additional options are aerosol epsilon (user defined = 1) and user defined alpha (ration of water reflectance in the red/NIR) bands) equal to 8.7 from (Ruddick et al., 2006).

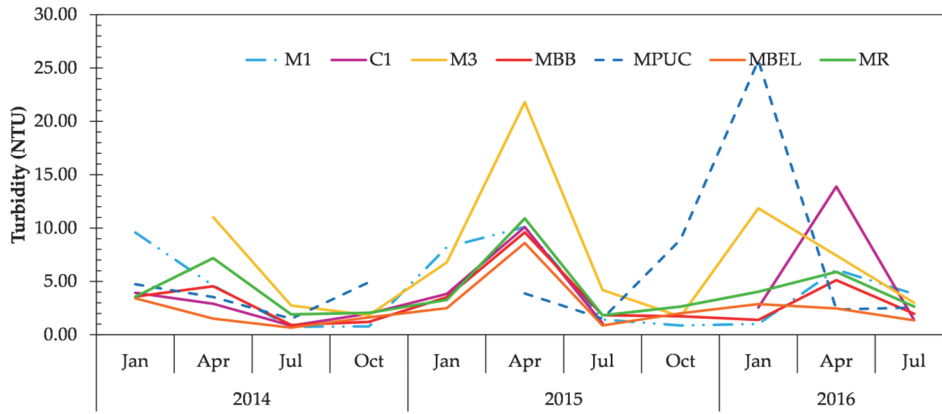
Rayleigh-corrected reflectance ( $\rho_c$ ) is obtained after subtraction of  $\rho_c$  from  $\rho_{\text{TOA}}$  with the following equation:

$$\rho_c = \rho_{\text{TOA}} - \rho_r = \rho_a + t_0 t_v \rho_w \quad (\text{Eq 3.2.5})$$

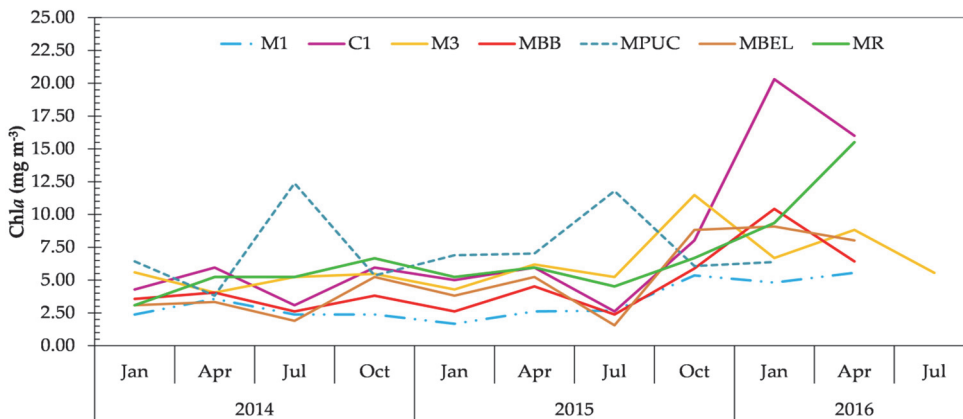
where,  $\rho_r$  and  $\rho_a$  are the reflectances resulting from Rayleigh and aerosol scattering;  $t_0$  and  $t_v$  are the sun and sensor diffusive transmittances;  $\rho_w$  is the water-leaving radiance reflectance.



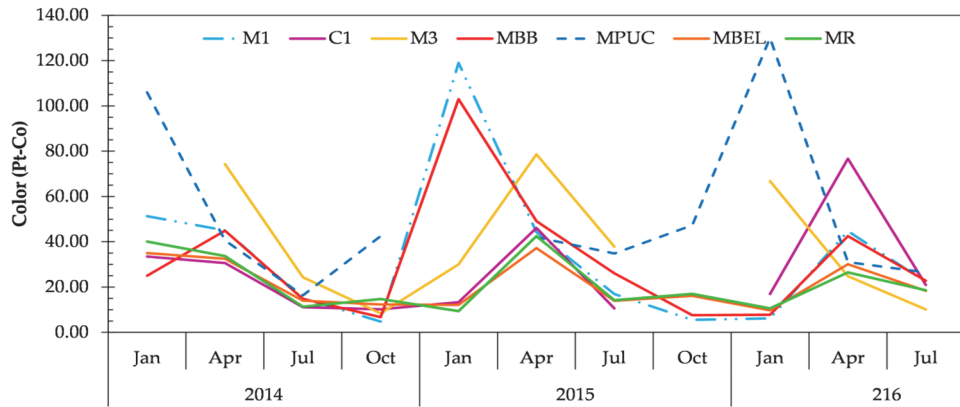
**Appendix 3.4** Maps of Chl-*a* concentration (mg m<sup>-3</sup>) estimated from OLI sensor using the OBPG algorithm for 16 June, 18 July and 03 August of 2013, respectively.



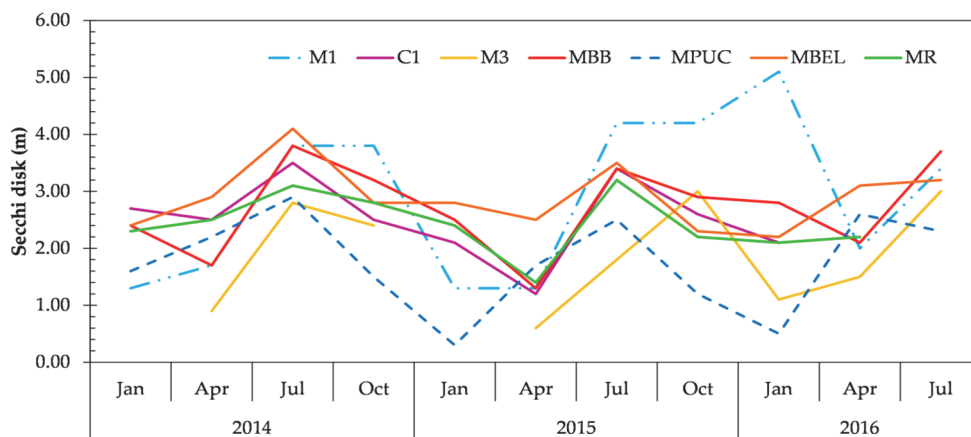
Appendix 3.5 Time series of turbidity in the Tucuruí hydroelectric reservoir from 2014 to



Appendix 3.6 Time series of Chl-*a* in the Tucuruí hydroelectric reservoir from 2014 to 2016.



**Appendix 3.8** Time series of color in the Tucuruí hydroelectric reservoir from 2014 to 2016.



**Appendix 3.7** Time series of Secchi disk in the Tucuruí hydroelectric reservoir from 2014 to 2016.

**Appendix 3.9** Cyanobacteria taxa and biovolume in percentage in April 2016.

<b>Taxa</b>	<b>Biovolume (%)</b>
<i>Anabaena circinalis</i>	1.78
<i>Aphanocapsa koordesi</i>	0.01
<i>Aphanocapsa elachista</i>	2.85
<i>Aphanocapsa bosaltica</i>	0.01
<i>Aphanizomenon gracile</i>	1.33
<i>Aphanocapsa sp.</i>	0.11
<i>Chroococcus dispersus</i>	2.05
<i>Chroococcus turgidus</i>	1.37
<i>Chroococcus minutus</i>	12.02
<i>Gloeocapsa sp.</i>	0.06
<i>Gloeocapsis rupestris</i>	0.02
<i>Jaaginema neglecta</i>	10.03
<i>Limnothrix redekei</i>	0.35
<i>Merismopedia minima</i>	0.03
<i>Merismopedia punctata</i>	0.19
<i>Microcystis aeruginosa</i>	27.71
<i>Microcystis robusta</i>	0.02
<i>Nostoc calcicola</i>	9.07
<i>Nostochopsis sp</i>	14.21
<i>Oscillatoria limosa</i>	1.41
<i>Oscillatoria refringens</i>	1.01
<i>Oscillatoria obtusa</i>	0.26
<i>Oscillatoria princeps</i>	0.11
<i>Oscillatoria sancta</i>	0.48
<i>Oscillatoria jenensis</i>	0.67
<i>Pseudoanabaena limnetica</i>	0.03
<i>Pseudoanabaena galeata</i>	0.05
<i>Plancktothrix agardhii</i>	0.10
<i>Planktolyngbya limnetica</i>	1.17
<i>Planktothrix mougeotii</i>	0.15
<i>Phormidium tergestinum</i>	0.35
<i>Rabdoderma elipsoidea</i>	0.02
<i>Raphidiopsis curvata</i>	9.77
<i>Synechocystis aquatilis</i>	0.14
<i>Synechococcus elongata</i>	1.05
<i>Snowella fennica</i>	0.04
<b>Total</b>	<b>100</b>

**Appendix 3.10** Cyanobacteria taxa and biovolume in percentage in July 2016.

<b>Taxa</b>	<b>Biovolume (%)</b>
<i>Anabaena circinalis</i>	2.11
<i>Anabaena flos-aquae</i>	0.05
<i>Anabaena fertilissima</i>	0.02
<i>Anabaena sp.</i>	0.05
<i>Aphanocapsa koordesi</i>	0.82
<i>Aphanocapsa biformis</i>	0.38
<i>Aphanocapsa delicatissima</i>	0.86
<i>Aphanocapsa elachista</i>	1.98
<i>Aphanocapsa hosaltica</i>	0.01
<i>Aphanocapsa montana</i>	0.00
<i>Aphanizomenon tropicalis</i>	0.02
<i>Aphanizomenon gracile</i>	1.89
<i>Aphanizomenon flos aquae</i>	0.06
<i>Aphanizomenon anabaena</i>	1.09
<i>Anabaena planktonik</i>	0.06
<i>Chroococcus dispersus</i>	1.03
<i>Chroococcus minutus</i>	16.62
<i>Chroococcus sonorensis</i>	0.96
<i>Coelomoron tropicalis</i>	0.07
<i>Cylindrospermopsis raciborskii</i>	1.31
<i>Chlorogloea microcystoides</i>	0.00
<i>Coelosphaerium kuetzingianum sp</i>	0.01
<i>Dactylococcopsis pectinatellophila</i>	0.01
<i>Dactylococcopsis raphidioides</i>	0.02
<i>Gloeocapsa sp.</i>	0.00
<i>Hydrococcus cesatii</i>	0.01
<i>Hydrococcus rivularis</i>	0.01
<i>Jaaginema neglecta</i>	6.58
<i>Limnothrix redekei</i>	0.20
<i>Merismopedia minima</i>	1.49
<i>Merismopedia tenuissima</i>	0.02
<i>Merismopedia punctata</i>	1.62
<i>Microcystis aeruginosa</i>	7.37
<i>Microcystis robusta</i>	0.07
<i>Microcystis protocistis</i>	0.11
<i>Microcystis pseudofilamentosa</i>	0.11

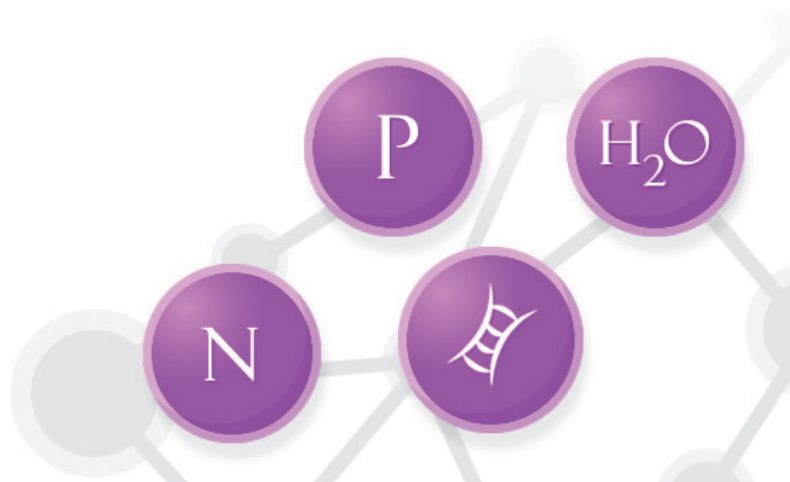
<i>Nostoc calcicola</i>	0.43
<i>Nostochopsis sp.</i>	1.58
<i>Oscillatoria refringens</i>	0.20
<i>Oscillatoria obtusa</i>	0.03
<i>Oscillatoria princeps</i>	0.24
<i>Oscillatoria sancta</i>	0.31
<i>Oscillatoria rubescens</i>	0.05
<i>Oscillatoria sp.</i>	0.05
<i>Oscillatoria jenensis</i>	0.08
<i>Pseudonabaena mucicola</i>	0.93
<i>Pseudoanabaena limnetica</i>	0.09
<i>Pseudoanabaena galeata</i>	0.03
<i>Pseudoanabaena catenata</i>	0.03
<i>Planktothrix agardhii</i>	1.84
<i>Planktolyngbya limnetica</i>	9.55
<i>Planktothrix mougeotii</i>	0.68
<i>Phormidium formosum</i>	0.02
<i>Rabdoderma elipsoidea</i>	2.13
<i>Raphidiopsis curvata</i>	30.16
<i>Synechocystis aquatilis</i>	0.86
<i>Synechococcus elongata</i>	1.96
<i>Snowella fennica</i>	0.01
<i>Snowella litoralis</i>	0.04
<i>Tychonema bourellyi</i>	1.66
<i>Woroninchia naegeliana</i>	0.14
<b>Total</b>	<b>100</b>

---

**Separation of hydrodynamic from bio-geochemical factors affecting eutrophication in a tropical hydropower reservoir using Generalized Linear Models**

---

4



### **Abstract\***

The eutrophication of hydroelectric reservoirs is influenced by both anthropogenic and natural factors. The trophic state of a water body is an important variable when characterizing water quality, due to nutrient inputs originating from anthropogenic sources. Few studies have examined the influence of reservoir hydrodynamics on the water quality of its limnological zones. In this context, the relationships between the hydrological cycle of an Amazon reservoir and the water quality in its limnological zones with respect to factors influencing eutrophication processes were assessed herein. Data were collected on the surface area, from 2005 to 2016, at twelve stations distributed upstream the dam. Chlorophyll-*a* (Chl-*a*), water transparency, dissolved oxygen (DO), total phosphorus, orthophosphate, total suspended solids (TSS) and turbidity were determined, as they undergo alterations during the hydrological cycle and present zonal variations. Generalized linear models were used to identify the response of limnological variables in relation to the influence of the hydrological cycle on the water quality of the longitudinal zones. The results indicate that more adequate eutrophication conditions occur during the reservoir filling stage. The lacustrine zone presented relatively low nutrient levels, with less total phosphorus and primary nutrients, limiting Chl-*a* concentrations, while the riverine zone presented higher total phosphorus, turbidity, TSS, DO and orthophosphate concentrations. Generalized linear models, gamma responses for Chl-*a* concentrations and inverse normal for transparency were able to capture the influence of the hydrological cycle and the longitudinal zone. The gamma model indicated that, during reservoir filling Chl-*a* is lower than when the reservoir is dry and that concentrations in the riverine and transitional zones are significantly higher than in the lacustrine zone, and when the reservoir is filling and full, transparency is lower than when the reservoir is dry. The transparency of the riverine zone is lower than the transparency of the lacustrine zone and total phosphorus displayed an inverse relationship with transparency, as expected. The results indicate that the filling and full cycles display higher eutrophication conditions than the dry and emptying cycles, with mean phosphorus values of 30.42  $\mu\text{gL}^{-1}$  and 30.15  $\mu\text{gL}^{-1}$ . The riverine zone presented higher eutrophication conditions, with mean phosphorus values of 32.32  $\mu\text{gL}^{-1}$ , higher than the limits established in the Brazilian CONAMA 357/2005 resolution for Class 2 lentic environments ( $< 30\mu\text{gL}^{-1}$ ).

---

\*This chapter is based on: Oliveira, T.F., **Brandão**, I.L.S., Hauser-Davis, R.A., Oliveira, A.A.F., Mannaerts, C.M., Saraiva, A.C.F., Oliveira, M.A., Ishihara, J.H. *Separation of hydrodynamic from biogeochemical factors affecting eutrophication in a tropical hydropower reservoir using Generalized Linear Models* (under review in the Science of the Total Environment).

## 4.1 Introduction

Eutrophication is an aquatic ecosystem nutrient enrichment process, which may be caused either by natural processes or induced by human activities. Excess nutrients in reservoirs lead to increased primary productivity and consequent development of aquatic algae and/or macrophytes. This may in turn impair the multiple use of water, including energy production, recreation and water supply, among others, implying in higher treatment costs for distribution and supply systems (Harremoës, 1998; Straškrabra and Tundisi, 2013; Vieira et al., 1998).

Excessive algae growth, known as a "blooms" caused by eutrophication are harmful not only to humans but also to aquatic ecosystems (Hess et al., 2017). Growth cannot always be detected, and these algae can accumulate on the surface, causing damage to aquatic ecosystems due to shading and consequent oxygen depletion (Tundisi and Tundisi, 2012).

Several variables are related to the eutrophication process, including Chlorophyll-*a* (Chl-*a*), water transparency, nutrients, conductivity, fecal coliforms, water residence time and dissolved oxygen (DO) (Haydée, 1997; Lamparelli, 2004; Tundisi et al., 1988; Wetzel, 2001). These variables are, thus, applied in the classification of water bodies according to trophic degree and in the calculation of trophic indices (Gupta, 2014; Vollenweider, 1968).

The creation of temperate zone lake trophic status indicators was much discussed by limnologists in the early 1970s (Carlson, 1977; Walker, 1979). Carlson (1977) used a linear regression analysis to identify the relationships between transparency, Chl-*a* and total phosphorus, creating a trophic state index that established the limits for these variables, since these parameters are simple, quick and cheap to determine.

Following this, several studies have evaluated the trophic behaviour of lakes and reservoirs, both through the Carlson trophic state indicator and its modifications (Alves et al., 2012; Barbosa et al., 2006; Cunha et al., 2013c; Devi Prasad, 2012; Garcia et al., 2012; Lamparelli, 2004; Saraiva et al., 2013). However, these indices cannot be universally applied, as the trophic conditions in each case will depend on the complexity of the ecosystems in which the reservoirs are inserted (Cunha et al., 2013a; Tundisi et al., 2006b)). In this case, other characteristics such as morphometry, hydrology, climatic factors and water nutrients, should be considered in eutrophication evaluation processes (Silvino and Barbosa, 2015).

Concerning reservoirs and the fact that they present multiple uses, it is essential to determine the water quality in these environments, as well as to monitor and evaluate future impacts to better understand the interactions that occur between basin uses, multiple reservoir uses and the preservation or deterioration of the local water quality (Tundisi and Tundisi, 2012).

Recently, Lobato et al. (2015a) and Lobato et al. (2015b) developed methodologies based on modern statistics to classify the trophic state of an Amazon reservoir, adapting the water quality indices proposed by Carlson and Lamparelli (Carlson, 1977; Lamparelli, 2004) and used the results to obtain a fuzzy classification system, considering the local hydrological cycle and the reservoir sampling site locations.

Generalized Linear Models (GLMs) were used for many years to describe random phenomena, even when not presenting a normally distributed variable response, and many types of transformations were usually suggested, in order to achieve data normality (Nelder and Baker, 1972). These models have been applied since then in many ecology and water quality studies (Damanik-Ambarita et al., 2016; Guisan et al., 2006; Nguyen et al., 2015; Thuiller, 2003).

Response variables in GLM follow a distribution belonging to the exponential family of distributions, and their linear structure is described by a set of independent variables. The relationship between the means of all observations and the linear structure is established by a binding function that must be appropriately chosen for this purpose. Nelder and Wedderburn also proposed an iterative process for parameter estimation and introduced the deviance, extensively applied to assess the quality of GLM adjustments, as well as in the development of residues and diagnostic measures (McCullagh and Nelder, 1989; Paula, 2013).

In this context, this study aims to apply GLMs, using regression models with gamma response and inverse normal response for the analysis of positive asymmetric data, to analyse the Tucuruí Hydroelectric Power Plant (HHP) reservoir, in the Brazilian Amazon, in order to identify the hydrological cycle and areas most vulnerable to eutrophication. The main hypothesis herein is that the hydrological cycles with higher eutrophic conditions will be the filling and full stages, where nutrient input is greater due to the higher occurrence of rains, and that the area with the greatest eutrophication vulnerability would be the riverine zone, that suffers the direct impact of organic material entry in the system.

## **4.2 Material and methods**

### **4.2.1 Sampling stations**

The Tucuruí HPP is located in the state of Pará, Brazil, from 5° 07' 54" S to 49° 17' 40" W to 3° 49' 46" to S 49° 39' 10" W. The dam was built in 1984 on the Tocantins River, at 7 km from the city of Tucuruí and 300 km from the city of Belém. The total flooded reservoir area varies throughout the year, ranging from 1500 km<sup>2</sup> to 2500 km<sup>2</sup> (Curtarelli et al., 2016) with a storage capacity of 45 km<sup>3</sup>. The reservoir length is of approximately 133 km and average width is of 13 km (Espíndola et al., 2000).

When HPP are constructed from a river damming, the tendency of the reservoir is to divide into three longitudinal zones: lacustrine, transitional and riverine. These zones are characterized by different depths, which, in turn, reflect horizontal and lateral water quality heterogeneity. Additionally, these zones present differences in water quality physical-chemical and biological variables (Chapman, 1996). The sampling stations of this study were identified as C1, C2, M1, MB, MBL, MR, MP, M3, ML, MJ, MIP and M5, located upstream of the HPP, in the different water quality longitudinal areas, displayed in Figure 4.1.

Plant management operates under four hydrological cycles: full (from March to May); filling (from December to February); dry (from September to November) and emptying (from June to August).

The Tucuruí HPP reservoir is one of the largest in the Amazon region, located in the eastern part of the Brazilian Amazon. The reservoir is surrounded by several environmental protection areas, related at the beginning of dam construction. These include an Environmental Protection Area (EPA), two Sustainable Development Reserves (SDR), which encourage the sustainable use of natural resources, and two Wildlife Conservation zones, presenting integral protection. The surrounding region is occupied by riverine populations, either dispersed or grouped into communities, and different-sized rural properties (Araújo et al., 2016).

The total estimated population in the surrounding area is of approximately 6,500 inhabitants, with higher concentrations at the Alcobaça and Pucuruí-Ararão SDRs. The area encompasses 3 major cities that have presented increased population growth from 1995 to 2017, totalling 105180 inhabitants (0.049% of the total Brazilian population). Despite the increase in population growth very little has been observed regarding changes in land use and land occupation in this area (INPE, 2017a).

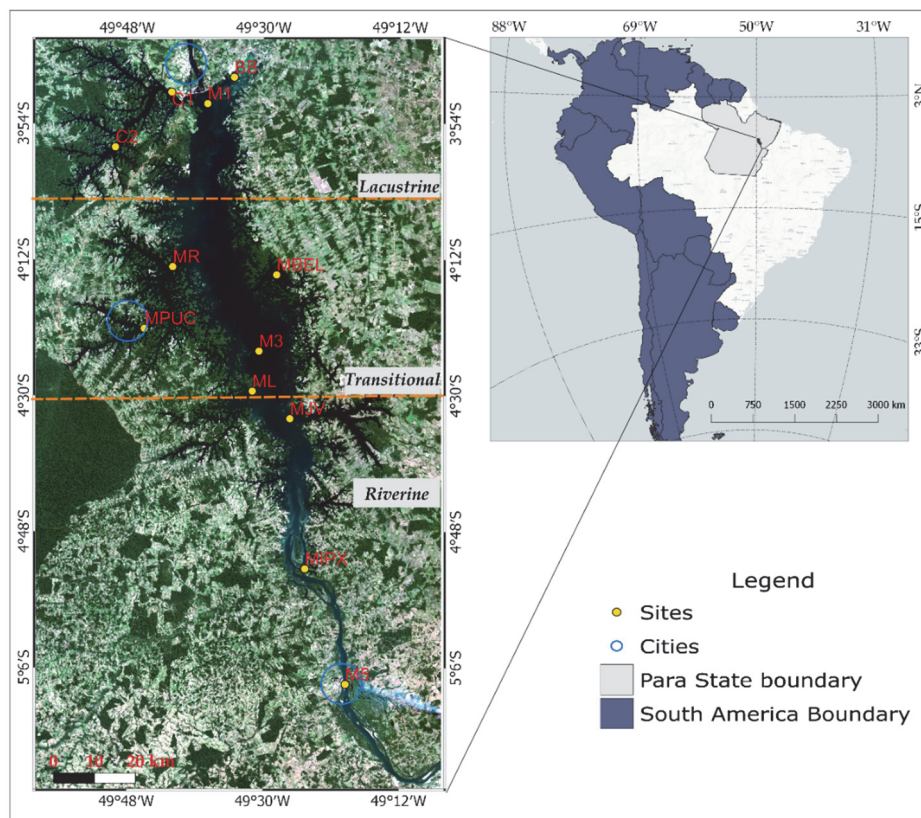


**Figure 4.1** Tucuruí HPP study area and sampling sites located throughout the reservoir, Pará, Brazil.

#### 4.2.1 Analysis and methods

Water parameters were determined from water surface reservoir samples collected from 2005 to 2016. Total phosphorus was determined by the ascorbic acid method, (Apha, 1995)); Chlorophyll-*a* was estimated using the acetone-extraction method (Gotterman et al., 1978); water transparency (m) was determined using a Secchi disk; turbidity was determined by the nephelometric method, SM (2130B); total suspended solids by the SM 2540-D method; DO by the SM 4500-OC method, oxygen by the azide modification method and orthophosphate by the

vanadomolybdo-phosphoric acid colorimetric method (SM 4500-PC) .(APHA, 2005).

### 4.3 Data analysis methodology

#### 4.3.1 Exploratory data analysis

Several statistical techniques were used in this stage to summarize and organize the data. The evaluation of reservoir zone division was carried out using a cluster analysis, applying the Ward aggregation and Euclidean distance method with score standardization. Student's t test was used to evaluate the difference of means per longitudinal zone and hydrological cycle, and a correlation analysis of the variables was performed. A  $\alpha=5\%$  significance level was adopted and all analyses were performed using the R software (R Team, 2016).

#### 4.3.2 Statistical model

The statistical model applied herein was used to identify the key environmental factors influencing the eutrophication process. After the exploratory analysis, the gamma response model was adopted for Chl-*a* as the response variable and the following explanatory variables: Chl-*a*, total phosphorus and DO.

##### *Gamma link function GLM description*

The gamma continuous distribution model is a type of GLM used in the analysis of non-negative data of a continuous nature that presents an increasing variance with the means and, more fundamentally, when the coefficient of variation of the data is approximately constant. The continuous gamma distribution model is applied in the estimation of variances in the analysis of variances and as approximate distribution of physical measures, survival times, equipment life analysis, faulty goods return time faults and reliability tests (Paula, 2013).

$Y_1, \dots, Y_n$  are independent random variables with distribution function (Eq. 4.1) Thus, it is assumed that these variables have different means and even coefficient of variation  $\phi^{-1/2}$ .

$$f(y_i; \mu_i; \phi) = \frac{\left(\frac{\phi}{\mu_i}\right)^\phi}{\Gamma(\phi)} y_i^{\phi-1} \exp\left(-\frac{\phi y_i}{\mu_i}\right) \quad (4.1)$$

where  $y_i > 0$ ,  $\phi > 0$ ,  $\mu_i > 0$  and  $\Gamma(\phi)$  is the gamma function.

In addition, supposing that  $g(\mu_i) = \eta_i$  with  $\eta_i = \mathbf{x}_i^T \boldsymbol{\beta}$ ,  $\mathbf{x}_i = (x_{i1}, \dots, x_{ip})^T$  containing values of explanatory variables and  $\boldsymbol{\beta} = (\beta_1, \dots, \beta_p)^T$  with the vector of parameters of interest estimated by the maximum likelihood method (McCullagh and Nelder, 1989). The most used link functions in the gamma case are identity ( $\mu_i = \eta_i$ ), logarithmic ( $\log \mu_i = \eta_i$ ) and reciprocal ( $\mu_i = \eta_i^{-1}$ ).

### ***Description of the model with an inverse normal***

The inverse normal continuous distribution model is a type of GLM used in the analysis of non-negative data of a continuous nature. Its main applications focus on the study of Brownian particle motion, regression analysis with considerably asymmetric data, reliability tests, sequential analysis, first pass time in random walks, among others.

Considering that  $Y_1, \dots, Y_n$  are independent random variables with distribution function (Eq. 4.2) in the same way that the gamma model assumes that these variables exhibit different means and same dispersion  $\phi^{-1}$ .

$$\mathbf{f}(\mathbf{y}_i; \boldsymbol{\mu}_i; \phi) = \frac{\phi^{1/2}}{\sqrt{2\pi y_i^3}} \exp \left\{ \frac{\phi(y_i - \mu_i)^2}{2\mu_i^2 y_i} \right\} \quad (4.2)$$

In which  $y_i > 0$ ,  $\phi > 0$ ,  $\mu_i > 0$ .

If  $Y_1, \dots, Y_n$  are independent random variables with distribution function. In addition, suppose that  $g(\mu_i) = \eta_i$  with  $\eta_i = \mathbf{x}_i^T \boldsymbol{\beta}$ ,  $\mathbf{x}_i = (x_{i1}, \dots, x_{ip})^T$  containing values of explanatory variables and  $\boldsymbol{\beta} = (\beta_1, \dots, \beta_p)^T$  being the vector of parameters of interest. The most commonly used link functions in the inverse normal case are identity ( $\mu_i = \eta_i$ ), logarithmic ( $\log \mu_i = \eta_i$ ) and reciprocal quadratic ( $\mu_i = \eta_i^{-2}$ ), the latter being the canonical link.

### ***Evaluation of the models through the diagnostic technique***

Deviance,  $D(\mathbf{y}; \hat{\boldsymbol{\mu}})$ , evaluates the discrepancy between the values adjusted by the saturated model and the values adjusted by the model proposed. For the model Gamma and normal inverse deviance  $D^{*G}(\mathbf{y}; \hat{\boldsymbol{\mu}})$  and  $D^{*IN}(\mathbf{y}; \hat{\boldsymbol{\mu}})$  are respectively obtained by (Eq. 4.3) and (Eq. 4.4).

$$D^{*G}(\mathbf{y}; \hat{\boldsymbol{\mu}}) = \phi D^G(\mathbf{y}; \hat{\boldsymbol{\mu}}) = 2\phi \sum_{i=1}^n \left[ \log \left( \frac{\hat{\mu}_i}{y_i} \right) + \frac{(y_i - \hat{\mu}_i)}{\hat{\mu}_i} \right] \quad (4.3)$$

$$D^{*IN}(\mathbf{y}; \hat{\boldsymbol{\mu}}) = \phi D^{IN}(\mathbf{y}; \hat{\boldsymbol{\mu}}) = \phi \sum_{i=1}^n \frac{(y_i - \hat{\mu}_i)^2}{y_i \hat{\mu}_i^2} \quad (4.4)$$

with  $\hat{\mu}_i, \hat{\eta}_i, \hat{\beta}$  the estimated values of  $\mu_i, \eta_i$  and  $\beta$  respectively, and  $y_i > 0$ .

If the postulated model is correct deviances (Eq. 4.3) and (Eq. 4.4) follow a chi-square distribution with  $(n-p)$  degrees of freedom. Thus, high values for deviation may indicate inadequacy of the model or lack of adjustment.

The standard deviation component residue for the Gamma and inverse normal models are obtained by (Eq. 4.5) and (Eq. 4.6)

$$t_{D_i}^G = \frac{\sqrt{2\phi}}{\sqrt{1-\hat{h}_{ii}}} \left\{ \log \left( \frac{\hat{\mu}_i}{y_i} \right) - (y_i - \hat{\mu}_i)/\hat{\mu}_i \right\}^{1/2} \quad (4.5)$$

$$t_{D_i}^{IN} = \frac{\sqrt{2\phi}}{\sqrt{1-\hat{h}_{ii}}} \frac{(y_i - \hat{\mu}_i)}{\hat{\mu}_i \sqrt{y_i}} \quad (4.6)$$

In which  $y_i > 0$  and  $\hat{h}_{ii}$  is the  $i$ -th element of the main diagonal of the matrix  $\mathbf{H} = \mathbf{W}^{1/2} \mathbf{X} (\mathbf{X}^T \mathbf{W} \mathbf{X})^{-1} \mathbf{X}^T \mathbf{W}^{1/2}$  with  $\omega_i = (d\mu_i/d\eta_i)^2 / \mu_i^2$ . Simulation studies indicate that these residues are close to normal for large  $\phi$  (Paula, 2013).

When the  $i$ -th observation and excluding the Cook distance is approximated similarly for the gamma and inverse normal model by (Eq. 4.7):

$$L_{D_i} = \frac{\phi \hat{h}_{ii}}{(1-\hat{h}_{ii})^2} \left( \frac{y_i - \hat{\mu}_i}{\hat{\mu}_i} \right)^2 \quad (4.7)$$

The graphs for  $t_{D_i}^G$ ,  $t_{D_i}^{IN}$  and  $L_{D_i}$  are recommended for diagnostic analyses (Paula, 2013). Due to the difficulty of evaluation if the normal plot of probabilities of the residuals moves away from an adjusted line, the construction of a reliable band type for the deviance components of standardized deviance can be very useful for detecting serious departures from normality. Atkinson (1985) suggests the construction of a type of confidence band by means of 19 simulations, which he called envelope. Thus, the probability that the largest residue of a particular envelope exceeds the upper limit is  $\approx 1/20$ . In this work the program described in Paula (2013) was used to generate the envelopes of the models considering 100 simulations.

Some authors suggest  $\hat{h}_{ii} \geq 2p/n$  as an indicator of leverage points but other diagnostic measures will be necessary to confirm this first diagnosis. Observations

will be considered influential when  $L_{D_i} \geq F_{50\%}(p, n - p)$ , and therefore it is recommended to examine the effects of the removal of these observations in the model fit (Cordeiro and Neto, 2004).

For the verification of the adequacy of the link function, the graph between the variable  $z$  and the linear predictor is constructed, so if the data plotted on the graph is approximately linear, the link function is correct (Paula, 2013).

In order to choose the best model with the same link function, the Akaike method was used, i.e. the parsimonious model was chosen, well-adjusted and with a reduced number of parameters  $p$ , with the lowest Akaike (AIC) given by (Eq. 4.8).

$$AIC = -L(\hat{\beta}) + p \quad (4.8)$$

where  $L(\hat{\beta})$  the logarithm of the likelihood function.

## ***4.4 Results and discussion***

### **4.4.1 Exploratory analyses results**

The water quality parameter analyses were performed using 573 samples collected on the water surface from 2005 to 2016 in the twelve Tucuruí upstream stations of the reservoir. The reservoir division was considered as lacustrine, transitional and riverine, according to Chapman (1996). To separate the zones, the cluster analysis was applied using the Ward aggregation method and the Euclidean distance with score standardization, which obtained 62% correct classification from the parameters used in the model: Chl-*a*, transparency, total phosphorus, STS, turbidity, DO and orthophosphate, but with the samples balanced for modelling in the zones and in the hydrological cycles of the region: Full (March, April and May); Filling (December, January and February); Dry (September, October and November) and Emptying (June, July and August) (Table 4.1).

**Table 4.1** Distribution of water samples by zone and hydrological cycle of the reservoir given by the cluster analysis

Zone	Cycle				Total	%
	Dry	Filling	Full	Emptying		
Lacustrine (C1, C2, M1 and MBB)	48	51	49	50	198	34.55
Transitional (M3, MBL, MP and MR)	39	60	43	50	192	33.51
Riverine (ML, MJ, MI and M5)	54	40	53	36	183	31.94
Total	141	151	145	136	573	100.00
%	24.61	26.35	25.31	23.73	100.00	

The lacustrine zone, presenting the largest and deepest basin with greater depth light availability, presented a mean water temperature of 29.93 °C ( $\pm 0.74$ ), relatively low nutrient levels with less total phosphorus and limited primary nutrients, reflecting lower Chlorophyll-*a* concentrations. The transition zone is broader and shallower than the lacustrine zone, with the highest mean temperature, of 30.28 °C ( $\pm 0.97$ ). Higher water temperatures in the transition zone can be attributed to the longer water retention time in this area, as the surface water temperature in reservoirs, as well as thermal distribution, are a function of the theoretical retention time (Straskraba and Tundisi, 2013). The riverine zone presents a narrow and channelized basin and mean water temperature of 29.97 °C ( $\pm 0.97$ ). In hydroelectric reservoirs, horizontal heterogeneous water temperature gradients are often observed, resulting in differences in this parameter in longitudinal zones (USGS, 2018). The heterogeneity of these gradients is observed not only in water temperature (physical system of the reservoir), but also in chemical and biological characteristics. These temporal and seasonal variations are dependent on water entering the reservoir during the different hydrological cycles (Tundisi and Tundisi, 2012).

#### **4.5 Results of the data used in the models**

The riverine, transitional and lacustrine zones presented mean total phosphorus concentration of 32.32 ( $\pm 17.56$ )  $\mu\text{g L}^{-1}$ , 23.15 ( $\pm 21.67$ )  $\mu\text{g L}^{-1}$  and 17.65 ( $\pm 9.99$ )  $\mu\text{g L}^{-1}$  respectively. These values were significantly different when compared in pairs, with *p*-value < 0.001. The greatest variability was observed for the transitional zone, with a coefficient of variation equal to 93.53%. The high variability of the total phosphorus concentration in the transition zone is due to the presence of sample

sites with different characteristics. As displayed in Figure 4.1, the MP site is located near the urbanized pole, where nutrient entry is higher than at the MBL site, located in a permanent preservation reserve.

The highest mean concentration of total phosphorus was observed during the Filling period followed by the Full period (Table 4.1). When comparing pairs, significant differences were observed for Full and Dry ( $p < 0.0001$ ); full and emptying ( $p < 0.001$ ); Filling and Dry ( $p < 0.001$ ) and Filling and Emptying ( $p = 0.001$ ). Changes in phosphorus concentrations occur according to the hydrological cycles. For example, during the flood seasons, the concentrations of this element are higher during the increase of the water volume of the reservoir than when it is in its decreasing phase (Straskraba and Tundisi, 2013).

**Table 4.2** Summary of the limnological parameter statistics from 2005-2016 during the different hydrological cycles at the Tucuruí reservoir.

Variable	Cycle	Mean	SD	CV	Min	Max
TP( $\mu\text{g L}^{-1}$ )	Dry	18.75	10.01	53.37	3.20	66.11
	Emptying	17.22	8.27	48.03	4.25	57.54
	Filling	30.42	25.96	85.36	3.89	195.59
	Full	30.15	16.67	55.27	5.24	91.31
Chl- <i>a</i> ( $\text{mg m}^{-3}$ )	Dry	6.91	4.72	68.35	0.71	32.34
	Emptying	4.88	2.67	54.66	0.95	15.95
	Filling	8.24	5.59	67.84	0.95	36.89
	Full	5.99	3.46	57.74	0.95	18.71
Transparency (m)	Dry	2.44	0.97	39.78	0.90	5.20
	Emptying	2.98	0.96	32.21	0.80	5.00
	Filling	1.70	0.92	53.77	0.30	5.00
	Full	1.76	0.81	46.18	0.40	3.20
Turbidity (NTU)	Dry	4.72	4.88	103.31	0.42	31.70
	Emptying	3.53	3.70	104.85	0.46	25.45
	Filling	15.19	19.70	129.74	0.11	125.00
	Full	11.59	16.29	140.56	0.73	123.00
TSS ( $\text{mg L}^{-1}$ )	Dry	2.90	3.06	105.49	0.20	27.17
	Emptying	2.00	2.85	142.66	0.10	19.40
	Filling	7.13	10.17	142.64	0.20	58.29
	Full	5.30	7.74	145.99	0.20	47.20
DO ( $\text{mg L}^{-1}$ )	Dry	6.07	0.81	13.30	2.94	8.32
	Emptying	6.12	0.80	13.07	3.80	8.06
	Filling	6.23	0.89	14.33	2.30	8.57
	Full	5.96	0.88	14.84	3.81	8.90
Orthophosphate ( $\mu\text{g L}^{-1}$ )	Dry	7.14	6.20	86.80	0.07	31.74
	Emptying	7.62	6.81	89.31	0.24	32.93
	Filling	9.38	9.62	102.60	0.18	51.01
	Full	12.27	7.79	63.44	0.24	33.56

The box-plots exhibited in Figure 4.2 indicate Chl-*a* and water transparency behaviour by zone and hydrological cycle.

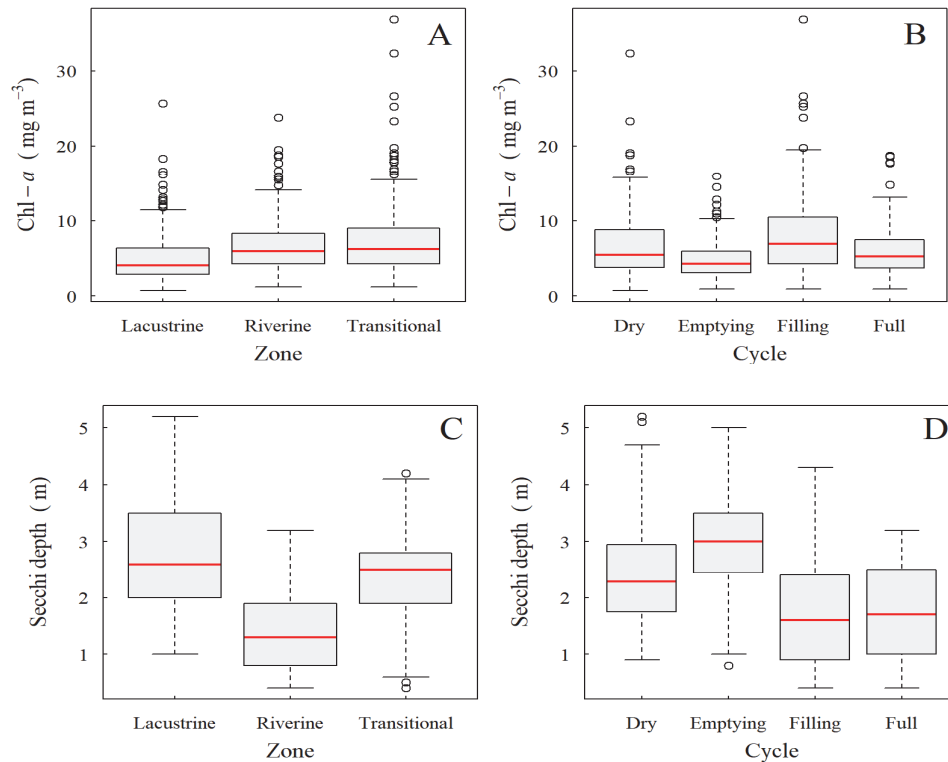


**Figure 4.2** Chl-*a* (mg m<sup>-3</sup>) concentration per zone (A) and cycle B), and Secchi depth per zone (C) and cycle (D).

Concerning Chl-*a*, the riverine, transitional and lacustrine zones presented mean Chl-*a* concentrations of 6.96 ( $\pm$  3.95) mg m<sup>-3</sup>, 7.61 ( $\pm$  5.34) mg m<sup>-3</sup>, and 5.16 ( $\pm$  3.61) mg m<sup>-3</sup> and the highest variability was observed in the transitional zone, with a coefficient of variation equal to 70.05%. The maximum development of Chlorophyll-*a* occurs in the transitional zone, due to phosphorus entry (Straskraba and Tundisi, 2013). The results suggest that nutrient availability, accompanied by favourable temperature, solar radiation and calm waters conditions in this zone are positive factors for algae growth and blooms (Dai et al., 2013). The highest Chl-*a* concentration was observed during the Filling period, followed by the Dry period, at 8.24 mg m<sup>-3</sup> and 6.91 mg m<sup>-3</sup> (Table 4.2). The differences between the Dry and Full periods, at  $p = 0.061$ , were not significant. High concentrations of Chlorophyll-*a* in the filling period of the reservoir are associated with nutrient uptake (organic

matter) with the increase of upstream flows. In the Dry period, high concentrations occur due to nutrient migration, mainly P, from the sediments to the more adjacent layers of water (Chapman, 2016).

Regarding water transparency, riverine, transitional and lacustrine zones presented average transparency, respectively, equal to 1.42 ( $\pm$  0.68) m, 2.34 ( $\pm$  0.83) m, and 2.79 ( $\pm$  1.02) m. The water transparency means from the zone sample sites were considered significant, at  $p = 0.000$ . In reservoirs, water transparency is a combined factor between colour, mineral turbidity and the presence of algae (Straskraba and Tundisi, 2013). Thus, the results suggest that the transparency in the riverine zone is affected by the presence of algae and mineral turbidity while in the transitional and lacustrine zones this effect is more influenced by the presence of algae. The highest mean transparency was observed during the Emptying period followed by the Dry period (Table 4.2). When compared pairwise, only the means of the Full and Filling cycles were not significantly different.

As for turbidity, the riverine, transitional and lacustrine zones presented average turbidity, respectively, of 15.34 ( $\pm$  19.86) NTU, 6.80 ( $\pm$  8.46) NTU and 4.26 ( $\pm$  4.33) NTU. The differences of the means of this parameter from the sample sites in the three zones were considered significant ( $p < 0.0001$ ).

The highest turbidity was observed during the Filling period, followed by the Full period (Table 4.2). When comparing pairwise, the emptying and dry and full to filling cycles did not present significant differences. Many factors influence water turbidity such as water colour, phytoplankton abundance and suspended matter. During high precipitation periods, turbidity increases due to the intense rains, which increase soil erosion at the reservoir margin. The entry of inorganic material composed of suspended solids commonly affects water turbidity, especially in the riverine and transitional zones. In the lacustrine zone, however, phytoplankton generally exerts greater influence on this parameter (USGS, 2018).

As for the total suspended solids, TSS, the riverine, transitional and lacustrine zones presented a mean concentration of 8.52 ( $\pm$  9.67) mgL<sup>-1</sup>, 2.75 ( $\pm$  2.75) mgL<sup>-1</sup> and 1.61 ( $\pm$  1.60) mgL<sup>-1</sup> respectively, similar to turbidity, and differences between the three zones were considered significant ( $p < 0.0001$ ).

The highest mean TSS was observed during the Filling period, followed by the Full period (Table 4.2). When comparing pairwise, the averages of the emptying and dry and full to filling cycles did not present significant differences.

The highest concentration of dissolved oxygen was observed in the riverine zone, at  $6.31 (\pm 0.84)$  mg L<sup>-1</sup>, followed by the lacustrine zone, which presented a mean concentration of  $6.02 (\pm 0.77)$  mg L<sup>-1</sup> and the transitional zone, at  $5.94 (\pm 0.92)$  mg L<sup>-1</sup>. Lower values of dissolved oxygen in the transition zone, accompanied by higher values of Chlorophyll-*a*, indicate its use in the algae respiration process (Esteves, 2011). The differences in means of this parameter were significant ( $p < 0.0001$ ) between the zones and, when compared singly, only the transitional-lacustrine pair was not significant ( $p = 0.721$ ).

The highest mean dissolved oxygen was observed in the filling period followed by the emptying period (Table 4.2). The concentration of dissolved oxygen ( $> 5$  mg L<sup>-1</sup>) in both periods suggests the possibility of using the reservoir to supply potable water (Straskraba and Tundisi, 2013). When comparing pairwise, only the averages in the full and filling periods presented significant differences ( $p = 0.011$ ).

The highest orthophosphate concentration was observed in the riverine zone, at  $11.31 (\pm 8.30)$  mg L<sup>-1</sup>, followed by the transitional zone, at  $8.50 (\pm 8.17)$  mg L<sup>-1</sup> and the lacustrine zone, at  $7.65 \pm 6.79$  mg L<sup>-1</sup>. The means of this parameter were significantly different between the zones ( $p < 0.0001$ ), and when comparing pairwise only the transitional-lacustrine pair did not present significantly different means ( $p = 0.5217$ ).

The highest dissolved orthophosphate concentration was observed during the full period, followed by the filling period. When pairwise comparisons were carried out, the means in the dry and emptying period, and emptying and filling did not present significant differences with  $p$ -values of 0.9652 and 0.3870, respectively.

#### **4.6 Model results**

Histogram asymmetries of the Chlorophyll-*a* and transparency responses were analysed (Figure 4.3) and the correlation analysis of the variables was performed. In the analysis of the general correlation, total phosphorus presented a significant correlation of 55.12% with orthophosphate, 58.41% with TSS and 51.85% with turbidity and very low and non-significant correlation with dissolved oxygen. Thus, total phosphorus and dissolved oxygen were chosen as the explanatory variables in the generalized linear model. In both models, the hydrological cycle and the longitudinal zone were considered factors, taking the lacustrine zone and the dry hydrological cycle as reference factors.

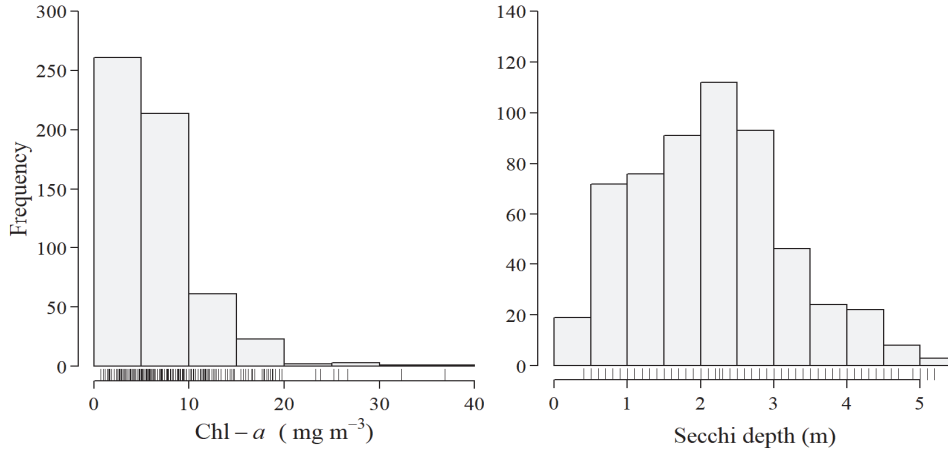


**Figure 4.3** Histograms for Chlorophyll-*a* concentration and transparency *S* (m).

After analysing several models with various binding functions, the most appropriate models for Chlorophyll-*a* and water transparency data were those that considered the factors and variables as main effects without iteration, since they fit well with the data and with the lowest AIC described in the methods (Equation 4.8).

#### 4.6.1 Chlorophyll-*a*

Chlorophyll-*a* concentrations differ between the means of the hydrological cycle, whereas the coefficients of variation differ less than the standard deviations. This indicates that the asymmetric behaviour of the chlorophyll-*a* concentration histogram (Figure 4.3) suggests that a gamma distribution of different means may be appropriate to explain the mean concentration of this variable per hydrologic cycle.

The maximum likelihood estimates of the model parameters (Equation 4.1),  $\mu_i = \exp \mathbf{x}_i^T \boldsymbol{\beta}$ , with logarithmic bond function ( $\eta_i = \log \mu_i = \mathbf{x}_i^T \boldsymbol{\beta}$ ) are given in Table 4.3. In the hydrological cycle emptying, chlorophyll-*a* concentrations are significantly lower than in the dry cycle at the 5% level, and although the difference for filling and full hydrologic cycles is not significant, chlorophyll-*a* concentration is higher. Considering the longitudinal zones, the concentrations of chlorophyll in the riverine and transitional zones are significantly higher when compared to the lacustrine zone, being in agreement with the descriptive statistics.

**Table 4.3** Model parameter estimates for Chlorophyll-*a*.

Coefficients	Estimate	SE	t value	p-value
(Intercept)	1.41	0.193	7.03	<b>0.000</b>
C1-Filling	0.157	0.073	2.21	0.033
C2-Full	-0.136	0.074	-1.85	0.064
C3-Emptying	-0.335	0.072	-4.62	<b>0.000</b>
Z1-Transitional	0.366	0.061	5.97	<b>0.000</b>
Z2-Riverine	0.270	0.066	4.05	<b>0.000</b>
TP	0.002	0.001	1.39	0.165
DO	0.041	0.030	1.36	0.173

The analysis of the deviance of the model  $D^{*G}(\mathbf{y}; \hat{\boldsymbol{\mu}})$  led to a value of  $p \cong 1.00$  indicating a suitable adjustment. Figure 4.4 displays the diagnostic graphs: Leverage, Cook Distance, and Linear Predictor. The elimination of the observations with  $h_{ii} \geq 2p/n = 0.05$  and that  $LL_{D_i}^G \geq F_{50\%}(p, n - p) = 0.94$ , which did not modify the inferential conclusions, and the linear predictor plot and z values are roughly linear, indicating that the log binding function was adequate.

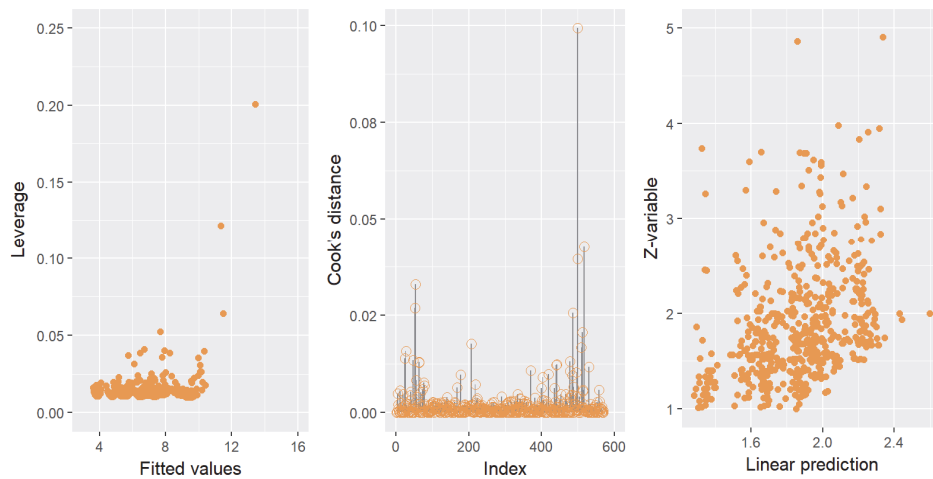


**Figure 4.4** Diagnostic charts for the concentration of Chlorophyll-*a*: leverage, Cook's distance and linear prediction with Range model.

### **4.6.2 Water transparency**

With a less marked asymmetry than the Chlorophyll-*a* concentration (Figure 4.4) and with the non-discrepant standard deviations (Table 4.2), the modelling was carried out with the inverse normal model (Equation 4.2) also with a logarithmic bonding function. The maximum likelihood estimates of the parameters for this model are given in Table 4.4.

In the filling and full hydrological cycles transparency was significantly lower than in the dry cycle at a significance level of 5%. The transparency of the riverine zone is significantly lower when compared to the transparency of the lacustrine zone and the total phosphorus presents an inverse ratio (the higher the transparency, the lower the total phosphorus, as expected).

**Table 4.4** Model parameter estimates for the inverse normal model transparency. References: Cycle: Dry and Zone: Lacustrine. Bold values are significant considering  $\alpha = 5\%$ .

Explanatory variable	Estimate	SE	t value	p-value
(Intercept)	1.227	0.106	11.56	<b>0.000</b>
C1-Filling	-0.383	0.041	-9.24	<b>0.000</b>
C2-Full	-0.229	0.042	-5.51	<b>0.000</b>
C3-Emptying	0.099	0.047	2.10	0.036
Z1-Transitional	-0.080	0.040	-2.03	0.041
Z2-Riverine	-0.550	0.037	-14.74	<b>0.000</b>
Chl- <i>a</i>	-0.006	0.002	-2.08	0.038
TP	-0.013	0.001	-18.26	<b>0.000</b>
DO	0.025	0.016	1.64	0.102

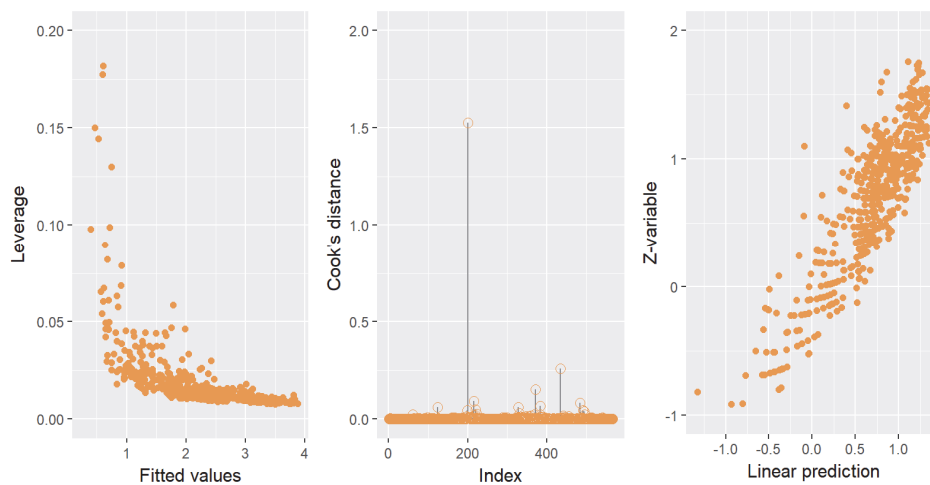


**Figure 4.5** Diagnostic diagrams for transparency: (a) leverage, (b) Cook distance and (c) linear predictor of the inverse normal model

The deviance of the model (Equation 4.4) led to the value of  $p \cong 1.00$  indicating an appropriate fit. Figure 4.5 shows the diagnostic graphs: lever, Cook distance, and linear predictor. As with the Gamma model for Chl-*a* concentration, the observations were evaluated with  $h_{ii} \geq 2p/n = 0.05$  and  $L_{D_i}^G \geq F_{50\%}(p, n - p) = 0.94$ . The elimination of these observations did not change the inferential

conclusions. The linear predictor and z values plots are roughly linear, indicating that the logarithmic binding function was adequate. The normal plot of envelope probabilities generated from 100 simulations (Figure 4.6) shows no evidence that the gamma distribution is inadequate to explain the Chl-*a* concentration nor the normal inverse distribution to explain water transparency.

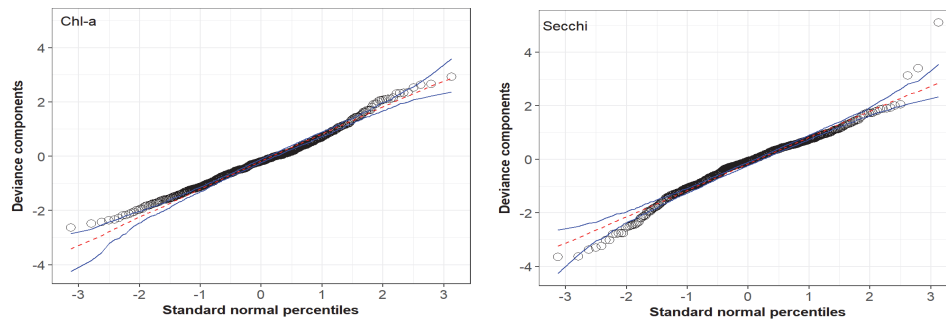


**Figure 4.6** Normal probability plot of deviance component standardized with envelope generated for the model (Range for Chl-*a* and Normal inverse for transparency (Secchi)).

#### 4.7 Conclusions

A model to identify key environmental factors influencing the eutrophication process in a hydroelectric power plant reservoir was developed, taking into account the local hydrological cycle and limnological zones.

Chlorophyll-*a*, water transparency, total phosphorus, orthophosphate, suspended solids, and turbidity were shown to vary according to the hydrological cycle and longitudinal zones. At the filling stage, eutrophication conditions are noted, since total phosphorus, Chlorophyll-*a* and suspended solids are higher, and, consequently, greater turbidity and less transparency occur.

The lacustrine zone presented relatively low nutrient levels with less total phosphorus and limited primary nutrients, resulting in lower Chlorophyll-*a* concentrations, while the riverine zone presented higher total phosphorus, turbidity, total suspended solids, dissolved oxygen and orthophosphate levels.

Two regression models were used for positive asymmetric data, the gamma response model utilized Chlorophyll-*a* as the response variable and total phosphorus and dissolved oxygen as the explanatory variables, while the inverse normal model utilized transparency as the response variable and Chlorophyll-*a*, total phosphorus and dissolved oxygen as the explanatory variables. The hydrological cycle and the longitudinal zone were considered as factors in both.

The gamma model indicated that, in the filling stage, Chlorophyll-*a* concentrations were lower than in the dry stage, and that concentrations in the riverine and transitional zones were significantly higher than in the lacustrine zone.

The use of GLMs was, thus, proven useful for determining reservoir areas and cycles most vulnerable to eutrophication processes. Contrary to what was hypothesized, the riverine zone was not the most vulnerable to the eutrophication process, as algae growth (Chl-*a* concentrations) is influenced not only by nutrient availability, but also by other optimal conditions such as light, calm waters, as found in the transitional zone. Thus, high Chl-*a* concentrations, which increase algal bloom occurrence, are strongly connected to the hydrological cycles, with consequences in the longitudinal zones.

GLMs, thus, provided crucial information that can aid in monitoring the water quality of hydroelectric reservoirs with dendritic characteristics and dynamic hydrological cycles, as these factors are well known to influence water quality in longitudinal zones. In addition, these models also provide information on the temporal and spatial scales and can be used in integrated approaches to ecosystem management in the area of influence of reservoirs.

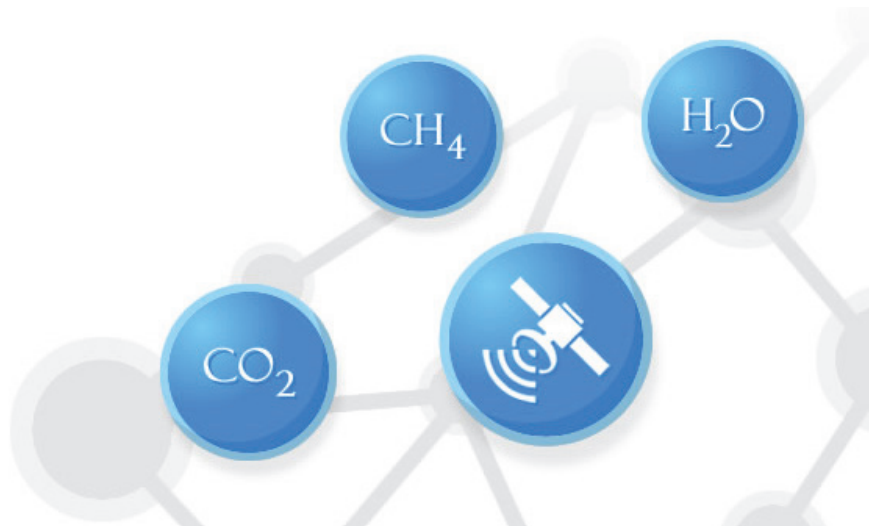
However, future research is required in order to provide a more precise integrated assessment of the main factors related to water quality in reservoirs, such as land use, human activities and degradation of surrounding areas, aiming to promote the sustainable use of the dam-lake-reservoir environment.

---

**Conjunctive use of in situ gas sampling and chromatograph with geospatial analysis to estimate greenhouse gas emissions of a large Amazonian hydroelectric reservoir**

---

5



### ***Abstract\****

Hydroelectric power reservoirs are considered potential contributors to the greenhouse effect in the atmosphere through the emittance of methane and carbon dioxide. We combined *in situ* sampling and gas chromatography with geostatistical and remote sensing approaches to estimate greenhouse gas (GHG) emissions of a large hydropower reservoir. We used remote sensing data to estimate the water surface and geospatial interpolation to calculate total emissions as a function of reservoir surface area. The CH<sub>4</sub> and CO<sub>2</sub> gas concentrations were linearly correlated to sampling time, confirming the adequacy of the *in situ* sampling method to measure GHG diffusive fluxes from reservoir water surfaces. The combination of high purity (99.99%) ISO-norm gas standards with a gas chromatograph, enabled us to achieve low measurement detection limits of 0.87 ppm and 1.22 ppm, respectively, for CH<sub>4</sub> (using a flame ionization or FID detector) and CO<sub>2</sub> (using a thermal conductivity or TCD detector). Our results show that CO<sub>2</sub> emissions are significantly (an order of  $5.10^2 - 10^3$ ) higher than those of CH<sub>4</sub> in both the spatial and temporal domain for this reservoir. The total diffusive GHG emissions over a year (June 2011 to May 2012) of the Tucuruí hydropower reservoir being in operation, in units of tons of carbon, added up to  $6.82 \times 10^3$  for CH<sub>4</sub> and  $1.19 \times 10^6$  for CO<sub>2</sub>. We show that *in situ* GHG sampling using small floating gas chambers and high precision gas chromatography can be combined with geospatial interpolation techniques and remote sensing data to obtain estimates of diffusive GHG emissions from large water bodies with fluctuating water surfaces such as hydropower reservoirs. We recommend that more measurements and observations on these emissions are pursued in order to support and better quantify the ongoing discussions on estimates and mitigation of GHG emissions from reservoirs in the Amazon region and elsewhere in the world.

---

\* This chapter is based on: **Brandão**, I.L.S., Mannaerts, C.M., Brandao, I.W.S., Queiroz, J.C.B., Verhoef, W., Saraiva, A. C. F., Filho, H.A.D. *Conjunctive use of in situ gas sampling and chromatography with geospatial analysis to estimate greenhouse gas emissions of a large Amazonian hydroelectric reservoir. Science of the total environment.* 650, p. 394-407 13 p., 650.

## 5.1 Introduction

Emissions of methane (CH<sub>4</sub>) and carbon dioxide (CO<sub>2</sub>) gases from hydroelectric reservoirs into the atmosphere form a growing concern among researchers around the world due to their potential to contribute to global warming (Huttunen et al., 2002; Kemenes et al., 2007; Soumis et al., 2004; St. Louis et al., 2000). Greenhouse gases (GHGs) and their greenhouse effect play an important role in Earth's climate as they are responsible for maintaining the temperature gradient in the atmosphere (Samimi and Zarinabadi, 2012). Carbon dioxide is distinguishable from other gases due to its ability to absorb and re-emit infrared energy, making it an effective heat-trapping greenhouse gas (Lacis et al., 2010; Somerville, 1998) and according to the European Environmental Agency (EEA, 2010) CO<sub>2</sub> emissions account for the largest share of GHGs, contributing 80-85% of emissions. Investigating methane emissions is also important, as reservoirs may create favourable conditions for the production of CH<sub>4</sub>, which has a global warming potential of 34 times that of CO<sub>2</sub>, considering the 100 time horizon years adopted by the Kyoto Protocol (Myhre et al., 2013).

Hydroelectric reservoirs have long been considered to be a source of “clean” GHG-free energy (Barros et al., 2011). However, recently there is increased awareness that these reservoirs could be contributing to the increase of GHGs in the atmosphere (Deemer et al., 2016). Concerns have been raised around the world (IHA, 2010), also creating awareness in the Amazon region, where several studies and monitoring campaigns have taken place (Devol et al., 1990; Kemenes et al., 2007; Lima, 2005; Richey et al., 2002; Rosa et al., 2016; Rosa et al., 2004; Santos et al., 2008; Santos et al., 2006).

Studies undertaken in the Amazon region have revealed diverging results regarding GHGs emitted by amazonian reservoirs, as the variables that might be contributing to the total emission by reservoirs are partly unknown. Rosa et al. (2002), for instance, who conducted earlier studies on estimates of GHGs emissions using a model of plane geometry to calculate emissions in unit of area, underestimated the total area of the Tucuruí Hydropower Reservoir (THR) by 15%, because they did not consider the variability occurring in the reservoir area during the year. An example of overestimation cited in the literature is the study conducted by Kemenes et al. (2007) in the Balbina reservoir, which found methane emissions exceeding those estimated by Rosa et al. (2002) by more than 20%. This was due to Kemenes et al. (2007) miscalculating the methane flux downstream of the Balbina reservoir. According to Santos et al. (2008), they should have based calculations on the mean

variation of this flux in the water column. Instead, they used the maximum depth, where methane emissions were higher, overestimating results.

Deshmukh (2013) also conducted a study on estimates of GHGs in a subtropical reservoir, revealing that the diffusive emission from the water surface has been the main source of release of carbon dioxide (CO<sub>2</sub>) into the atmosphere, namely 95% of total monthly emissions. A recent study, including a three-dimensional approach, conducted by Curtarelli et al. (2016) in the Tucuruí hydropower reservoir underestimated rather than overestimated the total emission by this reservoir. Despite the great achievements by these authors, the major drawback in their studies is not including the river downstream area or reference sites in their estimates, both necessary to allow emissions from a reservoir to be accurately estimated (IHA, 2010). With the uncertainties surrounding these researchers' results, concerns arise regarding the models used to estimate their emissions (Parekh and McCully, 2004; Santos et al., 2008) and whether hydropower reservoirs really provide "clean" GHGs-free energy. It is important to improve the available information regarding the GHG status of existing and new reservoirs and to provide tools to support decision making on mitigating measures that may be necessary, as stated in the guidelines for GHG measurement for freshwater reservoirs (IHA, 2010).

Despite progress made in GHG emission monitoring in amazonian reservoirs, more research is needed to provide a better understanding of the spatial and temporal distribution of GHG fluxes. Seasonal changes in climate, hydropower operations and carbon load may all affect spatial and temporal variations in GHG fluxes (IHA, 2010; Marcelino et al., 2015).

In this study we use an approach different from previous studies, which is based on a combination of *in situ* sampling with laboratory chemical analysis, geostatistics and remote sensing to model the spatial and temporal variations in CO<sub>2</sub> and CH<sub>4</sub> in the THR. Geostatistics, as a predictive tool, provides accurate and reliable estimations of phenomena at unsampled locations (Rivoirard, 2005).

The first step when applying geostatistic models is to determine the statistical relationship between sample points. In order to generate a surface model, some type of interpolation method must be used to estimate data values for locations where no samples were taken (Babish, 2000; Vieira and Paz Gonzalez, 2003). A fundamental tool in geospatial analysis is the variogram/semivariogram, which determines the amount of spatial dependency in the dataset (Spokas et al., 2003). The variogram/semivariogram is calculated based on the sampled sites. It is usually

recommended that at least 100 data points are used to develop an accurate variogram. However, in many circumstances, like in GHG sampling and analysis, it is difficult to obtain a high enough data density to fully characterize the surface emissions of GHGs. This is due to practical constraints such as the sampling time needed, and the displacement time on large reservoirs, such as Tucuruí (Spokas et al., 2003). The optimal GHG sampling accuracy recommended by the International Hydropower Association (IHA) requires between 20 and 30 sample sites, including areas such as the main upstream tributary, the main reservoir body and the downstream area. This recommendation was adopted in this research.

Remote sensing can be used to monitor surface water extent and its variation using visible and infrared next to Synthetic Aperture Radar (SAR) observations (Alsdorf et al., 2007; Prigent et al., 2007). Estimations of surface water extent using visible and infrared satellite measurements can be attained using open access data at medium-high (e.g. 30m) spatial resolution, but possibilities of detecting water surfaces under clouds or dense vegetation are limited (Papa et al., 2010). Interannual variability in methane surface emissions combined with water surface extent analysis has been studied by Bousquet et al. (2006), Papa et al. (2010), and Ringeval et al. (2010). The purpose of using remotely sensed water surface extent is to determine and monitor variations in the reservoir area in relation to the hydrological operation phases. It is already known that the surface area of this reservoir varies over the course of a year from 1500 km<sup>2</sup> to 2500 km<sup>2</sup> (Curtarelli et al., 2016).

The objective of this study was to evaluate a methodology, which may be used as input to the ongoing discussion regarding estimates of greenhouse gas emissions by hydroelectric power reservoirs in the Amazon region, as well as to provide information on the quantitative spatial and temporal variation in greenhouse gases based on geostatistics and remote sensing analysis. For this investigation, we considered reference sites in the reservoir's main impoundment, as well as in the upstream river inflow region and the area up to 30 km downstream of the dam.

## ***5.2 Methods***

### **5.2.1 Study area**

The Tucuruí Hydroelectric power Reservoir (THR) is located in the Tocantins watershed (Amazon region) between 3.39 S 50° 6' W and 4° 45' S 49° 23' W, Pará State, Brazil (Tundisi et al., 2014). It is one of the largest hydroelectric reservoirs in the Amazon with an upstream water surface area ranging from 1500 km<sup>2</sup> to 2500 km<sup>2</sup> over the year, and a storage capacity of 45 km<sup>3</sup>. The reservoir's length is

approximately 133 km and its average width is 13 km (Espíndola et al., 2000). Maximum water depth near the dam and spillway is 72 m. The climate of the study area is tropical monsoon (Am) (Curtarelli et al., 2016; Peel et al., 2007) with maximum temperatures of 33.12 °C measured in June 2011, 34.67 °C in September 2011, 33.02 °C in December 2011, and 31.54 °C in March 2012. The rainfall accumulated to 2677.2 mm for the January, 2011, to March, 2012, study period and was irregularly distributed over the year. The highest monthly rainfall was observed in March, 2012, with 499 mm in 29 days of precipitation, while the lowest rainfall was observed in August, 2011, with 21 mm in 3 days of precipitation (Figure 5.1).

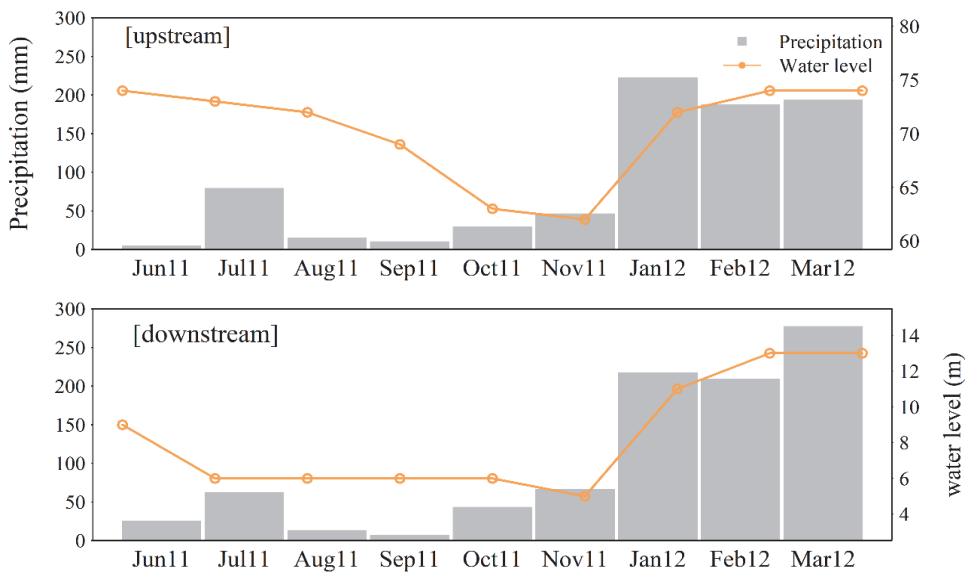


**Figure 5.1** Accumulated monthly precipitation and typical water levels in the THR (upstream and downstream of the dam) during the four fieldwork campaigns

This study included four fieldwork campaigns conducted every three months at 22 sites (Figure 5.2) distributed throughout the reservoir area, and took the different seasons into account, as well as the hydropower operation schedule (decreasing volume, low water level, filling and full capacity or maximum water level).

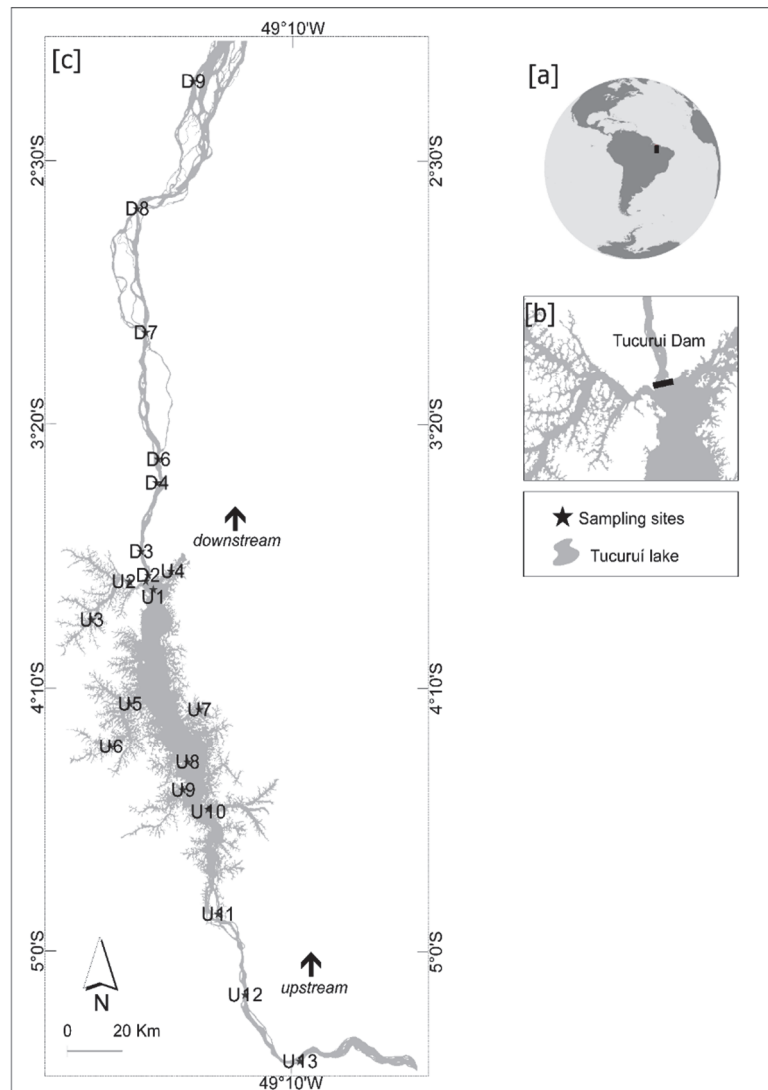


**Figure 5.2** Study area at (a) South America, (b) Tucuruí dam, and (c) sampling sites upstream (U) and downstream (D) locations at the THR reservoir.

### 5.2.2 Measurement of the diffusive fluxes of methane (CH<sub>4</sub>) and carbon dioxide (CO<sub>2</sub>)

Diffusive fluxes of methane (CH<sub>4</sub>) and carbon dioxide (CO<sub>2</sub>) were measured directly across the air-water interface of the 22 sites using static floating chambers (volume of 1L and surface of 0.0491 m<sup>2</sup>) using the method described in Devol et al. (1990) and in the IHA (2010). With this method a floating chamber is held upside down

for a few minutes just above the water to allow equilibrium with the air *in situ* to be established, after which the chamber is placed on the water. A 60 mL polyethylene syringe is then connected to the tubing of the floating chamber and pumped several times. This changes the air in the tube and homogenizes the air in the chamber. A first gas subsample of 40 mL is then collected at an initial time ( $t_0$ ), which is then transferred by needle injection in 40 mL pre-evacuated glass vials sealed with butyl rubber stoppers and stored until analysis (Kemenes et al., 2007; Lima, 2005). At 2 and 4 minute intervals (for a total of eight minutes) three other samples ( $t_2$ ,  $t_4$ , and  $t_8$ ) are taken (Lambert and Fréchet, 2005). All 22 sites were sampled in replicates during the operational regime of the THR, which starts to empty in June, has least water from September to November, fills up in December and is full by March. Measurements were taken between 7:00 and 17:00 hours with a maximum storage time of seven days, as suggested by Lambert and Fréchet (2005).

### **5.2.3 GHG diffusive flux analysis and calculations**

For quantitative analysis, we adapted the model proposed by Devol et al. (1990) and Damazio et al. (2013). Concentrations of methane ( $\text{CH}_4$ ) and carbon dioxide ( $\text{CO}_2$ ) (in units of  $\mu\text{mol mol}^{-1}$ ) were determined using a gas chromatograph (Bruker GC-450), coupled with a thermal conductivity detector (TCD) for carbon dioxide ( $\text{CO}_2$ ) and a flame ionization detector (FID) for methane ( $\text{CH}_4$ ). Porapak-Q and Hayesep standard columns were used in the analysis.

Validation of the gas chromatography of the methane and carbon dioxide determinations was accomplished using verification of linearity, detection limit, precision and accuracy. We used two standard gases ( $\text{CO}_2$  and  $\text{CH}_4$ ) from Multimix Linde with purities of 99.99%, as recommended by ISO (2015) and the statistic description by ICH (1996). The detection limit of the Bruker gas chromatograph used here is 1.22 ppm for  $\text{CO}_2$  and 0.87 ppm for  $\text{CH}_4$ . Full details on the validation of the gas chromatography method is provided in the appendices 1 to 12.

Gas fluxes were determined using linear regression of gas concentration versus time ( $t_0$ ,  $t_2$ ,  $t_4$  and  $t_8$ ). Fluxes were accepted or rejected following the method proposed by Lambert and Fréchet (2005). The correlation coefficient between gas concentration and time ( $R^2 > 0.90$ ) and analysis of variance ( $p < 0.05$ ) were determined according to Soumis et al. (2004) and Guérin and Abril (2007). Diffusive fluxes (DF) of methane and carbon dioxide in  $\text{mg m}^{-2} \text{d}^{-1}$  were determined using equations 5.1 and 5.2, respectively.

$$DF_{(CH_4)} = \left(\frac{P}{T}\right) \frac{\text{ChamberVolume (L)} * \text{MolecularWeight}(CH_4) * F1 * F2}{62.4 * \text{ChamberArea (m}^2)} * \text{Slope}(\mu\text{mol mol}^{-1}\text{min}^{-1}) \quad (\text{Eq 5.1})$$

$$DF_{(CO_2)} = \left(\frac{P}{T}\right) \frac{\text{ChamberVolume (L)} * \text{MolecularWeight}(CO_2) * F1 * F2}{62.4 * \text{ChamberArea (m}^2)} * \text{Slope}(\mu\text{mol mol}^{-1}\text{min}^{-1}) \quad (\text{Eq 5.2})$$

where, **P** stands for atmospheric pressure, which was measured in the laboratory and is given in mmHg; **T** is the laboratory temperature in Kelvin; the chamber volume is  $10^{-6}$  (that is the volume of 1 ppm of the floating chamber with 1000 mL); the molecular weights of  $CO_2$  and  $CH_4$  are  $44.01 \text{ g mol}^{-1}$  and  $16 \text{ g mol}^{-1}$ , respectively; **F1** is the conversion factor from minutes to a day (1440); **F2** is the conversion factor from g to mg (1000); 62.4 is the ideal gas constant ( $\text{LmmHgK}^{-1} \text{ mol}^{-1}$ ); the chamber area is  $0.0491 \text{ m}^2$ ; Slope is the regression slope of measured gas concentration versus observation time in  $\mu\text{molmol}^{-1}$ . For this study we considered  $P = 751 \text{ mmHg}$  and  $T = 300.15 \text{ K}$  ( $27 \text{ }^\circ\text{C}$ ).

#### 5.2.4 Water sampling and biogeochemical analysis

Water environmental and biogeochemical variables were measured coincidental with the *in situ* gas sampling and, for some variables, in the laboratory as well. Variables measured *in situ* included: water temperature (digital thermometer), water electrical conductivity (Hatch device, SM2510), and site depth (portable handy depth sounder Hondex PS-7). Analysed in the laboratory were dissolved oxygen (SM 4500-OC), Chlorophyll-*a* (extraction by acetone method and UV/VIS spectrometry), turbidity (nephelometric method, SM 2130B), ion ammonium (SM 4500-NH<sub>3</sub>-C), total phosphorus (ascorbic acid colorimetric method (USEPA, 1978)), orthophosphate (SM4500-PC), pH (PHTEK device, NBR 9896/1993), total suspended solids (SM 2540-D), and nitrate (SM 4500-NO<sub>3</sub><sup>-</sup>-B). GHG fluxes were related to environmental variables using a Pearson correlation analysis. On a spatial scale, a Kruskal-Wallis test was performed to verify differences between sample locations (reservoir upstream and downstream) and the types of environment where the samples were taken (lake, transition zone, river zone, and reference sites). Significance tests took into account a confidence level of 5%. The normality of the data was evaluated using the Lilliefors (Kolmogorov-Smirnov) test.

#### 5.2.5 Estimation of the reservoir surface water extent

The surface water extent was evaluated taking the seasonal runoff inflow and hydropower operation schedule (regulating the outflows) of the THR, which cause

great variability of its surface area, into consideration. To apply image processing to the water covered areas, an image masking method was applied. In the masking method, the near infrared band (0.76-0.89  $\mu\text{m}$ ) of the Landsat-5 satellite was used as threshold, since this band provides a good delineation to extract water bodies from other surface features (Baraúna et al., 2012). This processing was applied to the acquired scenes approximating the fieldwork dates and thus the THR total surface area was calculated.

The surface water extents were used as interpolation boundaries in the ordinary kriging of the *in situ* points of observed diffusive fluxes. This resulted in estimates of GHGs in spatial and temporal domains across the surface area of the THR for its different operational regimes. ArcMap (version 10.5.1) was used to manipulate the water masks and to calculate the emission ranges across the THR and for final map layouts.

#### **5.2.6 Geospatial analysis**

We used semivariograms to evaluate the distribution of our variables and ordinary kriging to generate models (images) of the spatial and temporal distribution of the GHG fluxes (Deutsch and Journel, 1998; Goovaerts, 1997; Houlding, 2012; Landim and Sturaro, 2002). Therefore, the procedure included the characterization and modeling of environmental variability, as well as the estimation of values at unsampled locations. The semivariance function was calculated for all directions (isotropic semivariogram) to assess the spatial dependence of the data as described in Souza et al. (2017).

The best model was assessed using a Jackknife test, which evaluates the consistency of the data estimated by kriging based on fitted semivariograms (on experimental data). The estimate is considered adequate when the mean ( $\mu_{jk}$ ) and variance ( $\sigma_{jk}$ ) of the reduced error are close to zero and one, respectively (Souza et al., 2017; Vieira et al., 2010).

Results of the interpolation establish a range of emissions per area, which are used to estimate the total emission per operational regime of the THR. Geostatistical analysis was performed using R (version 3.2.5) and the geoR and gstat libraries in the RStudio program (version 1.0.153) (R Development Core Team, 2010).

### 5.2.7 Evaluation of seasonal and total CH<sub>4</sub> and CO<sub>2</sub> emissions of the THR

Estimates of methane (CH<sub>4</sub>) and carbon dioxide (CO<sub>2</sub>) diffusive fluxes were obtained in the months June 2011, September 2011, December 2011, and March 2012, taking the operational regime of the THR, as well as the calculated areas upstream and downstream of the reservoir, into account.

Due to the high variability in gas emissions in the samples, it was not possible to adjust a known theoretical distribution such as a Gaussian distribution to the data. Therefore, we used the method of the M-estimators (Norušis, 2002) to assess information on the sample distribution. M-estimators include robust methods with smallest variance estimation compared to other estimators of variance (Susanti and Pratiwi, 2014). The M-estimator used in this study was the Tukey's biweight statistic. Though most studies on GHGs use the mean (arithmetic) and median as measure of central tendency, Damazio et al. (2013) suggested the use of more robust estimators when studying diffusive emissions of GHG fluxes by hydropower reservoirs, sampled and measured *in situ* using static floating chambers.

In this study, to estimate emissions per area, we first categorized fluxes according to the range given by the ordinary kriging (interpolation method) and calculated the M-estimator of each range. Secondly, in the upstream area we multiplied these results by the interpolated area given for each range, to obtain an estimate of emissions in those ranges, while downstream of the THR, an area 30km downstream from the dam was used.

In order to quantify anthropogenic impacts, we considered reference sites, characterized by similar land-use and climate to those in the reservoir area before impoundment. It is important to identify reference sites to ensure that normal variations due to climate or changes in land-use are taken into account and not seen as reservoir effects (Cole et al., 2001).

### 5.3 Results

#### 5.3.1 Spatial and temporal variation of CO<sub>2</sub> and CH<sub>4</sub> fluxes

Figure 5.3 shows flux emissions at each sampling site during the four fieldwork campaigns measuring CO<sub>2</sub> and CH<sub>4</sub>. Higher spatial and temporal variability for CH<sub>4</sub> was observed, with a variation coefficient of 213%. For CO<sub>2</sub>, a variation coefficient of 123% was found. The CO<sub>2</sub> fluxes varied from 31.75 to 42848.73 mg m<sup>-2</sup>day<sup>-1</sup> during the four field campaigns. The highest emissions were observed upstream of the reservoir at the U3, U8 and U9 sites in June 2011.

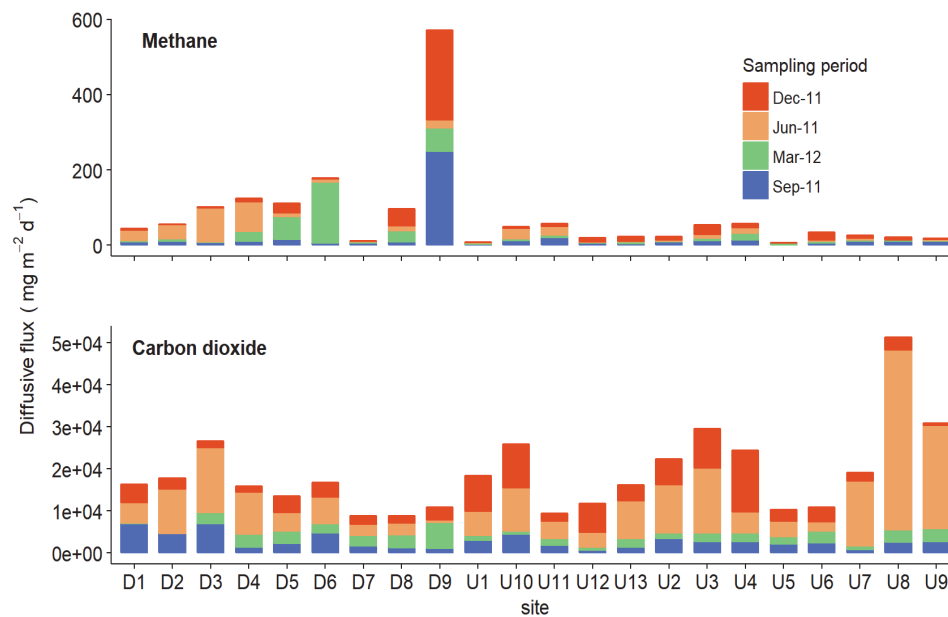


**Figure 5.3** Diffusive flux of CO<sub>2</sub> and CH<sub>4</sub> at each sampled site of the THR. Letters U and D stand for sites location upstream and downstream of the THR dam, respectively.

Diffusive fluxes of CH<sub>4</sub> were higher downstream of the THR and higher emissions were observed at D9 in September and December 2011, and at D6 in March 2012. Overall average emission values for CH<sub>4</sub> were 19.37 ( $\pm$  41.26) mg m<sup>-2</sup> d<sup>-1</sup> and for CO<sub>2</sub> they were 4731.66 ( $\pm$  5853.44) mg m<sup>-2</sup> d<sup>-1</sup> during the studied period. As described by Santos et al. (2006), sites located at deeper waters were usually responsible for lesser CH<sub>4</sub> emissions than shallow sites. The water depth upstream of the dam was much greater than downstream of the THR, even in the driest periods (Figure 1). Interestingly, CH<sub>4</sub> emissions from natural lakes and rivers are typically very high, and can reach values of 330 mg m<sup>-2</sup> d<sup>-1</sup> (Santos et al., 2006), as was also observed at the sites D4 and D5, which formed reference sites for this

study. These locations presented high values of CH<sub>4</sub> emission, but their total (area) emissions were low if emitted flux and area were considered. Therefore, they presented only a small contribution to the CH<sub>4</sub> emissions in the THR.

### 5.3.2 Statistical relationships between biogeochemical variables and GHG fluxes

Water temperature and Chlorophyll-*a* were the only environmental variables significantly different between the sample sites ( $p_{(wt)} = 0.004$ ;  $p_{(Chl-a)} = 0.030$ ), months ( $p_{(wt)} = 0.005$ ;  $p_{(Chl-a)} = 0.013$ ) and sampled environment ( $p_{(wt)} = 0.000$ ;  $p_{(Chl-a)} = 0.030$ ). Temperature varied from 26.7 to 32 °C with mean values of 29.87 ( $\pm 0.95$  °C). Minimum values of Chlorophyll-*a* in the THR were recorded in June, 2011, varying from 1.19 to 8.09 mg m<sup>-3</sup> with mean values of 5.22 ( $\pm 3.50$  mg m<sup>-3</sup>). Whereas, maximum values of 21.42 mg m<sup>-3</sup> were recorded in March, 2012, with a mean of 7.50 ( $\pm 4.68$  mg m<sup>-3</sup>).

Significant differences between sites were found for water depth ( $p_{(wd)} = 0.000$ ), total phosphorus ( $p_{(TP)} = 0.005$ ), nitrate ( $p_{(NO_3^-)} = 0.027$ ), and TSS ( $p_{(TSS)} = 0.003$ ). Between months, dissolved oxygen ( $p_{(DO)} = 0.000$ ), pH ( $p_{(pH)} = 0.004$ ), EC ( $p_{(EC)} = 0.000$ ), turbidity ( $p_{(TURB)} = 0.000$ ), TSS ( $p_{(TSS)} = 0.001$ ), ion ammonium ( $p_{(NH_4^+)} = 0.012$ ) and orthophosphate ( $p_{(PO_4)} = 0.006$ ) significantly differed. Considering the environment where samples were collected, significant differences were found for dissolved oxygen ( $p_{(DO)} = 0.010$ ), nitrate ( $p_{(NO_3^-)} = 0.000$ ) and water depth ( $p_{(wd)} = 0.000$ ).

Significant differences in CH<sub>4</sub> fluxes were observed between sites ( $p_{(CH_4)} = 0.001$ ), limnologic zones ( $p_{(CH_4)} = 0.010$ ) *i.e.* lacustrine, transitional, and riverine, and sampling locations ( $p_{(CH_4)} = 0.003$ ) *i.e.* upstream and downstream. In CO<sub>2</sub> fluxes, statistically significant differences were noted only between studied periods ( $p_{(CO_2)} < 0.001$ ).

To assess possible factors controlling GHG fluxes, a Pearson correlation analysis between environmental and biogeochemical variables and the measured GHG was performed (Table 5.1). Significant correlations were found between methane fluxes and water temperature ( $r = -0.56$ ,  $p = 0.007$ ,  $n = 22$ ); Chl-*a* ( $r = -0.58$ ,  $p = 0.014$ ,  $n = 18$ ); DO ( $r = -0.45$ ,  $p = 0.036$ ,  $n = 22$ ) in June, 2011, pH in September, 2011 ( $r = 0.43$ ,  $p < 0.05$ ,  $n = 22$ ), and NO<sub>3</sub><sup>-</sup> ( $r = 0.49$ ,  $p = 0.032$ ,  $n = 20$ ) in March, 2012. Fluxes of carbon dioxide were significantly correlated with TSS ( $r = -0.46$ ,  $p = 0.023$ ,  $n = 19$ ), NO<sub>3</sub><sup>-</sup> ( $r = 0.58$ ,  $p = 0.010$ ,  $n = 19$ ) in September, 2011, and with NO<sub>3</sub><sup>-</sup> ( $r = 0.48$ ,  $p = 0.028$ ,  $n = 20$ ) and Chl-*a* ( $r = 0.65$ ,  $p = 0.002$ ,  $n = 20$ ) in March, 2012.

**Table 5.1** Correlation between GHG fluxes and water environmental and biogeochemical variables. Variables included water temperature (wt), total suspended solids (TSS), total phosphorus (TP), nitrate (NO<sub>3</sub><sup>-</sup>), Chlorophyll-*a* (Chl-*a*), electrical conductivity (EC), pH, dissolved oxygen (DO), turbidity (Turb), ion ammonium (NH<sub>4</sub><sup>+</sup>) and orthophosphate (PO<sub>4</sub><sup>-3</sup>).

gas	wt	TSS	TP	NO <sub>3</sub> <sup>-</sup>	Chl- <i>a</i>	EC	pH	DO	Turb	NH <sub>4</sub> <sup>+</sup>	PO <sub>4</sub> <sup>-3</sup>
<b>June 2011</b>											
CO <sub>2</sub>	-0.02	-0.14	-0.03	-0.06	0.12	0.23	0.19	0.21	0.25	-0.29	-0.05
CH <sub>4</sub>	-0.56**	0.35	0.38	0.43*	-0.58**	-0.47	-0.25	-0.45*	-0.18	0.18	0.29
<b>September 2011</b>											
CO <sub>2</sub>	-0.09	-0.46*	-0.24	0.58**	-0.13	-0.23	0.08	-0.35	-0.03	-0.23	-0.42
CH <sub>4</sub>	-0.16	0.17	-0.02	-0.04	0.29	-0.04	0.43*	0.40*	-0.05	-0.16	0.22
<b>December 2011</b>											
CO <sub>2</sub>	-0.19	-0.14	-0.25	-0.25	-0.13	-0.08	0.05	0.20	-0.19	0.09	0.13
CH <sub>4</sub>	-0.17	0.25	0.02	-0.22	0.17	0.11	-0.05	0.16	-0.10	-0.03	0.04
<b>March 2012</b>											
CO <sub>2</sub>	-0.43*	0.13	0.27	0.48*	0.65**	-0.30	-0.14	-0.29	0.15	0.01	0.09
CH <sub>4</sub>	-0.33	-0.06	-0.21	0.49*	0.19	-0.05	-0.10	-0.11	0.12	0.01	-0.25

\*\* Correlation is significant at the 0.01 level; \* correlation is significant at the 0.05 level.

### 5.3.3 Geostatistical analysis results

#### 5.3.3.1 Semivariogram estimation and modeling results

Semivariogram models were estimated using CH<sub>4</sub> and CO<sub>2</sub> fluxes shown in Figure 5.3. The semivariogram models showing the best results for CH<sub>4</sub> were exponential models for the fieldwork undertaken in June 2011, December 2011, and March 2012, and a spherical model for fieldwork undertaken in September 2011. They were selected from the mean and variance of the reduced error, respectively. For CO<sub>2</sub>, the models that showed the best results were gaussian, eyefit, spherical and exponential, respectively, for the successive months studied. They were also selected according to their mean and variance of the reduced error. Results in Table 5.2a show that the CH<sub>4</sub> semivariograms have a lower nugget effect in relation to the sill than those of CO<sub>2</sub> (Table 5.2b), which is reflected in the higher degree of spatial dependence of this variable. More information on semivariogram graphs is available in appendices 5.18 and 5.19.

**Table 5.2** Geostatistical parameters for CH<sub>4</sub> and CO<sub>2</sub> fluxes in the THR.

<b>(a) Parameters used in the variogram fitting model for CH<sub>4</sub></b>							
<b>Fieldwork</b>	<b>Model</b>	<b>C<sub>0</sub></b>	<b>C</b>	<b>Range [m]</b>	<b>μ<sub>jk</sub></b>	<b>σ<sub>jk</sub></b>	<b>DR (%)</b>
Jun/2011 (field 1)*	Exponential	0.77	3.52	59.81	0.00107	0.65854	81.98
Sep/2011 (field 2)**	Spherical	2.24	25.05	57.73	-0.01039	0.75542	91.79
Dec/2011 (field 3)*	Exponential	0.89	1.76	44.60	0.01156	0.84330	66.27
Mar/2012 (field 4)**	Exponential	0	1239.15	44.76	0.02414	1.37046	100.00
<b>(b) Parameters used in the variogram fitting model for CO<sub>2</sub></b>							
<b>Fieldwork</b>	<b>Model</b>	<b>C<sub>0</sub></b>	<b>C</b>	<b>Range [m]</b>	<b>μ<sub>jk</sub></b>	<b>σ<sub>jk</sub></b>	<b>DR (%)</b>
Jun/2011 (field 1)**	Gaussian	1.11x10 <sup>7</sup>	3.33x10 <sup>7</sup>	18.64	-0.01421	0.43603	75.00
Sep/2011 (field 2)**	EyeFit	3.03x10 <sup>5</sup>	9.75x10 <sup>5</sup>	62.39	-0.01223	0.89416	76.32
Dec/2011 (field 3)**	Spherical	6.10x10 <sup>5</sup>	4.57x10 <sup>6</sup>	16.64	0.0051	0.96567	88.24
Mar/2012 (field 4)**	Exponential	1.31x10 <sup>5</sup>	9.09x10 <sup>5</sup>	24.74	0.02582	0.72655	87.40

\*\* (square root data transformation); \*\* (data is not transformed); C<sub>0</sub> (nugget effect); C (dispersion of variance); DR (spatial dependence ratio =  $(C/(C_0+C)) \times 100$  (Vieira et al., 2010); high DR value means strong spatial dependence); μ<sub>jk</sub> (average reduced error); σ<sub>jk</sub> (reduced error variance)

The kriging interpolation resulted in five main classes for CH<sub>4</sub> and eight for CO<sub>2</sub> and they are shown as areal surface emissions in Figures 5.4 and 5.5, respectively. The areal surface of methane (CH<sub>4</sub>) in Figure 5.4 reveals that larger values were found in the same regions having the highest fluxes, which are areas close to inlets in high waters, and to the cities such as Cametá (D9) and Marabá (U13) (September and December) in low waters. Lowest values were observed in the transition and lake zones of the reservoir and correspond to the largest emission zones. The transition and lake zones of this reservoir are deeper than other areas with sampled sites showing minimum depth of 21.4 m and maximum of 70.1 m, respectively, in high waters.

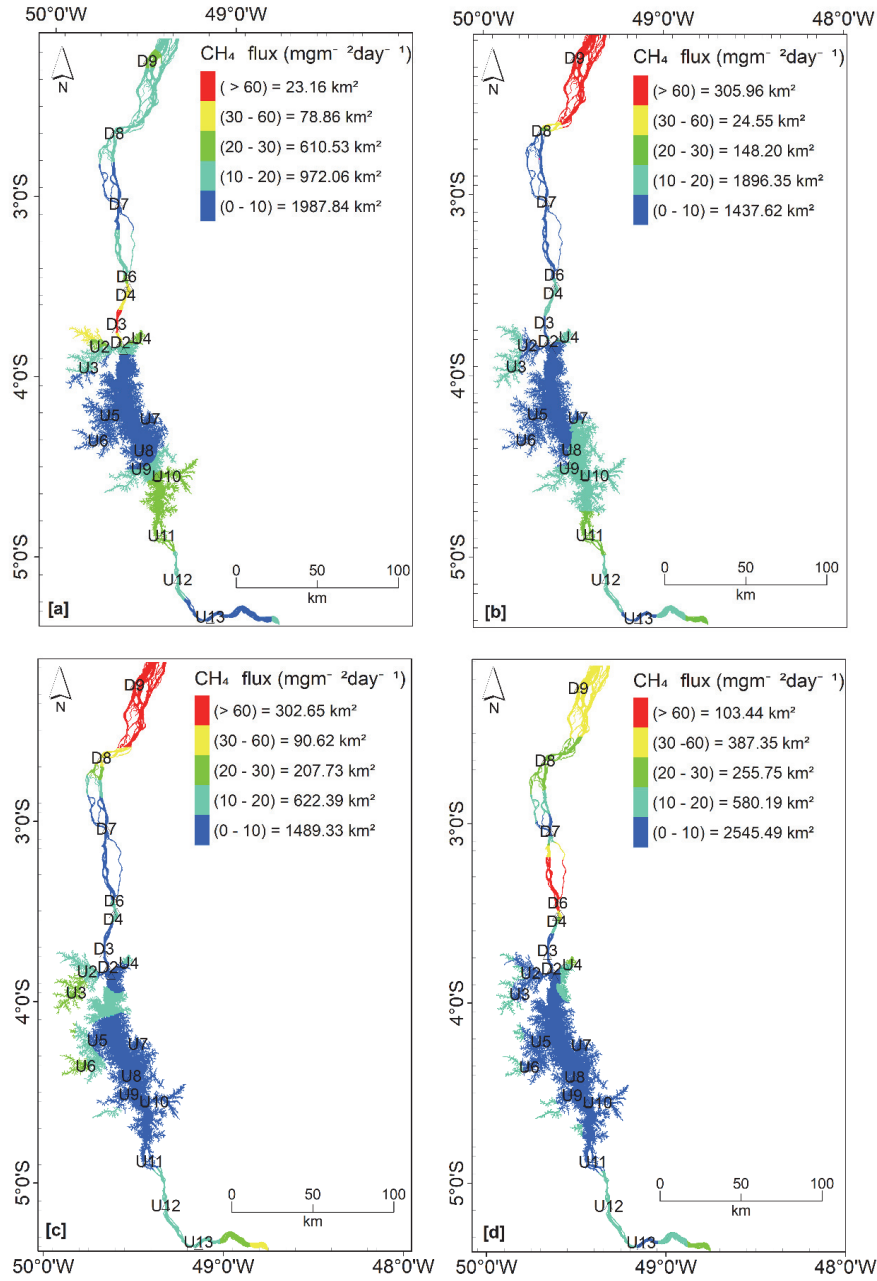


**Figure 5.4** Spatial and temporal distribution of CH<sub>4</sub> fluxes in the entire THR system (including river upstream and downstream) corresponding to: (a) June; (b) September; and (c) December of 2011; (d) March of 2012.

Figure 5.5 shows the areal surface of CO<sub>2</sub> emissions obtained from kriging interpolation with eight main classes. These classes reveal that larger fluxes were observed in June and December, 2011. In June, higher fluxes were observed in the transition zone and part of the lake zone, which is consistent with sampling sites in these areas, as shown in Figure 5.3. Sources of carbon for GHG emissions are likely to be derived from organic matter imported to or produced in the reservoir by biodecay. None of the analysed variables showed significant correlation with CO<sub>2</sub> fluxes. However, just days before the measurements in June, 2011, rainfall events were observed with accumulated values of 116.6 mm (Figure 5.1) and a wind speed average of 1.34 m/s ( $\pm 0.30$ ). Greater areas with low fluxes were observed in September, 2011, and March, 2012, and these areas were mostly consistent with fluxes shown in Figure 5.3. In September, CO<sub>2</sub> fluxes were negatively correlated with suspended solids ( $r = -0.46$ ) and positively with NO<sub>3</sub> ( $r = 0.58$ ) and in March, 2012, they were correlated negatively with water temperature ( $r = -0.43$ ) and positively with NO<sub>3</sub> ( $r = 0.48$ ), and Chl-*a* ( $r = 0.65$ ).

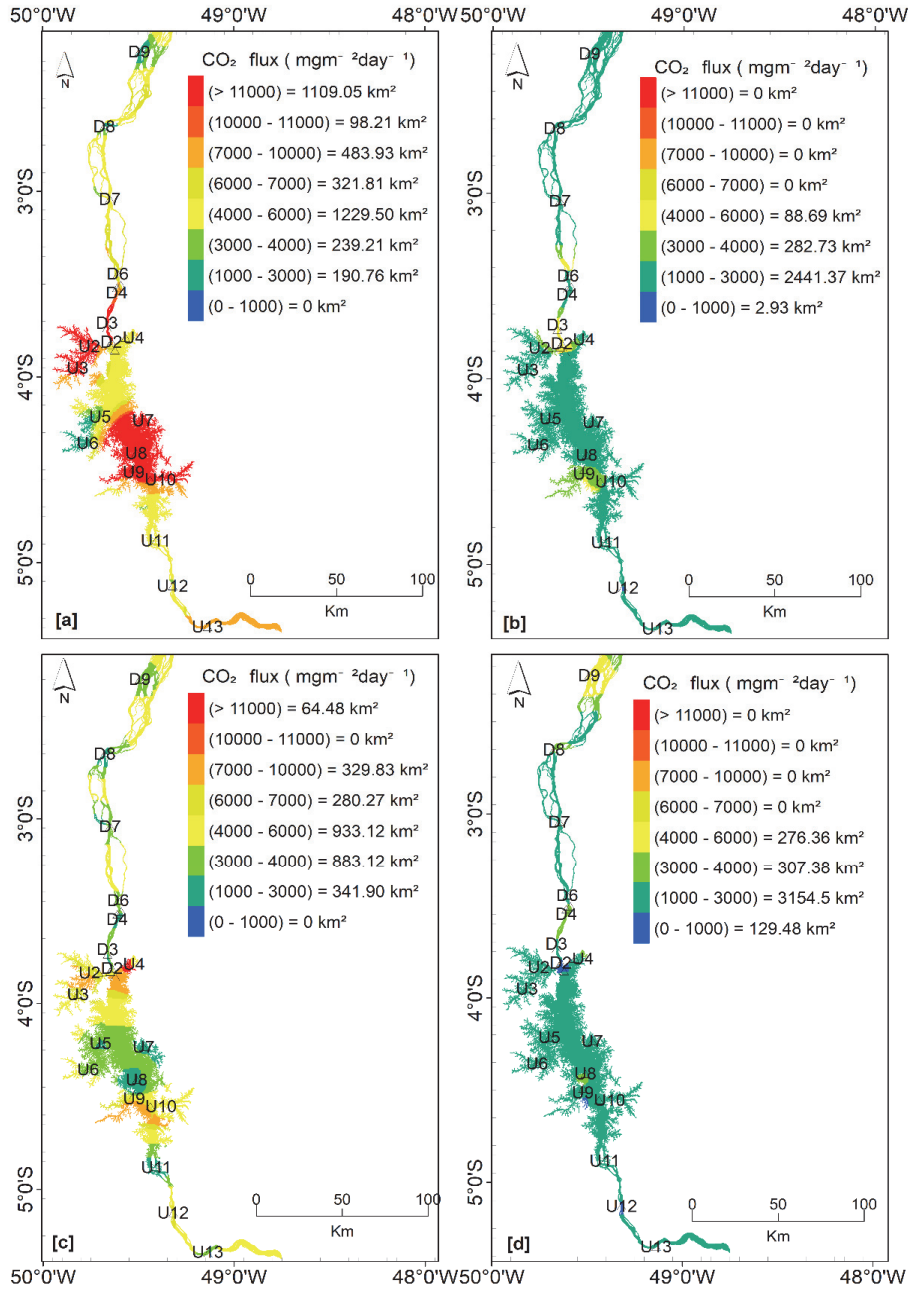


**Figure 5.5** Spatial and temporal distribution of CO<sub>2</sub> in the entire THR system (including river upstream and downstream) corresponding to: a) June-2011; b) September-2011; c) December -2011; and d) March of 2012.

Using geostatistical analysis and subsequent kriging interpolation, it was possible to create layers that estimated the average of the two GHG fluxes across the entire reservoir. The best geospatial model used in the interpolation was selected using the Jackknife test, which evaluates the consistency of the interpolated data, based on fitted semivariograms. Interpolated areas allowed for a direct visualization of the geographical distribution of the GHG fluxes per area, as well as the identification of emission hot spots.

The total surface GHG emissions were calculated using the estimated areas derived from the geostatistical analysis. Diffusive emissions of CH<sub>4</sub> and CO<sub>2</sub> were grouped according to their emission range to obtain the M-estimator for each area. In this study, an area 30 km downstream of the dam was considered to be background source, meaning that diffusive emissions of CH<sub>4</sub> and CO<sub>2</sub> from this distance would gradually be reduced to natural emission levels. This distance varied for each field work date due to the hydropower operation and flows as well as the number of days used in the calculations displayed in Tables 5.3 and 5.4. We considered the periods in the THR operation according to their number of days, *i.e.* emptying (85 days), dry (85 days), filling (85 days), and full capacity (111 days).

**Table 5.3** Calculation of CH<sub>4</sub> emissions over the entire THR system during the monitoring period.

Fieldwork	DE upstream area (kg d <sup>-1</sup> )	DE downstream area <sup>(1)</sup> (kg d <sup>-1</sup> )	[A+B] x days (kg tri <sup>-1</sup> )	CH <sub>4</sub> (ton tri <sup>-1</sup> )	CH <sub>4</sub> -C Carbon (tons tri <sup>-1</sup> )
	(A)	(B)	(C)	(D)	(E)
Jun/2011	3.34E+04	1.15E+03	2.93E+06	2.93E+03	2.20E+03
Sep/2011	2.07E+04	4.75E+02	1.80E+06	1.80E+03	1.35E+03
Dec/2011	2.13E+04	1.22E+03	1.91E+06	1.91E+03	1.43E+03
Mar/2012	2.00E+04	2.02E+03	2.45E+06	2.45E+03	1.84E+03

<sup>(1)</sup> Background area at 30 km distance downstream and DE= diffusive emission; the ratio of 12/16 stands for: Carbon molecular weight/ CH<sub>4</sub> molecular weight; tri = trimester.

Table 5.3 shows that the total CH<sub>4</sub> emitted flux by the entire reservoir system (including upstream and downstream) during its hydropower operational cycle was estimated on 9.09 x 10<sup>3</sup> ton of CH<sub>4</sub>, corresponding to 6.82 x 10<sup>3</sup> ton of carbon into the atmosphere during the 10-month (Jun-2010 to Mar-2012) monitoring period. When expressed in daily mean emission flux, these totals correspond to 9.12 mg CH<sub>4</sub> m<sup>-2</sup>d<sup>-1</sup> or 6.48 mg CH<sub>4</sub>-C m<sup>-2</sup>d<sup>-1</sup>. Fluxes per area were higher upstream in June, 2011, while lowest values were observed downstream in September, 2011.

**Table 5.4** Calculation of CO<sub>2</sub> emissions over the entire THR system during the monitoring period.

Fieldwork	DE upstream area (kg d <sup>-1</sup> )	DE downstream area <sup>(1)</sup> (kg d <sup>-1</sup> )	[A+B] x days (kg tri <sup>-1</sup> )	CO <sub>2</sub> (ton tri <sup>-1</sup> )	CO <sub>2</sub> -C Carbon (tons tri <sup>-1</sup> )
	(A)	(B)	(C)	(D)	(E)
Jun/2011	2.62E+07	2.13E+05	2.24E+09	2.24E+06	6.11E+05
Sep/2011	7.34E+06	1.87E+05	6.40E+08	6.40E+05	1.74E+05
Dec/2011	8.60E+06	1.61E+05	7.44E+08	7.44E+05	2.03E+05
Mar/2012	6.54E+06	1.72E+05	7.45E+08	7.45E+05	2.03E+05

The ratio of 12/44 stands for: Carbon molecular weight/ CO<sub>2</sub> molecular weight.

Table 5.4 shows that the total CO<sub>2</sub> emitted flux by the entire reservoir system (including upstream and downstream) during its hydropower operational cycle was estimated at 4.37 x 10<sup>6</sup> ton of CO<sub>2</sub>, corresponding to 1.19 x 10<sup>6</sup> ton of C into the atmosphere during the studied period. When expressed in daily mean emission flux, these totals correspond to 4,384.5 mg CO<sub>2</sub> m<sup>-2</sup>d<sup>-1</sup> or 1,195.6 mg CO<sub>2</sub>-Carbon m<sup>-2</sup>d<sup>-1</sup>. CO<sub>2</sub> fluxes per area were observed to be higher upstream in June, 2011, and lower downstream in December, 2011. Overall, the GHG fluxes were higher in June, 2011. High fluxes of CO<sub>2</sub> and no correlation with the analysed environmental variables suggest that CO<sub>2</sub> production is likely to be related to the incoming of particulate organic carbon from surrounded areas due to rainfall events.

### **5.4 Discussion**

Diffusive fluxes of methane (CH<sub>4</sub>) and carbon dioxide (CO<sub>2</sub>) gases from the THR were determined through *in situ* sampling using floating chambers, followed by gas chromatographic analysis and validation to certified standards. The determination coefficient (R<sup>2</sup>) was 0.99 for both CH<sub>4</sub> and CO<sub>2</sub> gas, yet the sensibility of the method was greater for CH<sub>4</sub>. Detection limits of quantification were 0.16 µmolmol<sup>-1</sup> and 0.60 µmolmol<sup>-1</sup>, respectively, for CH<sub>4</sub> and CO<sub>2</sub>. Precision (error) was less than 2% for both gases, which is considered good, for both method and analysis. Results of the accuracy were according to the accuracy range established in the method section, namely between 90 and 100%.

Results of gas diffusive flux estimations from the sampling time linear regression model presented some spatial and temporal variability. The presence of some doubtful measurements (outliers) using a linear model to estimate both gases was

noted. These values were attributed to uncertainties from various sources, including bubble interference at the beginning of the *in situ* gas chamber deployment (Lima, 2002; Richey et al., 2002) and wind speed, which were also considered responsible for fluctuations in the CO<sub>2</sub> fluxes (Bastviken et al., 2004). These observed fluctuations illustrate the continuous environmental variability occurring in gas exchanges at the air-water interface. We suggest that these fluctuations do not present errors, but in fact show the natural variability related to a realistic *in situ* sampling and evaluation of GHG emissions from reservoirs and water impoundments.

Interpolation results show a large spatial variability in CO<sub>2</sub> fluxes at the reservoir surface in June and December, 2011. Figure 5.5 shows the spatial distribution of CO<sub>2</sub> fluxes for all field campaigns, with a CO<sub>2</sub> minimum of 31.75 and an extreme maximum of 42,848.48 mg m<sup>-2</sup> d<sup>-1</sup>. Only the surface fluxes of CO<sub>2</sub> were significantly different between the studied periods ( $\chi^2 = 26.87$ ,  $p$ -value < 0.0001). Highest fluxes of CO<sub>2</sub> per area were observed upstream of the reservoir and are likely related to rainfall runoff inflow events. Precipitation events are responsible for the flush of terrestrial carbon into surface waters, increasing CO<sub>2</sub> concentrations and emissions through degradation of organic matter (Deemer et al., 2016).

Large areas emitting CH<sub>4</sub> fluxes were found in the main body of the THR, with some individual fluxes being less than 10 mg m<sup>-2</sup> d<sup>-1</sup>. Sites nearby the dam (outlets) such as D1, D2 and D3 revealed high CH<sub>4</sub> fluxes in June, 2011, suggesting that fluxes may increase due to higher turbulence in the zone immediately downstream of the dam (Vachon et al., 2010; Zhao et al., 2013); moreover, these sites are located in shallower areas than those upstream, with a maximum average depth of 18.10 m in September, 2011. CH<sub>4</sub> fluxes at reservoir outlets (e.g. spillways, etc.) have been reported to contribute significantly to the total emission (DelSontro et al., 2011; IHA, 2010). Although no significant correlation was observed between water depth and CH<sub>4</sub> fluxes in this research, CH<sub>4</sub> emissions have been reported to be depth dependent (Bastviken et al., 2004). Greater water depths favour dilution rates of CH<sub>4</sub> gas in the water column, therefore deeper areas in the reservoir are likely to cause lower CH<sub>4</sub> emissions to the atmosphere (Bambace et al., 2007; Zhao et al., 2013).

Relatively increased CH<sub>4</sub> fluxes were observed at sites located near populated areas such as the D9 site, which showed greater fluxes in the sampling periods of b, c, and d (Figure 4). Sites influenced by anthropogenic activities such as soil degradation and/or release of wastewater, may add to the risk of increasing GHG emissions (IHA, 2010). The excess of nutrients, released to the reservoir from anthropogenic

activities, is a causal factor for eutrophication, which can eventually promote hypoxic or anoxic conditions in the reservoir, therefore increasing CH<sub>4</sub> emissions (Straskraba and Tundisi, 2013). In this study, we observed a significant correlation between CH<sub>4</sub> fluxes and nitrate, Chl-*a*, dissolved oxygen, and temperature in June, 2011, and a weak correlation between these parameters during the other sampling periods.

The value range of CH<sub>4</sub> and CO<sub>2</sub> gas emissions but also the high spatial and temporal variations in GHG emissions observed here are in agreement with previous measurements and findings of Santos and Rosa (2005) and others. These authors reported values for GHG emissions from the Tucuruí reservoir during two campaigns in 1998-1999 with significant variation from 15 to 129 mgm<sup>-2</sup>d<sup>-1</sup> for CH<sub>4</sub> and 5,350 to 10,433 mg m<sup>-2</sup>d<sup>-1</sup> for CO<sub>2</sub>, but collate with the measured spatial and temporal variability in our four (2011-2012) observation campaigns.

We also compared the THR to other tropical hydroelectric reservoirs. The total mean diffusive fluxes from the THR in the studied period were 19.37 mg m<sup>-2</sup> d<sup>-1</sup> for CH<sub>4</sub> and 4731.66 mg m<sup>-2</sup> d<sup>-1</sup> for CO<sub>2</sub>. Compared to mean fluxes of 3050 mg m<sup>-2</sup> d<sup>-1</sup> for CO<sub>2</sub> of the Gatun Lake in Panama, THR shows similar results, while mean flux of CH<sub>4</sub> is considerably lower as the Gatun Lake mean values are 537 mg m<sup>-2</sup> d<sup>-1</sup> (Therrien, 2003). The THR showed lower values of both CH<sub>4</sub> and CO<sub>2</sub> of those reported in the Petit Saut reservoir in French Guiana, with mean values of 824 mg m<sup>-2</sup> d<sup>-1</sup> and 8475 mg m<sup>-2</sup> d<sup>-1</sup> (Therrien, 2004).

The results presented in this study come from an analysis different from those used in the consulted literature. The methodology of these works usually use mean values to estimate emissions over a certain spatial and temporal scales, while here the Tukey's biweight M-estimator was used. These findings indicate that deriving mean or average values of GHG emissions of reservoirs will be accompanied by a high uncertainty. However, this reinforces the value of experimental measurements and assessment of the spatial and temporal variabilities of these emission processes. Additionally, each reservoir has its own environmental and biochemical characteristics and history, which makes comparisons between them purely descriptive.

The GHG emissions observed in the THR has been a focus of ongoing discussions in the Amazon region for a while, however these emissions cannot be attributed solely to the impoundment per se. It is because a large part of the organic material causing these emissions comes from surrounding vegetated areas and anthropic activities outside the reservoir, *e.g.* the inflow of domestic sewage without treatment

of urban areas located in the same drainage basin (Straskraba and Tundisi, 2013). Certainly, Amazonian dams contribute in some way, to the increase of GHG emissions. However, it must be accounted that these emissions are fundamentally due to the lack of management of the water resources in the area of influence of the reservoir and not the presence of the reservoir itself (Tundisi and Tundisi, 2012). Thus, the management of resources should aim at reducing eutrophication sources, to avoid not only local problems such as, harmful algal blooms and fish kills, but also, to avoid increasing the GHG emissions into the atmosphere, which is a global concern.

### **5.5 Conclusions**

This study showed that a conjunctive use of *in situ* sampling, high precision gas chromatography and geospatial analysis (including use of remote sensing data) is an appropriate methodology to estimate GHG emissions of large reservoirs, taking the fluctuating water surfaces into account. We fully admit that much more still needs to be understood, especially about the production of carbon dioxide and methane gases and spatiotemporal behaviour of gas emissions in reservoir impoundments and areas. In this study, we analysed the possibility of generating total reservoir GHG fluxes from a number of *in situ* observations using integration of the site sampling and laboratory GHG determination results over the whole reservoir grid area based on geospatial analysis and interpolation. The evaluation of the seasonal fluctuations in the reservoir water surface area using satellite data permitted the calculation of the average emissions as a function of the seasons as well as the reservoir operation rules. These analysis outputs are essential to assessing the GHG emission impact of the entire system over longer periods.

In this study, the total CH<sub>4</sub> emitted into the atmosphere during the study period (June 2011-May 2012) by the entire reservoir system was estimated to be  $6.82 \times 10^3$  ton of carbon, while the total CO<sub>2</sub> emitted was estimated to be  $1.19 \times 10^6$  ton of carbon, a much higher contribution than by methane.

At the seasonal scale, the spatial heterogeneity of CO<sub>2</sub> surface fluxes could be linked to natural short-term variations at the different sampling environments and to weather phenomena such as tropical storm events with high precipitation and winds. Higher spatial variability was observed in June (when the reservoir begins the emptying phase) and December (when the reservoir starts the filling phase).

We observed that results of GHG fluxes at the upstream and downstream reference sites showed higher emission values than those in the main body of the reservoir,

therefore these reference site measurements were not used in the emission calculations of the reservoir impoundment

In our opinion, drawbacks of this study remain the field conditions (and sampling of a very large complex dendritic reservoir surface area) and the relatively limited number of sampling sites for this spatial scale, making improvement to the fitting of the empirical semivariograms difficult. This constraint may increase the uncertainty in the results, and we suggest that more sampling sites must be included to improve the interpolation method used here. We can, however, comment that the technical feasibility of spatially denser and more frequent *in situ* sampling of such large reservoir systems will come at considerable financial cost, including equipment and manpower requirements. Additionally, we believe that the natural variability in gas emission at the air-water interface is contributing to the lesser fitting of the experimental semivariograms.

A main advantage of the approach used here is the visualization of the temporal and spatial distribution of the GHG fluxes, which allows for the identification of emission hot spots. Although, we used only point-based sampling with gas diffusion chambers, combined with surface area assessment and geospatial interpolation, the seasonal patterns of GHG emissions could be determined from the 22 sampling sites covering the reservoir regions, including the main water body, and the upstream and downstream and comparison sites.

## Appendix 5.1 Validation results

**Linearity:** values obtained in this experiment are described in appendices 5.1-5.4.

Appendix 5.1 Linearity results of CH<sub>4</sub>

C ( $\mu\text{mol mol}^{-1}$ )	Area 1 ( $\mu\text{Vmin}$ )	Area 2 ( $\mu\text{Vmin}$ )	Area 3 ( $\mu\text{Vmin}$ )	Mean
0.984	36.5	36.8	35.9	36.4
1.962	76.9	76.0	77.8	76.9
3.065	122.1	121.3	120.9	121.4

Appendix 5.2 Linearity results of CO<sub>2</sub>

C ( $\mu\text{mol mol}^{-1}$ )	Area 1 ( $\mu\text{Vmin}$ )	Area 2 ( $\mu\text{Vmin}$ )	Area 3 ( $\mu\text{Vmin}$ )	Mean
1.509	14.6	14.8	14.9	14.8
379.1	3656.9	3647.3	3634.0	3646.1
705.3	6778.7	6799.8	6767.0	6781.8

Appendix 5.3 Residuals from CH<sub>4</sub> linearity.

C ( $\mu\text{mol mol}^{-1}$ )	Predicted value	R <sub>1</sub>	R <sub>2</sub>	R <sub>3</sub>	SD	95% confidence
0.984	36.6	-0.1	0.2	-0.7	0.46	1.14
1.962	76.5	0.4	-0.5	1.3	0.90	2.24
3.065	121.6	0.5	-0.3	-0.7	0.61	1.52

Appendix 5.4 Residuals from CO<sub>2</sub> linearity

C ( $\mu\text{mol mol}^{-1}$ )	Predicted value	R <sub>1</sub>	R <sub>2</sub>	R <sub>3</sub>	SD	95% confidence
1.509	15.0	-0.4	-0.2	-0.1	0.15	0.38
379.1	3645.6	11.3	1.7	-11.6	11.50	28.57
705.3	6782.6	-3.9	17.2	-15.6	16.62	41.29

### Detection and quantification limits

Data used in the detection limits was obtained from the analytical curve and the established acceptance criteria was that analysed sampling concentration may be equal or greater than the calculated quantification limit. Results are in appendix 5.5.

**Appendix 5.5** Detection and quantification limits obtained from gas chromatography of CH<sub>4</sub>.

Intercept (y)		Slope	LOD ( $\mu\text{mol/mol}$ )	LOQ ( $\mu\text{mol/mol}$ )
Correlation coefficient	SE			
3.6082	0.648	40.8514	0.05	0.16

**Appendix 5.6** Detection and quantification limits obtained from gas chromatography of CO<sub>2</sub>.

Intercept (y)		Slope	LOD ( $\mu\text{mol/mol}$ )	LOQ ( $\mu\text{mol/mol}$ )
Correlation coefficient	SE			
0.4733	0.566	9.6152	0.20	0.60

### Precision

Repeatability was accomplished by multiple injections of the samples by the same analyst under the same analytical conditions at the same day and intermediate precision was determined using two analysts under different analytical conditions, during two days. Results are in appendices 5.7 and 5.8.

The sensitivity (or precision) and intermediate precision were determined using the coefficient of variation (%CV) or relative standard deviation (RSD). The results in appendices 5.9 and 5.10 show values lower than 2%, indicating a good precision of the method and of the analyst.

Appendix 5.7 Repeatability for CH<sub>4</sub>.

Injections	CH <sub>4</sub> (μmol mol <sup>-1</sup> )	Peak area (μVmin)	%CV
1 <sup>a</sup>	0.984	36.5	1.26
2 <sup>a</sup>		36.8	
3 <sup>a</sup>		35.9	
1 <sup>a</sup>	1.962	76.9	1.17
2 <sup>a</sup>		76.0	
3 <sup>a</sup>		77.8	
1 <sup>a</sup>	3.065	122.1	0.50
2 <sup>a</sup>		121.3	
3 <sup>a</sup>		120.9	

Appendix 5.8 Repeatability for CO<sub>2</sub>.

Injections	CO <sub>2</sub> (μmol mol <sup>-1</sup> )	Peak area(μVmin)	%CV
1 <sup>a</sup>	1.509	14.6	1.03
2 <sup>a</sup>		14.8	
3 <sup>a</sup>		14.9	
1 <sup>a</sup>	379.1	3656.9	0.32
2 <sup>a</sup>		3647.3	
3 <sup>a</sup>		3634.0	
1 <sup>a</sup>	705.3	6778.7	0.25
2 <sup>a</sup>		6799.8	
3 <sup>a</sup>		6767.0	

**Appendix 5.9** Intermediate precision of CH<sub>4</sub>.

Injections	CH <sub>4</sub> (μmol mol <sup>-1</sup> )	Area 1 (μVmin)	Area 2 (μVmin)	%CV
1 <sup>a</sup>	0.984	36.5	36.6	1.78
2 <sup>a</sup>		36.8	38.3	
3 <sup>a</sup>		35.9	37.2	
1 <sup>a</sup>	1.962	76.9	76.7	1.20
2 <sup>a</sup>		76.0	76.3	
3 <sup>a</sup>		77.8	78.1	
1 <sup>a</sup>	3.065	122.1	122.4	0.54
2 <sup>a</sup>		121.3	121.0	
3 <sup>a</sup>		120.9	121.6	

**Appendix 5.10** Intermediate precision of CO<sub>2</sub>.

Injections	CO <sub>2</sub> (μmol mol <sup>-1</sup> )	Area 1 (μVmin)	Area 2 (μVmin)	%CV
1 <sup>a</sup>	1.509	14.6	14.8	1.03
2 <sup>a</sup>		14.8	14.6	
3 <sup>a</sup>		14.9	14.9	
1 <sup>a</sup>	379.1	3656.9	3646.4	0.75
2 <sup>a</sup>		3647.3	3628.2	
3 <sup>a</sup>		3634.0	3710.6	
1 <sup>a</sup>	705.3	6778.7	6791.5	0.23
2 <sup>a</sup>		6799.8	6821.2	
3 <sup>a</sup>		6767.0	6801.7	

### Accuracy

Results on the accuracy are shown in tables 5.11 and 5.12. The acceptance range was between 90 and 110%.

Appendix 5.11 Accuracy for CH<sub>4</sub>.

Injections	CH <sub>4</sub> standard ( $\mu\text{mol mol}^{-1}$ )	CH <sub>4</sub> found ( $\mu\text{mol mol}^{-1}$ )	Percent recovery
1	0.984	0.972	
2	0.984	0.966	
3	0.984	0.999	
4	0.984	0.960	
5	0.984	0.999	
6	0.984	0.989	100.3%
7	0.984	0.984	
8	0.984	1.011	
9	0.984	0.982	
10	0.984	0.982	

Appendix 5.12 Accuracy for CO<sub>2</sub>.

Injections	CH <sub>4</sub> standard ( $\mu\text{mol mol}^{-1}$ )	CH <sub>4</sub> found ( $\mu\text{mol mol}^{-1}$ )	Percent recovery
1	379.1	372.82	
2	379.1	373.14	
3	379.1	373.02	
4	379.1	371.86	
5	379.1	376.06	
6	379.1	385.86	99.9%
7	379.1	371.05	
8	379.1	377.29	
9	379.1	386.53	
10	379.1	402.92	

**Semivariogram fitting model parameters**

**Appendix 5.13** Methane – Field 1 (Jun/2011): data transformed with square root.

Model	C <sub>0</sub>	C	Range [m]	μ <sub>jk</sub>	σ <sub>jk</sub>	DR (%)
Spherical	0.826	2.471	80.355	0.005	0.639	74.937
Exponential	<b>0.774</b>	<b>3.520</b>	<b>59.811</b>	<b>0.001</b>	<b>0.659</b>	<b>81.976</b>
Gaussian	1.211	2.157	41.653	0.005	0.651	64.053
Eyefit	1.190	3.020	59.280	0.006	0.713	71.734

**Appendix 5.14** Methane – Field 2 (Sep/2011): data not transformed.

Model	C <sub>0</sub>	C	Range [m]	μ <sub>jk</sub>	σ <sub>jk</sub>	DR (%)
Spherical	<b>2.240</b>	<b>25.053</b>	<b>57.731</b>	<b>-0.010</b>	<b>0.755</b>	<b>91.792</b>
Exponential	<b>0.000</b>	<b>28.628</b>	<b>23.780</b>	<b>-0.025</b>	<b>0.728</b>	<b>100.000</b>
Gaussian	5.987	21.409	28.693	-0.001	0.720	78.147
Eyefit	6.220	23.330	32.180	0.003	0.764	78.951

**Appendix 5.15** Methane – Field 3 (Dec/2011): data transformed with square root.

Model	C <sub>0</sub>	C	Range [m]	μ <sub>jk</sub>	σ <sub>jk</sub>	DR (%)
Spherical	1.018	1.398	86.351	0.012	0.868	57.871
Exponential	<b>0.896</b>	<b>1.760</b>	<b>44.595</b>	<b>0.012</b>	<b>0.843</b>	<b>66.270</b>
Gaussian	1.242	1.208	44.987	0.014	0.924	49.307
Eyefit	1.090	1.440	32.640	0.016	0.850	56.917

**Appendix 5.16** Methane – Field 4 (Mar/2012): data not transformed.

Model	C <sub>0</sub>	C	Range [m]	μ <sub>jk</sub>	σ <sub>jk</sub>	DR (%)
Spherical	0.000	999.759	61.578	0.025	1.462	100.000
Exponential	<b>0.000</b>	<b>1239.145</b>	<b>44.758</b>	<b>0.024</b>	<b>1.370</b>	<b>100.000</b>
Gaussian	98.499	908.551	30.086	-0.006	2.375	90.219
Eyefit	137.170	1063.030	38.600	-0.008	2.018	88.571

**Appendix 5.17** Geospatial analysis and semivariograms details.

Equations used in geospatial analysis:

$$\gamma(L) = \frac{1}{2N(L)} \sum_{i=1}^{N(L)} [Z(x_i + L) - Z(x_i)]^2$$

where,  $\gamma(L)$  is the semivariogram function,  $Z(x_i + L)$  is the value of the variable at point  $x_i + L$ ,  $Z(x_i)$  is the value of the variable at point  $x_i$ ,  $N(L)$  is the number of pairs separated by a distance  $L$ , and  $x_i$  is a measure of position  $x_i$ .

The theoretical semivariogram models were fitted using the method of weighted least squares, which was previously used to evaluate the performance of three semivariogram models: spherical, exponential, and gaussian, respectively.

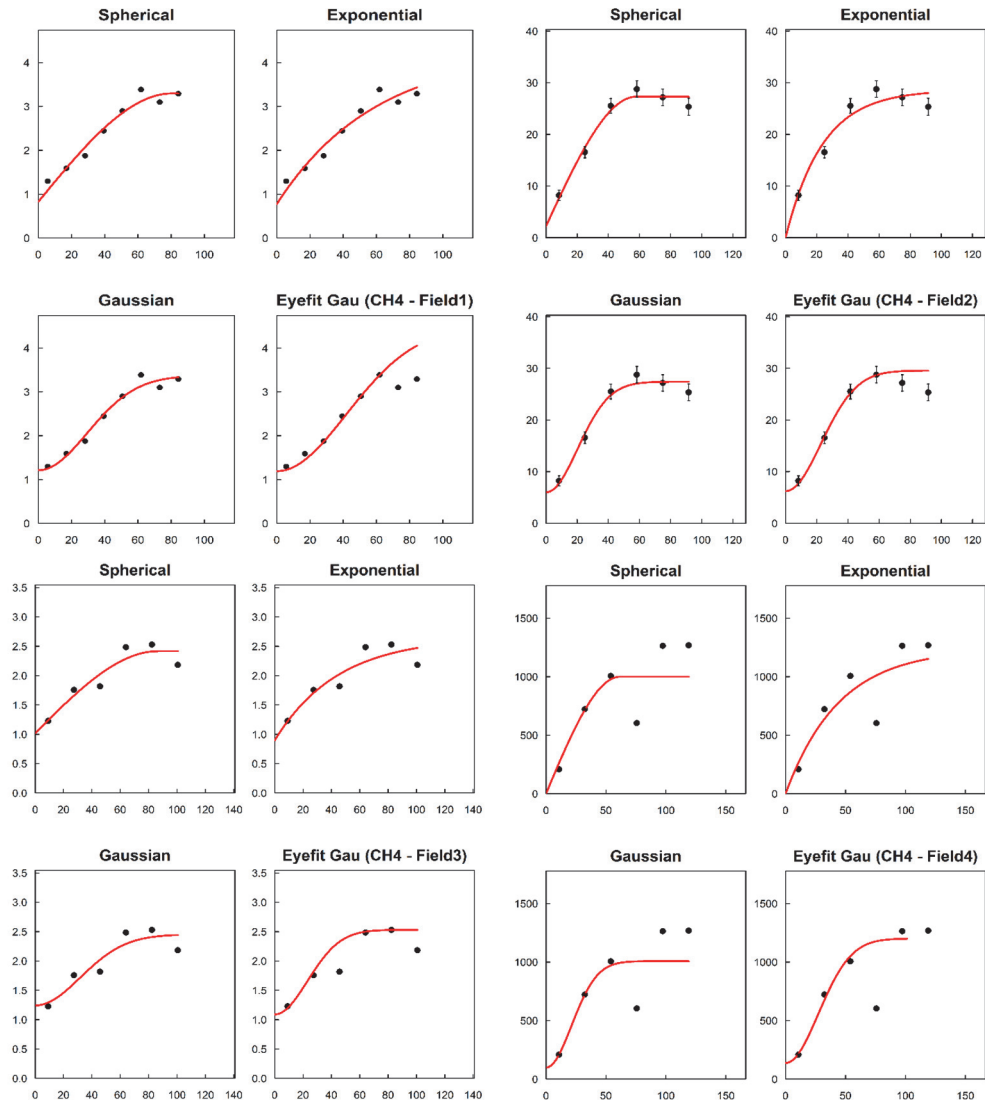
$$\gamma(L) = \begin{cases} C_0 + C \left[ \frac{3h}{2A} - \frac{1}{2} \left( \frac{h}{A} \right)^3 \right] & \text{for } 0 < h \leq A \\ C_0 + C & \text{for } h > A \\ 0 & \text{for } h = 0 \end{cases}$$

$$\gamma(L) = \begin{cases} C_0 + C \left[ 1 - \exp\left(-\frac{h}{A}\right) \right] & \text{for } 0 < h \\ 0 & \text{for } h = 0 \end{cases}$$

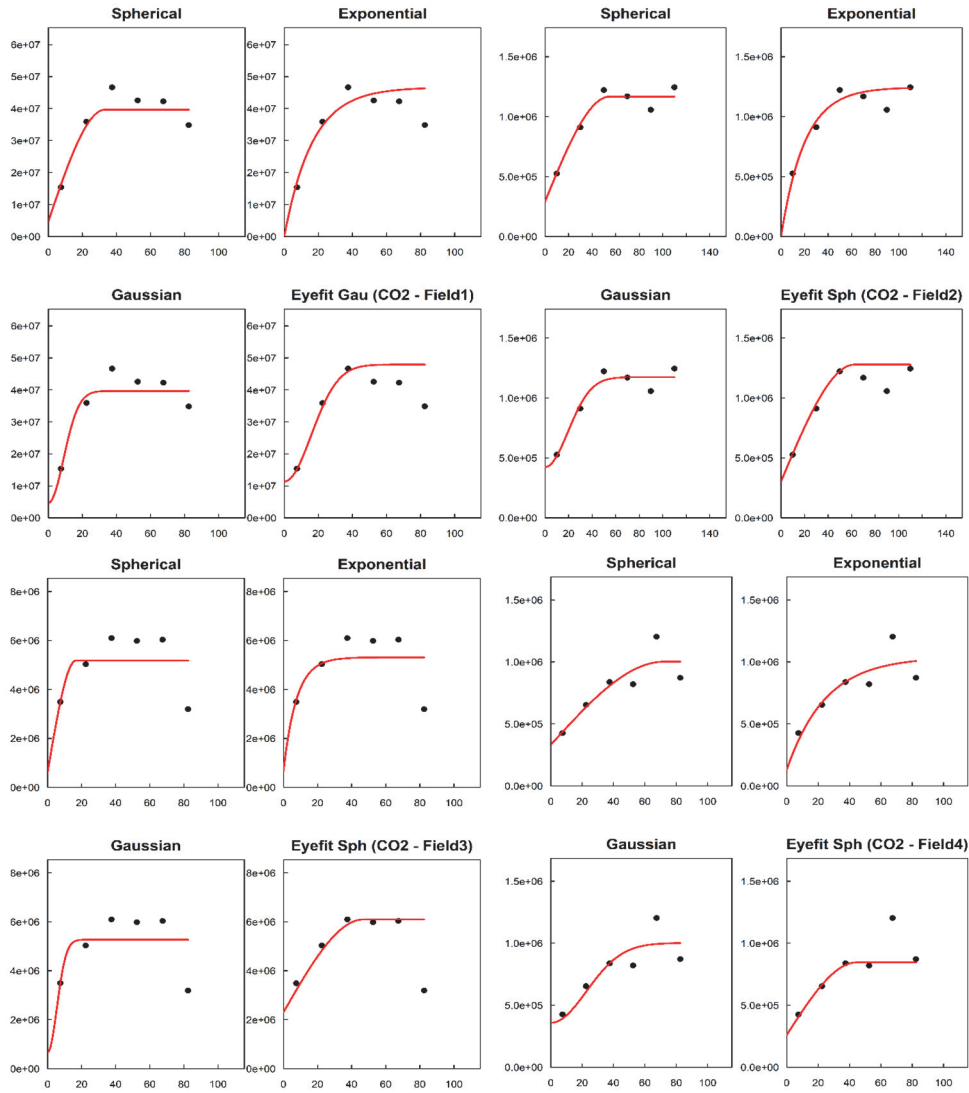
$$\gamma(L) = \begin{cases} C_0 + C \left[ 1 - \exp\left(-\frac{h^2}{A^2}\right) \right] & \text{for } 0 < h \\ 0 & \text{for } h = 0 \end{cases}$$

Where  $C_0$  is the nugget effect,  $C$  is the dispersion of variance,  $C_0 + C$  estimates the variance of a random process and is known as the “sill” (Oliver and Webster, 2014), and  $A$  is the range [m].

Appendix 5.18 Semivariograms for methane.



Appendix 5.19 Semivariograms for carbon dioxide.







## **6.1 Introduction**

Several hydroelectric power dams were built in the Amazon region as a result of industrial and socio-economic developments of Brazil in the last decades. These constructions are well known for causing certain environmental impacts. Anthropogenic modifications of the natural aquatic ecosystem, such as the conversion of water courses into hydroelectric reservoir impoundments are known to cause several disturbances within these ecosystems namely, changes in the storage of nutrients and their recycling for instance (Tundisi et al., 2014). Regional and local anthropic actions can also have a significant influence on regional and global carbon balance as well as on the surface and subsurface water biogeochemistry.

Hydropower reservoirs are aquatic ecosystems characterized by complex functioning subsystems (physical, chemical and biological). They have different hydrological and morphometric characteristics with both horizontal and vertical patterns, which may vary with the geographic region in which they are located. The main uses of reservoirs are electric power generation, domestic water supply, flood control, recreation, amongst others (Chapman, 2016).

Conservation and management of water resources in hydropower reservoirs depends significantly on information about water quality and how it changes in the spatial and temporal domains (Straskraba and Tundisi, 2013). Conventionally, the study of water quality within these ecosystems is based on systematic point sampling which however does not represent the whole system, especially in the case of large reservoirs. Remote sensing data have a potential to observe and study these large aquatic environments because they provide synoptic information over the whole reservoir areas, by capturing the spectral signals and their variabilities that occur and reflect from the water body.

This research proposed to integrate geospatial information with *in situ* water quality monitoring to improve on the cost efficiency of environmental management schemes for hydropower reservoirs. Accordingly, with results obtained in the various investigations conducted in this study, it is possible to conclude that the synergy between geospatial analysis and *in situ* observation is a most desirable and efficient approach to monitor the water quality of these large aquatic tropical ecosystems.

## 6.2 Main results

### i. Seasonal variation of phytoplankton is an indicator of anthropic activities in surrounding areas of hydroelectric reservoirs.

Hydroelectric reservoirs are considered semi-enclosed water bodies with characteristics of rivers and lakes, usually having a high social and economic importance (Straskraba and Tundisi, 2013) as they usually are constructed with the purpose of promoting multiple uses, such as water supply for agriculture and human population, energy generation, fishing and tourism (Tundisi et al., 2012).

The construction of dams affects the dynamics of aquatic ecosystems because it alters the water flow from a lotic to the lentic regime (Bunn and Arthington, 2002). Changes of the water velocity complement these transformations and divide the longitudinal gradient of the water body into three distinct zones (riverine, transitional and lacustrine), with unique physical, chemical and biological characteristics (Chapman, 2016).

In general, reservoirs are subjected to complex functions of natural and artificial forces with dynamics that are distinguished from other natural aquatic ecosystems. In this lake-like habitat, rapid changes occur in the horizontal and vertical circulation patterns, which alter the ecological mechanisms of the formed lake (Tundisi et al., 2008). Additionally, all these changes will depend on other factors such as age, retention time, reservoir operation rules and morphometry (Tundisi et al., 2012).

Reservoirs with dendritic morphometry and which are connected to tributaries are likely to present distinct water chemical compositions, which is due to the spatial and temporal heterogeneity of inflows (Tundisi et al., 1993). Beyond that, reservoir ecosystems are also subject of riparian land occupation and use by populations living in surrounding areas which may contribute to increase point and diffuse sources of water pollution. Among these factors, the increase of nutrients such as phosphorus and nitrogen are a typical cause of excessive algae growth, being harmful to the animal and human health (Conley et al., 2009) (Bellinger and Sigee, 2015). Excessive inputs of nutrients may increase the concentration of organic matter in the reservoirs, and when it is not entirely decomposed in the natural carbon cycle, it leads to the eutrophication process, with consequently water quality degradation and loss of biodiversity (Friedl and Wüest, 2002).

One way to identify the level of degradation and to qualify the trophic state of a water body is through the monitoring of its physical, chemical and biological characteristics. Trophic indexes are useful and aim to classify aquatic bodies in

different trophic classes, and they are assessed through nutrient levels and their effect on algal growth and water transparency (Carlson) (Cunha et al., 2013a). Another way to assess eutrophication in a water body is through the analysis of its phytoplankton community (Reynolds, 2006). This is because phytoplankton is an important indicator of the aquatic environmental conditions. Phytoplankton has a spatial distribution characterized by a great differentiation both along the water column (vertical distribution) and along the surface (horizontal distribution); it has a short life cycle, giving immediate responses to environmental changes (Lee, 2008).

Thus the combined study of phytoplankton taxonomic composition and their successions in space and time provides essential information on spatial and temporal gradients caused by environmental changes of a local water body (Reynolds, 2006).

In chapter 2 of this dissertation the primary goal was to investigate phytoplankton response to nutrient loadings in the surrounding areas of a Brazilian Amazonian reserve, located in a hydropower reservoir area. As phytoplankton typically perform vertical migrations as a result of any change in the environment, it was proposed to take measurements in the temporal and vertical (i.e. water depth) scales. The vertical dimension is the major axis responsible for explaining phytoplankton heterogeneity due to its effect on primary production (Mellard et al., 2011a) as well as energy transfer to high trophic levels (Lampert et al., 2003). The hypothesis of this chapter was that the phytoplankton vertical and temporal distribution correlates with nutrient loads likely caused by human activities in the surrounding areas of this reserve.

The results of this research showed that phytoplankton biomass is largely determined by seasonal changes in the water level of the reservoir and also influenced by abiotic variables such as water temperature, pH, water transparency and nutrient loads.

The water level fluctuations (also introduced by the hydrological operation cycles of the hydropower), within this reservoir is a factor causing changes in phytoplankton structure and composition and not directly human interference (nutrient loading) as established in the hypothesis. Low water levels favor *Desmids* and *Bacillariophyta* phytoplankton groups, indicating a mixed water column while high water levels favor *Cyanophyta*. Even though there are no reports of harmful algae blooms in the waters of this Brazilian Amazonian reserve, the dominance of *Cyanophyta* raises concern to the water management due to their potential impact on human health and aesthetic degradation of aquatic ecosystems.

Other interesting results of this chapter can be cited as i) in the dry season, with less accumulated precipitation and low water levels, turbidity levels increased, whereas, contrastingly suspended solids decreased. The conclusion is that the increase in phytoplankton biomass contributes to increasing turbidity, which is high in the euphotic layer decreasing towards the metalimnion and increasing in the hypolimnion. However, due to the lack of measurements deeper than 15 m, results reported in this chapter are not able to explain that this tendency appears after 10 m where low levels of turbidity are detected increasing towards the bottom layer; ii) regardless of the phytoplankton biomass increase from rainy to dry season, Chl-*a* concentrations decreased. This may be due to *Bacillariophyta* division presenting lower Chl-*a* pigment percentage than the other algal groups. The method used for chlorophyll estimation (extraction by acetone) also did not include absorbance for fucoxanthin, the major pigment of this phytoplankton division.

**ii. The synergy between water limnology and satellite imagery to identify algal blooms extent.**

Algal blooms are potentially detectable through satellite imagery because of the magnitude and spectral behavior of the remote sensing reflectance ( $R_{rs}$ ,  $sr^{-1}$ ) vary due to the presence of pigments other than chlorophyll-*a*, such as chlorophyll-*b*, *c*, and *d*, carotenoids or phycobilins which also contribute to the phytoplankton absorption coefficient (IOCCG, 2014). These pigments can however generate flat features or features with peaks at specific wavelengths in absorption spectra.

Blooms of certain phytoplankton groups such as coccolithophore can be detected due to their high reflectance across the visible spectrum (Smyth et al., 2004). Remote sensing reflectance spectra associated with phytoplankton dominance have minimal values in the spectral region around 440 nm, given the higher absorption of light by the pigments and maximum magnitude in the green region (Kirk, 2010). In optically complex waters, such as hydropower reservoirs, light absorption by colored and dissolved organic matter (CDOM) and other particulate organic materials also contribute to declining remote sensing reflectance in the blue region (Watanabe et al., 2018).

Cyanobacteria of fresh and ocean waters contain phycocyanin and phycobilins as accessory pigments. In diatoms, accessory pigments are chlorophyll-*b* and fucoxanthin (Uitz et al., 2006). To differentiate cyanobacteria from diatoms, authors take into account that backscattering does not vary significantly between these two groups and that the variation in remote sensing reflectance during bloom conditions, is primarily due to the phytoplankton absorption coefficient (Johnsen and Sakshaug,

2007; Whitmire et al., 2007). Thus, these characteristics make it possible to differentiate diatoms and cyanobacteria through remote sensing reflectance during bloom conditions. However, it is essential to take into account that the size of the dominant phytoplankton organism changes the absorption coefficient showing a more flat spectrum in the blue range than in the green of the spectrum (Bricaud et al., 2004).

Cyanobacteria blooms can develop in diverse environments (Bellinger and Sigeo, 2015), and it is because of this algae group is formed by strategic organisms adapted to a wide variety of environmental conditions. Their specific characteristics are determined by a range of features, including cellular physiology (presence of gas vesicles within cells allow regulation of buoyancy) and physiological response (light and nutrient availability), cell size and structure, and general morphology allow them to become prevalent over other phytoplankton groups (Havens, 2008).

Cyanobacteria harmful algal blooms (CHABs) form an increasing problem globally in all types of water bodies due to increasing eutrophication (Chorus, 2012; Figueiredo et al., 2004; Repavich et al., 1990; Sivonen et al., 1989). The presence or absence of particular cyanobacteria species may signal the ecological status of a water body; the dominance of cyanobacteria has been particularly useful as an indicator for a high nutrient status (Chorus and Bartram, 1999). Thus, monitoring of cyanobacteria blooms in drinking water and reservoirs with secondary uses is necessary (Randolph et al., 2008). However, estimating the occurrence of CHABs hot spots in unmeasured locations using traditional sampling methods is very difficult (Backer, 2002; Pitois et al., 2000; Randolph et al., 2008).

Several studies have focused on detecting phytoplankton blooms using satellite imagery in the ocean and coastal waters (IOCCG, 2014; Morales et al., 2011). In inland waters, such as reservoirs, however, these studies are scarce, or few of those studies are using hyperspectral sensors (Hestir et al., 2015; Kudela et al., 2015). Even with their free access and availability, multispectral satellite sensor, such as Landsat 8 and Sentinel are not being greatly explored in inland waters studies. This is due to difficulties of implementing algorithms for a small number of spectral bands (Ogashawara et al., 2014).

The Operational Land Imager (OLI) sensor onboard the Landsat-8 satellite has shown potential regarding application in studies on aquatic environments (Pahlevan et al., 2014). OLI images were used by Torbick and Corbiere (2015) to estimate cyanobacteria density using empirical models, and Huang (2016b) emphasized the

value of OLI images based on the blue to green spectral region for assessing waters with a low to medium amount of biomass of blue-green algae.

In chapter 3 of this dissertation, a multidisciplinary approach is presented, based on both the ecological and the optical perspective to identify algal blooms extent. The primary goal of this research was to investigate if the combination of water limnology and satellite imagery is a suitable approach to identify CHAB extent in hydroelectric reservoirs. The motivation of this study was based on the characteristics of an Amazonian hydroelectric reservoir water conditions (with low/medium Chlorophyll-a) and using the literature review of Huang (2016b) and Ogashawara et al. (2017).

An understanding of the ecological characteristics of reservoirs, including biophysical and chemical features, is vital for their water management. Biological studies are essential to assess uses of water in reservoirs due to their close relation to the effects of algal blooms (Reichwaldt and Ghadouani, 2012). Enhanced phytoplankton growth is a primary concern for policy and management mainly when the reservoir is used for recreation, aquaculture or potable water supplies (Chapman, 2016).

Main conclusions of this chapter are i) even though the ecological and optical approaches showed both drawbacks and advantages, the main finding is that the OBPG algorithm exhibited good performance for estimating the spatial and temporal variability in Chl-a concentrations. However, this algorithm may be applied using OLI/L8 imagery to study areas with periods of little cloud cover on a temporal scale and with good understanding of the study area water limnology; ii) the OBPG algorithm showed a good performance for this study area, which was not expected due to the use of the blue-green ratio. However, the explanation for such a result might be that the oligotrophic to mesotrophic classification between July and September yielded remote sensing reflectance towards the blue-green region. Additionally, this study area presents low turbidity and color concentrations from July to September as shown in the supplementary material (Figures S3 and S5); iii) Despite the limitations of the  $SA_{red-NIR}$  algorithm, it showed that it is possible to flag algal bloom occurrence with some a priori knowledge of the study area and availability of limnological and remote sensing data.

A general conclusion is that further study on the bio-optical properties of Amazonian reservoir waters would be beneficial in order to better understand the water quality issues in these areas.

**iii. Identifying environmental factors influencing the eutrophication process in hydroelectric reservoirs**

Chapter 4 and 5 present the results of our research on two main environmental issues of hydropower reservoirs i.e., **eutrophication and greenhouse gas emissions**, with particular focus on the Tucuruí, as an example of a large tropical impoundment. The objective of chapter 4 was to assess the eutrophication status in hydropower reservoirs considering their operational hydrological cycles and longitudinal zones formed after dam construction. The main motivation of this study was the absence of a trophic index that is adequately calibrated for Amazon waters. Cunha et al. (2013a) calibrated the trophic index that Carlson (1977), first developed for temperate zones, for tropical and subtropical reservoirs. However, their study only uses data sampled in the Southeast region of Brazil, not including the Amazon, which presents different water chemistry, climatic, topological and morphological features. These indexes cannot be universally applied, as the trophic conditions in each case will depend on the complexity of the ecosystems in which the reservoirs are inserted (Cunha et al., 2013a; Tundisi et al., 2006b)). In this case, other characteristics such as morphometry, hydrology, climatic factors and water nutrients, should be considered in eutrophication evaluation processes (Silvino and Barbosa, 2015).

In the study carried out in chapter 4, generalized linear models were applied, using linear regression with gamma and inverse normal response for the analysis of positive asymmetric data, to assess the water quality in the Tucuruí hydroelectric reservoir, with the aim to distinguish between the impact of the hydrological operation cycle and biogeochemical variables on eutrophication and reservoir areas or zones most vulnerable to eutrophication.

Questions arising and posed were **i)** will the hydrological operation cycles i.e. the filling and full stages, where nutrient input is typically greater due to the higher occurrence of rainfall and runoff inflow induce higher eutrophication conditions? **ii)** is the area with the greatest eutrophication vulnerability the riverine zone that suffers most from the direct impact of organic material entry in the system? To answer these questions, two generalized linear regression models were used for positive asymmetric data: the gamma response model utilizes for chlorophyll-a as the response variable and total phosphorus and dissolved oxygen as the explanatory variables, while the inverse normal model utilizes transparency as the response variable and chlorophyll-a, total phosphorus and dissolved oxygen as the explanatory variables. The hydrological cycle and the longitudinal zones were considered factors in both analyses.

Using this approach, the gamma model indicated that, in the filling stage, chlorophyll-a concentrations were lower than in the dry stage, and concentrations in the riverine and transitional zones were significantly higher than in the lacustrine zone. The conclusion was that the use of GLMs are, thus, useful for determining reservoir areas and operation cycles most vulnerable to eutrophication processes. Contrary to what was hypothesized, the riverine zone was not the most vulnerable to the eutrophication process, as algae growth (chlorophyll-a concentration) is influenced not only by nutrient availability but also by other optimum growth conditions such as light, calm waters, as found in the transitional zone. Thus, high chl-a concentrations, which is expected to increase the risk of algal bloom occurrence, are strongly connected to the hydrological operation cycle of reservoirs, with consequences in the longitudinal zones.

The approach developed and applied in chapter 4 offers a good prospect for future work because it provides crucial information that can aid in monitoring the water quality of hydroelectric reservoirs with dendritic features and dynamic hydrological operation cycles, as these factors are well known to influence the water quality. In addition, these statistical inference models can also provide information on the temporal and spatial scales and can be used in integrated approaches for ecosystem management in the area of influence of reservoirs.

**iv. Conjunctive use of geospatial analysis with *in situ* monitoring to estimate greenhouse gas emissions from reservoirs.**

Eutrophication of inland waters is a global concern because this process may contribute to accelerating water quality degradation. Eutrophication and associated massive algal growth is also related to primary production of aquatic ecosystems, which in turn has an impact on the global carbon and other biogeochemical cycles. Typical consequences of eutrophication are an increase of suspended and dissolved matter, decreased oxygen concentrations in the water, the release of phosphorus from sediments, harmful algal blooms, fish deaths and risk to human health (Straskraba and Tundisi, 1999).

Generally, reservoirs built with the purpose of electric power generation face two stages. The first stage goes from the initial period of filling the reservoir and lasts approximately five years (Tundisi et al., 2012). In this stage greenhouse gas emissions are known to rapidly increase, reaching a short-term peak with a trend to decline over the years. Impacts caused by reservoirs during the filling phase have been much discussed (Richard et al 2005, Abe et al 2005). During this phase, there are rapid and intensified processes occurring in the newly formed lake, such as the abrupt

transition of a lotic into a lentic environment, flooding of different biomes with several types of vegetation having different amounts of biomass, and showing different decomposition rates (Bunn and Arthington, 2002; Ferreira, 2015).

The second stage corresponds to the dominance of the permanent emissions of the reservoir. In this phase, the main sources of gases are the biomass formed in the reservoir itself, which reaches the reservoir by its tributaries and the contribution of the residual biomass (Tremblay, 2005). Over the years, after the filling stage, reservoirs tend to stabilize because of the decay of the main sources of organic matter that contribute to the GHG production (St. Louis et al., 2000).

In hydroelectric reservoirs, GHG gases are produced when the organic matter available (dissolved) in the water and in the sediments is degraded under aerobic and/or anaerobic conditions (Rosa et al., 2004). This organic matter is derived from different sources including surrounding land occupation, organic matter submerged during the filling phase, allochthonous origin (from the drainage basin), and autochthonous material (generated in the reservoir system itself due to photosynthesis) (Bunn and Arthington, 2002). Emissions are affected by several factors including the physiographic features of the reservoir, climatic conditions and the hydrological operation cycle (Straskraba and Tundisi, 1999).

Researchers have been dedicated to understanding the complexity of the biogeochemical and physical processes behind the GHGs emission in reservoirs. Although it is known that they are spatially heterogeneous systems, most surveys lack the consideration of this spatial and temporal heterogeneity.

Chapter five of this dissertation describes an approach different from previous studies, which is based on a combination of *in situ* gas sampling with laboratory chemical analysis, geostatistics, and remote sensing to model the spatial and temporal variations in CO<sub>2</sub> and CH<sub>4</sub> emissions from the THR.

Diffusive fluxes of methane (CH<sub>4</sub>) and carbon dioxide (CO<sub>2</sub>) gases from the THR were determined using *in situ* gas sampling with floating chambers, followed by gas chromatographic analysis and validation to certified gas standards.

In this study, we examined the possibility of generating the entire reservoir GHG fluxes from a number of *in situ* observations integrating the site sampling and laboratory results over the whole reservoir grid area based on geospatial analysis and interpolation. The evaluation of the seasonal fluctuations in the reservoir water

surface area using satellite data permitted the calculation of the average emissions as a function of the seasons as well as the reservoir operation rules. These analysis outputs are essential in assessing the GHG emission impact of the entire system over more extended time periods and e.g. full operation cycle of the hydropower reservoir system.

The results of chapter 5 show that a conjunctive use of *in situ* sampling, high precision gas chromatography and geospatial analysis (including the use of remote sensing data) is an appropriate methodology to estimate GHG emissions of large reservoirs, taking the fluctuating water surfaces into account. However, this study also admits that much more still needs to be understood, especially about the production of carbon dioxide and methane gases and the spatiotemporal behavior of gas emissions of tropical reservoir impoundments and reservoir areas.

Another advantage of the approach used in chapter 3 is the visualization of the temporal and spatial distribution of the GHG fluxes, which allows for the identification of emission hot spots. The drawbacks of this study remain the field conditions (and sampling of a very large complex dendritic reservoir surface area) and the relatively limited number of sampling sites for this spatial scale, making spatial interpolation and an improvement to the fitting of the empirical semivariograms difficult. We can however observe that in fact, any methodology for GHG emission monitoring of large fluctuating water bodies will be confronted with the *in situ* observation and sample number problem. This is due to the technical feasibility and the considerable financial cost related to these environmental monitoring activities.

### **6.3 Research contributions**

- i. This research explores perspectives and possibilities of extending conventional point-based monitoring of water quality in tropical hydroelectric reservoirs with remote sensing and geospatial analysis methods.
- ii. It provides an in-depth analysis of two main environmental problems associated with hydroelectric reservoirs: eutrophication and greenhouse gases emission. Results are described in chapters 4 and 5, respectively;
- iii. The combined use of *in situ* gas sampling, laboratory gas chromatography with remote sensing data to obtain information of the seasonal reservoir area fluctuations and geospatial interpolation techniques, permitted to assess the greenhouse gas (GHG) emissions as a function of the seasons as well as the reservoir operation rules. This spatio-temporal analysis can be considered essential to assess the GHG emission impact of entire reservoir systems over more extended periods.

- iv. Another advantage of the approach used in chapter 5 is its visualization capacity of the temporal and spatial distribution of the GHG fluxes, which allows for the identification of emission hot spots.
- v. This study also contributed to improving phytoplankton sampling strategies (number of sampling depths and repetitions in time during a day) to obtain total phytoplankton biomass for reservoirs or lakes with medium deep (e.g. > 10m) water columns. The main advantage of sampling phytoplankton in vertical and temporal scales is the ability to identify species response to environmental changes. This experiment permitted to advise on sampling strategies for monitoring phytoplankton in lakes and reservoirs.
- vi. This research also contributed to deliver a search approach algal bloom occurrence patterns in space and time, and based on ecological preferences for conditions (such as physical, chemical and biological). We think that, maps showing algal bloom probable occurrence can be of great help to water management decision-makers.
- vii. Overall, this research contributed to developing and validating approaches that can aid monitoring the water quality of tropical hydroelectric reservoirs with dendritic characteristics and dynamic hydrological operation cycles. Approaches developed here, provide information in temporal and spatial scales and can be used in integrated water management monitoring in reservoirs.

#### **6.4 Research recommendations**

- i. The use of statistical GLMs was proven useful for determining reservoir areas and hydrological operation cycles most vulnerable to eutrophication processes. Future research is suggested in order to provide a more precise integrated assessment of the main factors related to water quality in reservoirs, such as riparian land use, human activities and degradation of surrounding areas, aiming to promote the sustainable use of the dam-lake-reservoir environment.
- ii. As described in chapter 5, the drawbacks of this study remained the field conditions (and sampling of a very large complex dendritic reservoir surface area), resulting in a relatively limited number of sampling sites for this spatial scale. This makes direct application of geospatial interpolation and improvement to the fitting of the empirical semivariograms difficult. This constraint may increase the uncertainty in the results, and this dissertation suggests that more sampling sites must be included to improve the interpolation method used here. It can, however, be commented that the technical feasibility of spatially denser and more frequent *in situ* sampling of

such large reservoir systems will come at a considerable financial cost, including equipment and workforce requirements.

In this dissertation, the use of robust estimators when studying diffusive emissions of GHGs sampled with static gas chambers in dendritic hydroelectric reservoirs, is greatly advised. It is because of the natural variability in gas emission at the air-water interface within these complex environments, with different compartments and limnological characteristics. These factors significantly contribute to fluctuations in the analysis and should not always be considered as outliers or sampling errors.

- iii. This study recommends that cyanobacteria or phytoplankton continue to be carefully monitored in this area to ensure that their ecological functioning is wisely considered when attempting to map their occurrence, using limited available satellite imagery (due to cloud cover).
- iv. It is suggested that further studies on the bio-optical properties of Amazonian reservoir waters will be beneficial to local water management in order to better understand the water quality issues in these areas, and to use new and future remote sensing systems.

### ***6.5 Future research paths:***

- i. Assess phytoplankton functional type response to GHGs emission in reservoirs due to their interference in the carbon cycle;
- ii. Consider the applicability of other and new remote sensing products for simulation and validation of GHGs emission in reservoirs such as newly launched satellites, Landsat 8 and the ESA Sentinel's series among others;
- iii. Consider the development of a model to parameterize optically active components in tropical lakes and reservoirs of the Amazon region using *in situ* radiometric measurements.
- iv. Study the impacts of climate change and climate variability at regional and local scales and their potential effects on eutrophication and CHABs formation.



---

## Bibliography

---

- Alsdorf D, Bates P, Melack J, Wilson M, Dunne T. Spatial and temporal complexity of the Amazon flood measured from space. *Geophysical Research Letters* 2007; 34: n/a-n/a.
- Alves ICC, El-Robrini M, Santos MdLS, Monteiro SdM, Barbosa LPF, Guimarães JTF. Qualidade das águas superficiais e avaliação do estado trófico do Rio Arari (Ilha de Marajó, norte do Brasil). *Acta Amazonica* 2012; 42: 115-124.
- ANA. Agencia Nacional de Aguas. 2017, 2017.
- Ansari AA, Gill SS, Lanza GR, Rast W. *Eutrophication: causes, consequences and control*: Springer, 2011.
- APHA. American Public Health, Association. *Standard Methods for the Examination of Water and Wastewater*. 21st ed, Washington DC, 2005, pp. 1220p.
- Apha A. WPCF, *Standard methods for the examination of water and wastewater*. American Public Health Association/American Water Works Association/Water Environment Federation, Washington DC, USA 1995.
- Araújo FR, González-Pérez SE, Lopes MA, Viégas IdJM. Ethnobotany of babassu palm (*Attalea speciosa* Mart.) in the Tucuruí Lake Protected Areas Mosaic-eastern Amazon. *Acta Botanica Brasilica* 2016; 30: 193-204.
- Atkinson AC. *Plots, transformations and regression; an introduction to graphical methods of diagnostic regression analysis*, 1985.
- Babish G. *Geostatistics without tears. A Practical Guide to Geostatistics (Variograms, Kriging, eds)* 2000; 4.
- Backer LC. Cyanobacterial Harmful Algal Blooms (CyanoHABs): Developing a Public Health Response. *Lake and Reservoir Management* 2002; 18: 20-31.
- Bambace L, Ramos F, Lima I, Rosa R. Mitigation and recovery of methane emissions from tropical hydroelectric dams. *Energy* 2007; 32: 1038-1046.
- Barata ASdN. *Ambiente e o ordenamento do território: a questão ambiental dos desmatamentos em áreas protegidas na Amazônia: estudo de caso na RDS (Reserva de Desenvolvimento Sustentável) Alcobaça, Tucuruí, Pará-Brasil*, 2011.
- Baraúna RA, Graças DA, Miranda PR, Ghilardi R, Barbosa MS, Schneider MPC, et al. Prokaryotic Diversity of the Tucuruí Hydropower Plant Reservoir in the Brazilian Amazon. *Aquatic Science and Technology* 2012; 1.
- Barbosa JEdL, Souza Andrade R, Paiva Lins R, Diniz CR. Diagnóstico do estado trófico e aspectos limnológicos de sistemas aquáticos da Bacia Hidrográfica

- do Rio Taperoá, Trópico semi-árido Brasileiro. *Revista de Biologia e Ciências da Terra* 2006.
- Barros N, Cole JJ, Tranvik LJ, Prairie YT, Bastviken D, Huszar VL, et al. Carbon emission from hydroelectric reservoirs linked to reservoir age and latitude. *Nature Geoscience* 2011; 4: 593-596.
- Bastviken D, Cole J, Pace M, Tranvik L. Methane emissions from lakes: Dependence of lake characteristics, two regional assessments, and a global estimate. *Global biogeochemical cycles* 2004; 18.
- Bastviken D, Tranvik LJ, Downing JA, Crill PM, Enrich-Prast A. Freshwater methane emissions offset the continental carbon sink. *Science* 2011; 331: 50-50.
- Becker V, Caputo L, Ordonez J, Marce R, Armengol J, Crossetti LO, et al. Driving factors of the phytoplankton functional groups in a deep Mediterranean reservoir. *Water Research* 2010; 44: 3345-3354.
- Bellinger EG, Sigeo DC. *Freshwater algae: identification and use as bioindicators*: John Wiley & Sons, 2015.
- Bicudo C, Menezes M. *Cyanophyceae/Cyanobacteria*, 2006.
- Bicudo CEM, Bicudo RMT. *Algas de águas continentais brasileiras. Algas de águas continentais brasileiras*. Funbec, 1970.
- Bilous OP, Barinova SS, Ivanova NO, Huliaieva OA. The use of phytoplankton as an indicator of internal hydrodynamics of a large seaside reservoir – case of the Sasyk Reservoir, Ukraine. *Ecohydrology & Hydrobiology* 2016.
- Bonansa M, Rodriguez MC, Pinotti L, Ferrero S. Using multi-temporal Landsat imagery and linear mixed models for assessing water quality parameters in Río Tercero reservoir (Argentina). *Remote Sensing of Environment* 2015; 158: 28-41.
- Bousquet P, Ciais P, Miller J, Dlugokencky E, Hauglustaine D, Prigent C, et al. Contribution of anthropogenic and natural sources to atmospheric methane variability. *Nature* 2006; 443: 439-443.
- Boyer JN, Kelble CR, Ortner PB, Rudnick DT. Phytoplankton bloom status: Chlorophyll a biomass as an indicator of water quality condition in the southern estuaries of Florida, USA. *Ecological Indicators* 2009; 9: S56-S67.
- Brandao ILdS, Mannaerts CM, Saraiva ACF. Seasonal variation of phytoplankton indicates small impacts of anthropic activities in a Brazilian Amazonian reserve. *Ecohydrology & Hydrobiology* 2017.
- Bricaud A, Claustre H, Ras J, Oubelkheir K. Natural variability of phytoplanktonic absorption in oceanic waters: Influence of the size structure of algal populations. *Journal of Geophysical Research: Oceans* 2004; 109.

- Brivio PA, Giardino C, Zilioli E. Determination of chlorophyll concentration changes in Lake Garda using an image-based radiative transfer code for Landsat TM images. *International Journal of Remote Sensing* 2001; 22: 487-502.
- Bukata RP, Jerome JH, Kondratyev AS, Pozdnyakov DV. *Optical Properties and Remote Sensing of Inland and Coastal Waters*: CRC Press, 1995.
- Bunn SE, Arthington AH. Basic Principles and Ecological Consequences of Altered Flow Regimes for Aquatic Biodiversity. *Environmental Management* 2002; 30: 492-507.
- Carl JS, Stuart RJ, Stephen JH, Alan AM, Pedro R, José P, et al. Models of open populations with space-limited recruitment in stochastic environments: relative importance of recruitment and survival in populations of *Semibalanus balanoides*. *Marine Ecology Progress Series* 2004; 275: 185-197.
- Carlson RE. A trophic state index for lakes. *Limnology and oceanography* 1977; 22: 361-369.
- Chapman D. *Water quality assessment-a guide to the use of biota, sediments and water in environmental monitoring*. CRC Press, New York, 2016.
- Chapman DV. *Water quality assessments: a guide to the use of biota, sediments, and water in environmental monitoring*. 1996.
- Chenl Y. Effects of pH on the growth and carbon uptake of marine phytoplankton. *Marine Ecology Progress Series* 1994.
- Chien YC, Wu SC, Chen WC, Chou CC. Model simulation of diurnal vertical migration patterns of different-sized colonies of *Microcystis* employing a particle trajectory approach. *Environmental engineering science* 2013; 30: 179-186.
- Chorus EI, Bartram J. *Toxic cyanobacteria in water: a guide to their public health consequences, monitoring and management*. London: WHO, 1999.
- Chorus I. *Cyanotoxins: occurrence, causes, consequences*. Berlin: Springer Science & Business Media, 2012.
- Chorus I, Bartram J. *Toxic Cyanobacteria in Water*. London: Taylor & Francis, 2002.
- Coesel PF. Structural characteristics and adaptations of desmid communities. *The Journal of Ecology* 1982: 163-177.
- Cole JJ, Cole JJ, Caraco NF, Caraco NF. Carbon in catchments: connecting terrestrial carbon losses with aquatic metabolism. *Marine and Freshwater Research* 2001; 52: 101-110.
- Cole JJ, Prairie YT, Caraco NF, McDowell WH, Tranvik LJ, Striegl RG, et al. Plumbing the global carbon cycle: integrating inland waters into the terrestrial carbon budget. *Ecosystems* 2007; 10: 172-185.

- Conley DJ, Paerl HW, Howarth RW, Boesch DF, Seitzinger SP, Havens KE, et al. Controlling eutrophication: nitrogen and phosphorus. *Science* 2009; 323: 1014-1015.
- Cooke GD, Welch EB, Peterson S, Nichols SA. Restoration and management of lakes and reservoirs: CRC press, 2016.
- Cordeiro GM, Neto EdAL. Modelos paramétricos. Pernambuco: UFRPE 2004.
- Costa LS, Huszar VLM, Ovale AR. Phytoplankton Functional Groups in a Tropical Estuary: Hydrological Control and Nutrient Limitation. *Estuaries and Coasts* 2009; 32: 508-521.
- Cunha CJs. Variação espacial e temporal do fitoplâncton do reservatório da usina hidrelétrica de Tucuruí-Pará. Instituto de Ciências Biológicas. Master degree. Universidade Federal do Pará, Belém, Brazil, 2013.
- Cunha DGF, do Carmo Calijuri M, Lamparelli MC. A trophic state index for tropical/subtropical reservoirs (TSI tsr). *Ecological Engineering* 2013a; 60: 126-134.
- Cunha EDdS, Cunha ACd, Silveira Jr AMd, Faustino SMM. Phytoplankton of two rivers in the eastern Amazon: characterization of biodiversity and new occurrences. *Acta Botanica Brasílica* 2013b; 27: 364-377.
- Cunha RW, Garcia Jr MDN, Albertoni EF, Palma-Silva C. Qualidade de água de uma lagoa rasa em meio rural no sul do Brasil. *Revista Brasileira de Engenharia Agrícola e Ambiental-Agriambi* 2013c; 17.
- Curtarelli MP, Ogashawara I, Alcântara EH, Stech JL. Coupling remote sensing bio-optical and three-dimensional hydrodynamic modeling to study the phytoplankton dynamics in a tropical hydroelectric reservoir. *Remote Sensing of Environment* 2015; 157: 185-198.
- Curtarelli MP, Ogashawara I, de Araújo CAS, Lorenzetti JA, Leão JAD, Alcântara E, et al. Carbon dioxide emissions from Tucuruí reservoir (Amazon biome): New findings based on three-dimensional ecological model simulations. *Science of The Total Environment* 2016; 551: 676-694.
- Daggers TD, Kromkamp JC, Herman PMJ, Van Der Wal D. A model to assess microphytobenthic primary production in tidal systems using satellite remote sensing. *Remote sensing of environment* 2018; 211: 129-145.
- Dai H, Mao J, Jiang D, Wang L. Longitudinal Hydrodynamic Characteristics in Reservoir Tributary Embayments and Effects on Algal Blooms. *PLOS ONE* 2013; 8: e68186.
- Dall'Olmo G, Gitelson AA. Effect of bio-optical parameter variability on the remote estimation of chlorophyll-a concentration in turbid productive waters: experimental results. *Applied Optics* 2005; 44: 412-422.

- Damanik-Ambarita MN, Everaert G, Forio MAE, Nguyen THT, Lock K, Musonge PLS, et al. Generalized Linear Models to Identify Key Hydromorphological and Chemical Variables Determining the Occurrence of Macroinvertebrates in the Guayas River Basin (Ecuador). *Water* 2016; 8: 297.
- Damazio JM, SANTOS M, Xavier VL, Medeiros AM, MARCELINO A, Amorim MA, et al. Uso da mediana para estimativa robusta de taxa de emissão difusiva de gases de efeito estufa em reservatórios a partir de medições pontuais com câmaras flutuantes espacialmente distribuídas. XX Simpósio Brasileiro de Recursos Hídricos 2013.
- Davidson Thomas A, Audet J, Svenning J-C, Lauridsen Torben L, Søndergaard M, Landkildehus F, et al. Eutrophication effects on greenhouse gas fluxes from shallow-lake mesocosms override those of climate warming. *Global Change Biology* 2015; 21: 4449-4463.
- Deemer BR, Harrison JA, Li S, Beaulieu JJ, DelSontro T, Barros N, et al. Greenhouse Gas Emissions from Reservoir Water Surfaces: A New Global Synthesis. *BioScience* 2016; 66: 949-964.
- Dekker AG. Detection of optical water quality parameters for eutrophic waters by high resolution remote sensing. PhD. Vrije Universiteit, Amsterdam, 1993a.
- Dekker AG. Detection of optical water quality parameters for eutrophic waters by high resolution remote sensing. 1993b.
- DelSontro T, Kunz MJ, Kempton T, Wüest A, Wehrli B, Senn DB. Spatial Heterogeneity of Methane Ebullition in a Large Tropical Reservoir. *Environmental Science & Technology* 2011; 45: 9866-9873.
- Deshmukh C. Greenhouse gas emissions (CH<sub>4</sub>, CO<sub>2</sub> and N<sub>2</sub>O) from a newly flooded hydroelectric reservoir in subtropical South Asia: The case of Nam Theun 2 Reservoir, Lao PDR. Université Paul Sabatier-Toulouse III, 2013.
- Desikachary T. Cyanophyta Indian Council of Agricultural Research New Delhi, India. New Delhi: Indian Council of Agricultural Research, 1959.
- Deus R, Brito D, Kenov IA, Lima M, Costa V, Medeiros A, et al. Three-dimensional model for analysis of spatial and temporal patterns of phytoplankton in Tucuruí reservoir, Pará, Brazil. *Ecological Modelling* 2013; 253: 28-43.
- Deutsch CV, Journel A. Geostatistical software library and user's guide. Oxford University Press, New York 1998.
- Devi Prasad AG. Carlson's Trophic State Index for the assessment of trophic status of two lakes in Mandya district. *Advances in Applied Science Research* 2012; 3: 2992-2996.
- Devol A, Richey J, Forsberg BR, Martinelli L. Seasonal dynamics in methane emissions from the Amazon River floodplain to the troposphere. *Journal of Geophysical Research* 1990; 95: 16417-16426.

- Dowell M, Platt T. Partition of the Ocean into Ecological Provinces: Role of Ocean-Colour Radiometry. 2009.
- EEA S. The European Environment: State and Outlook 2010. European Environment Agency, Joint Research Centre. Publications Office of the European Union, Luxembourg. European Environment Agency, Copenhagen, Denmark, 2010.
- Eichner M, Rost B, Kranz SA. Diversity of ocean acidification effects on marine N<sub>2</sub> fixers. *Journal of experimental marine biology and ecology* 2014; 457: 199-207.
- Eletronorte. Usinas do setor elétrico brasileiro. 2016, 2016.
- Espíndola ELG, Matsumura-Tundisi T, Rietzler AC, Tundisi JG. Spatial heterogeneity of the Tucuruí Reservoir (State of Pará, Amazonia, Brazil) and the distribution of zooplanktonic species. *Revista Brasileira de Biologia* 2000; 60: 179-194.
- Esteves FdA. Fundamentos de limnologia, 2011.
- Felip M, Catalan J. The relationship between phytoplankton biovolume and chlorophyll in a deep oligotrophic lake: decoupling in their spatial and temporal maxima. *Journal of Plankton Research* 2000; 22: 91-106.
- Ferreira SP. Estimativa de emissões de gases de efeito estufa em reservatórios de hidrelétricas utilizando técnicas de sensoriamento remoto. Doctor. Universidade Federal do Rio Grande do Sul, Porto Alegre, 2015.
- Figueiredo DRd, Azeiteiro UM, Esteves SM, Gonçalves FJ, Pereira MJ. Microcystin-producing blooms—a serious global public health issue. *Ecotoxicology and environmental safety* 2004; 59: 151-163.
- Finkel ZV, Beardall J, Flynn KJ, Quigg A, Rees TAV, Raven JA. Phytoplankton in a changing world: cell size and elemental stoichiometry. *Journal of plankton research* 2009; 32: 119-137.
- Franz BA, Bailey SW, Kuring N, Werdell PJ. Ocean color measurements with the Operational Land Imager on Landsat-8: implementation and evaluation in SeaDAS. *Journal of Applied Remote Sensing* 2015; 9: 096070-096070.
- Friedl G, Wüest A. Disrupting biogeochemical cycles-Consequences of damming. *Aquatic Sciences* 2002; 64: 55-65.
- Gamito S. Caution is needed when applying Margalef diversity index. *Ecological Indicators* 2010; 10: 550-551.
- Garcia HL, Silva VLd, Marques LP, Garcia CAB, Carvalho FdO. Avaliação da qualidade da água utilizando a teoria fuzzy. 2012.
- Gholizadeh MH, Melesse AM, Reddi L. A comprehensive review on water quality parameters estimation using remote sensing techniques. *Sensors* 2016; 16: 1298.

- Giardino C, Pepe M, Brivio PA, Ghezzi P, Zilioli E. Detecting chlorophyll, Secchi disk depth and surface temperature in a sub-alpine lake using Landsat imagery. *Science of The Total Environment* 2001; 268: 19-29.
- Golterman HL, Clymo RS, Ohnstad MAM. *Methods for Physical and Chemical Analysis of Fresh Waters*. Wageningen: Blackwell Scientific, 1978.
- Gomes AMdA, Sampaio PL, da Silva Ferrão-Filho A. Florações de cianobactérias tóxicas em uma lagoa costeira hipereutrófica do Rio de Janeiro/RJ (Brasil) e suas consequências para saúde humana. *Oecologia brasiliensis* 2009; 13: 329-345.
- Goovaerts P. *Geostatistics for natural resources evaluation: Oxford University Press on Demand*, 1997.
- Gordon HR, Wang M. Retrieval of water-leaving radiance and aerosol optical thickness over the oceans with SeaWiFS: a preliminary algorithm. *Applied optics* 1994; 33: 443-452.
- Gotterman H, Clymo R, Ohnstad M. *IBP Handbook No. 8, Methods for Physical and Chemical Analysis of fresh waters*. Black Well Scientific Publications. Oxford Edinburgh London, Melbourne, 1978.
- Gu B, Schelske CL, Coveney MF. Low carbon dioxide partial pressure in a productive subtropical lake. *Aquatic Sciences* 2011; 73: 317-330.
- Guérin F, Abril G. Significance of pelagic aerobic methane oxidation in the methane and carbon budget of a tropical reservoir. *Journal of Geophysical Research: Biogeosciences* 2007; 112.
- Guisan A, Lehmann A, Ferrier S, Austin M, Overton J, Aspinall R, et al. Making better biogeographical predictions of species' distributions. *Journal of Applied Ecology* 2006; 43: 386-392.
- Gupta M. A New Trophic State Index for Lagoons. *Journal of Ecosystems* 2014; 2014: 8.
- Gurlin D, Gitelson AA, Moses WJ. Remote estimation of chl-a concentration in turbid productive waters—Return to a simple two-band NIR-red model? *Remote Sensing of Environment* 2011; 115: 3479-3490.
- H. SV, Schindler DW. "Eutrophication science: where do we go from here?". *Trends in Ecology & Evolution* 2009; 24: 6.
- Häder DP, Gao K. The Impacts of Climate Change on Marine Phytoplankton. *Climate Change Impacts on Fisheries and Aquaculture: A Global Analysis* 2017; 2: 897-924.
- Harremoës P. The challenge of managing water and material balances in relation to eutrophication. *Water Science and Technology* 1998; 37: 9-17.

- Havens KE. Cyanobacteria blooms: effects on aquatic ecosystems. Cyanobacterial harmful algal blooms: state of the science and research needs. Springer, New York, 2008, pp. 733-747.
- Haydée TO. Aplicação de índices de estado trófico e de qualidade da água na avaliação da qualidade ambiental de um reservatório artificial (Reservatório de Barra Bonita, estado de São Paulo, Brasil). Reservatório de Barra Bonita, estado de São Paulo, Brasil 1997.
- Hess P, Villacorte LO, Dixon MB, Boerlage SF, Anderson DM, Kennedy MD, et al. Harmful Algal Blooms (HABs) and Desalination: A Guide to Impacts, Monitoring and Management. 2017.
- Hestir EL, Brando VE, Bresciani M, Giardino C, Matta E, Villa P, et al. Measuring freshwater aquatic ecosystems: The need for a hyperspectral global mapping satellite mission. *Remote Sensing of Environment* 2015; 167: 181-195.
- Hillebrand H, Dürselen C-D, Kirschtel D, Pollinger U, Zohary T. BIOVOLUME CALCULATION FOR PELAGIC AND BENTHIC MICROALGAE. *Journal of Phycology* 1999; 35: 403-424.
- Hoek C, Mann D, Jahns HM. *Algae: an introduction to phycology*: Cambridge university press, 1995.
- Hollister JW, Milstead WB, Kreakie BJ. Modeling lake trophic state: a random forest approach. *Ecosphere* 2016; 7.
- Houlding S. *3D geoscience modeling: computer techniques for geological characterization*: Springer Science & Business Media, 2012.
- Hu C. A novel ocean color index to detect floating algae in the global oceans. *Remote Sensing of Environment* 2009; 113: 2118-2129.
- Huang J. Detecting the Spatial Patterns of Blue-green Algae in Harsha Lake using Landsat 8 Imagery. Master degree. East China Normal University, Louisiana, 2016a.
- Huang J. Detecting the Spatial Patterns of Blue-green Algae in Harsha Lake using Landsat 8 Imagery. East China Normal University, 2016b.
- Hunter P, Gilvear D, Tyler A, Willby N, Kelly A. Mapping macrophytic vegetation in shallow lakes using the Compact Airborne Spectrographic Imager (CASI). *Aquatic Conservation: Marine and Freshwater Ecosystems* 2010; 20: 717-727.
- Hunter P, Tyler A, Willby N, Gilvear D. The spatial dynamics of vertical migration by *Microcystis aeruginosa* in a eutrophic shallow lake: A case study using high spatial resolution time-series airborne remote sensing. *Limnology and Oceanography* 2008; 53: 2391-2406.
- Hunter PD, Tyler AN, Gilvear DJ, Willby NJ. Using remote sensing to aid the assessment of human health risks from blooms of potentially toxic cyanobacteria. *Environmental Science & Technology* 2009; 43: 2627-2633.

- Huttunen JT, Väisänen TS, Hellsten SK, Heikkinen M, Nykänen H, Jungner H, et al. Fluxes of CH<sub>4</sub>, CO<sub>2</sub>, and N<sub>2</sub>O in hydroelectric reservoirs Lokka and Porttipahta in the northern boreal zone in Finland. *Global Biogeochemical Cycles* 2002; 16.
- ICH. ICH harmonised tripartite guideline: guideline for good clinical practice E6 (R1). International Conference on Harmonisation of Technical Requirements for Registration of Pharmaceuticals for Human Use. 10. Washington, DC, 1996.
- Ideflor-bio. Reserva de Desenvolvimento Sustentável Alcobaça | Ideflor-bio. 2017, 2015.
- Ideflor-bio. Reserva De Desenvolvimento Sustentável Alcobaça, Ideflor-Bio. 2017, 2017.
- IHA. GHG Measurement Guidelines for Freshwater Reservoirs: Derived from: the UNESCO/IHA Greenhouse Gas Emissions from Freshwater Reservoirs Research Project: International Hydropower Association (IHA), 2010.
- INMET. Instituto Nacional de Meteorologia. 2017, 2017.
- INPE. PRODES - Desflorestamento nas Unidades de Conservação. 2018, 2017a.
- INPE. PRODES - Desflorestamento nas Unidades de Conservação. 2017, 2017b.
- IOCCG. Ocean-Color Observations from a Geostationary Orbit. In: Group RotIO-CC, editor. IOCCG, Dartmouth, Canada, 2012, pp. 110.
- IOCCG. Phytoplankton Functional Types from Space. In: Stuart V, editor. IOCCG. Reports and Monographs of the International Ocean-Colour Coordinating Group, Dartmouth, Canada, 2014.
- IOCCG. Remote Sensing of Ocean Colour in Coastal, and Other Optically-Complex, Waters. Vol N0.3. Dartmouth, Canada: IOCCG, 2000.
- ISO. Gas analysis -- Preparation of calibration gas mixtures -- Part 1: Gravimetric method for Class I mixtures (ISO 6142-1:2015), Geneva, 2015, pp. 39.
- Johnsen G, Sakshaug E. Biooptical characteristics of PSII and PSI in 33 species (13 pigment groups) of marine phytoplankton, and the relevance for pulse-amplitude-modulated and fast-repetition-rate fluorometry 1. *Journal of Phycology* 2007; 43: 1236-1251.
- Johnson N, Revenga C, Echeverria J. Managing Water for People and Nature. *Science* 2001; 292: 1071.
- Juanes JA, Guinda X, Puente A, Revilla JA. Macroalgae, a suitable indicator of the ecological status of coastal rocky communities in the NE Atlantic. *Ecological Indicators* 2008; 8: 351-359.
- Kallio K, Kutser T, Hannonen T, Koponen S, Pulliainen J, Vepsäläinen J, et al. Retrieval of water quality from airborne imaging spectrometry of various lake

- types in different seasons. *Science of the Total Environment* 2001; 268: 59-77.
- Kasprzak P, Padisák J, Koschel R, Krienitz L, Gervais F. Chlorophyll a concentration across a trophic gradient of lakes: An estimator of phytoplankton biomass? *Limnologia - Ecology and Management of Inland Waters* 2008; 38: 327-338.
- Kemenes A, Forsberg BR, Melack JM. Methane release below a tropical hydroelectric dam. *Geophysical research letters* 2007; 34.
- Kirk JT. *Light and photosynthesis in aquatic ecosystems*. UK: Cambridge university press, 1994.
- Kirk JTO. *Light and Photosynthesis in Aquatic Ecosystems*: Cambridge University Press, 2010.
- Komárek J, Huber-Pestalozzi G, Fott B. *Das Phytoplankton des Süßwassers: Systematik und Biologie. Teil 7: Hälfte 1. Chlorophyceae (Grünalgen), Ordnung: Chlorococcales*: Schweizerbart, 1983.
- Koponen S, Attila J, Pulliainen J, Kallio K, Pyhälähti T, Lindfors A, et al. A case study of airborne and satellite remote sensing of a spring bloom event in the Gulf of Finland. *Continental Shelf Research* 2007; 27: 228-244.
- Koponen S, Pulliainen J, Kallio K, Hallikainen M. Lake water quality classification with airborne hyperspectral spectrometer and simulated MERIS data. *Remote Sensing of Environment* 2002; 79: 51-59.
- Kudela RM, Palacios SL, Austerberry DC, Accorsi EK, Guild LS, Torres-Perez J. Application of hyperspectral remote sensing to cyanobacterial blooms in inland waters. *Remote Sensing of Environment* 2015; 167: 196-205.
- Kutser T, Pierson DC, Kallio KY, Reinart A, Sobek S. Mapping lake CDOM by satellite remote sensing. *Remote Sensing of Environment* 2005; 94: 535-540.
- Lacis AA, Schmidt GA, Rind D, Ruedy RA. Atmospheric CO<sub>2</sub>: Principal control knob governing Earth's temperature. *Science* 2010; 330: 356-359.
- Lambert M, Fréchet J-L. *Analytical techniques for measuring fluxes of CO<sub>2</sub> and CH<sub>4</sub> from hydroelectric reservoirs and natural water bodies. Greenhouse Gas Emissions—Fluxes and Processes*. Springer, 2005, pp. 37-60.
- Lamparelli MC. *Graus de trofia em corpos d'água do estado de São Paulo: avaliação dos métodos de monitoramento*. 2004.
- Lampert W, McCauley E, Manly BF. Trade-offs in the vertical distribution of zooplankton: ideal free distribution with costs? *Proceedings of the Royal Society of London B: Biological Sciences* 2003; 270: 765-773.
- Landim PMB, Sturaro JR. *Krigagem indicativa aplicada à elaboração de mapas probabilísticos de riscos*. Rio Claro: DGA 2002.
- Lee RE. *Phycology*. New York: Cambridge University Press, 2008.

- Lee S-W, Hwang S-J, Lee S-B, Hwang H-S, Sung H-C. Landscape ecological approach to the relationships of land use patterns in watersheds to water quality characteristics. *Landscape and Urban Planning* 2009; 92: 80-89.
- Lees AC, Peres CA, Fearnside PM, Schneider M, Zuanon JAS. Hydropower and the future of Amazonian biodiversity. *Biodiversity and conservation* 2016; 25: 451-466.
- Li WK, McLaughlin FA, Lovejoy C, Carmack EC. Smallest algae thrive as the Arctic Ocean freshens. *Science* 2009; 326: 539-539.
- Lim J, Choi M. Assessment of water quality based on Landsat 8 operational land imager associated with human activities in Korea. *Environmental monitoring and assessment* 2015; 187: 384.
- Lima IBT. Biogeochemical distinction of methane releases from two Amazon hydroreservoirs. *Chemosphere* 2005; 59: 1697-1702.
- Lima IBTd. Emissão de metano por reservatórios hidrelétricos amazônicos através de leis de potência. Universidade de São Paulo, 2002.
- Lobato TC, Hauser-Davis RA, Oliveira TF, Silveira AM, Silva HAN, Tavares MRM, et al. Construction of a novel water quality index and quality indicator for reservoir water quality evaluation: A case study in the Amazon region. *Journal of hydrology* 2015b; 522: 674-683.
- Lobato TdC, Hauser-Davis RA, de Oliveira TF, Maciel MC, Tavares MRM, da Silveira AM, et al. Categorization of the trophic status of a hydroelectric power plant reservoir in the Brazilian Amazon by statistical analyses and fuzzy approaches. *Science of The Total Environment* 2015; 506-507: 613-620.
- Lobato TdC, Hauser-Davis RA, de Oliveira TF, Maciel MC, Tavares MRM, da Silveira AM, et al. Categorization of the trophic status of a hydroelectric power plant reservoir in the Brazilian Amazon by statistical analyses and fuzzy approaches. *Science of The Total Environment* 2015a; 506-507: 613-620.
- Manyari WV, de Carvalho OA. Environmental considerations in energy planning for the Amazon region: Downstream effects of dams. *Energy Policy* 2007; 35: 6526-6534.
- Marcelino A, Santos M, Xavier V, Bezerra C, Silva C, Amorim M, et al. Diffusive emission of methane and carbon dioxide from two hydropower reservoirs in Brazil. *Brazilian Journal of Biology* 2015; 75: 331-338.
- Margalef R. *Limnología*: Ediciones Omega, 1983.
- McCullagh P, Nelder JA. *Generalized Linear Models*, Second Edition: Taylor & Francis, 1989.
- Mellard JP, Yoshiyama K, Litchman E, Klausmeier CA. The vertical distribution of phytoplankton in stratified water columns. *J Theor Biol* 2011a; 269: 16-30.

- Mellard JP, Yoshiyama K, Litchman E, Klausmeier CA. The vertical distribution of phytoplankton in stratified water columns. *Journal of theoretical biology* 2011b; 269: 16-30.
- Mello NASTd, Brighenti LS, Barbosa FAR, Staehr PA, Bezerra Neto JF. Spatial variability of methane (CH<sub>4</sub>) ebullition in a tropical hypereutrophic reservoir: silted areas as a bubble hot spot. *Lake and Reservoir Management* 2018; 34: 105-114.
- Mendonça R, Barros N, Vidal LO, Pacheco F, Kosten S, Roland F. Greenhouse gas emissions from hydroelectric reservoirs: what knowledge do we have and what is lacking? *Greenhouse Gases-Emission, Measurement and Management*. InTech, 2012.
- Mobley CD. *Light and water : radiative transfer in natural waters*. 1994.
- Morales J, Stuart V, Platt T, Sathyendranath S. *Handbook of Satellite Remote Sensing Image Interpretation: Applications for Marine Living Resources Conservation and Management: EU PRESPO Project*, 2011.
- Moses WJ, Gitelson AA, Berdnikov S, Povazhnyy V. Estimation of chlorophyll- a concentration in case II waters using MODIS and MERIS data—successes and challenges. *Environmental Research Letters* 2009; 4: 045005.
- Mur R, Skulberg OM, Utkilen H. *Cyanobacteria in the environment: A guide to their public health consequences, monitoring and management*. In: Bartram ICAJ, editor. WHO, London, 1999, pp. 15-40.
- Myhre G, Shindell D, Bréon F-M, Collins W, Fuglestedt J, Huang J, et al. Anthropogenic and natural radiative forcing. *Climate change* 2013; 423: 658-740.
- Nelder JA, Baker RJ. *Generalized linear models: Wiley Online Library*, 1972.
- Nguyen THT, Boets P, Lock K, Ambarita MND, Forio MAE, Sasha P, et al. Habitat suitability of the invasive water hyacinth and its relation to water quality and macroinvertebrate diversity in a tropical reservoir. *Limnologica-Ecology and Management of Inland Waters* 2015; 52: 67-74.
- Noernberg MA, Evelyn M. L. de Moraes Novo, Thelma Krug. *Radar System Application For The Management Of Aquatic Plant Infestation In Reservoirs: Advantages And Disadvantages*. *Bol. Ciênc. Geod.* 1999; 5: 41-54.
- Norušis M. *SPSS Base 11.0 guide to data analysis*. Prentice Hall, Upper Saddle River, New Jersey, 2002.
- Novotny V. The danger of hypertrophic status of water supply impoundments resulting from excessive nutrient loads from agricultural and other sources. *Journal of Water Sustainability* 2011; 1: 1-22.
- Nybakken JW, Bertness MD. *Marine biology: an ecological approach: Pearson/Benjamin Cummings*, 2005.

- Ogashawara I, Alcântara EHD, Stech JL, Tundisi JG. Cyanobacteria detection in Guarapiranga Reservoir (São Paulo State, Brazil) using Landsat TM and ETM+ images. *Revista Ambiente & Água* 2014; 9: 224-238.
- Ogashawara I, Li L, Moreno-Madriñán MJ. Slope algorithm to map algal blooms in inland waters for Landsat 8/Operational Land Imager images. *Journal of Applied Remote Sensing* 2017; 11: 012005-012005.
- Okogwu OI, Ugwumba AO. Response of phytoplankton functional groups to fluctuating water level in two shallow floodplain lakes in Cross River, Nigeria. *Inland Waters* 2012; 2: 37-46.
- Oliveira EN, Fernandes AM, Kampel M, Cordeiro RC, Brandini N, Vinzon SB, et al. Assessment of remotely sensed chlorophyll-a concentration in Guanabara Bay, Brazil. *Journal of Applied Remote Sensing* 2016; 10: 026003.
- Oliver M, Webster R. A tutorial guide to geostatistics: Computing and modelling variograms and kriging. Vol 113, 2014.
- Orlik K, Blomqvist P, Brettum P, Cronberg G, Eloranta P. Methods for quantitative assessment of phytoplankton in freshwaters. P. 1: Sampling, processing, and application in freshwater environmental monitoring programmes, 1998.
- Padisák J, Crossetti LO, Naselli-Flores L. Use and misuse in the application of the phytoplankton functional classification: a critical review with updates. *Hydrobiologia* 2009; 621: 1-19.
- Pahlevan N, Lee Z, Wei J, Schaaf CB, Schott JR, Berk A. On-orbit radiometric characterization of OLI (Landsat-8) for applications in aquatic remote sensing. *Remote Sensing of Environment* 2014; 154: 272-284.
- Palmer SCJ, Kutser T, Hunter PD. Remote sensing of inland waters: Challenges, progress and future directions. Elsevier, 2015.
- Papa F, Prigent C, Aires F, Jimenez C, Rossow WB, Matthews E. Interannual variability of surface water extent at the global scale, 1993–2004. *Journal of Geophysical Research: Atmospheres* 2010; 115: n/a-n/a.
- Parekh P, McCully P. A preliminary review of the impact of dam reservoirs on carbon cycling. International Rivers Network, Massachusetts. Massachusetts Institute of Technology, Cambridge, USA, 2004, pp. 8.
- Patz JA, Campbell-Lendrum D, Holloway T, Foley JA. Impact of regional climate change on human health. *Nature* 2005; 438: 310.
- Paula GA. On diagnostics in double generalized linear models. *Computational Statistics & Data Analysis* 2013; 68: 44-51.
- Peel MC, Finlayson BL, McMahon TA. Updated world map of the Köppen-Geiger climate classification. *Hydrology and earth system sciences discussions* 2007; 4: 439-473.

- Perkins T, Adler-Golden S, Matthew MW, Berk A, Bernstein LS, Lee J, et al. Speed and accuracy improvements in FLAASH atmospheric correction of hyperspectral imagery. *Optical Engineering* 2012; 51: 111707-1.
- Pettersson LH, Pozdnyakov D. *Monitoring of harmful algal blooms*. Chichester, UK: Springer Science & Business Media, 2012.
- Pitois S, Jackson M, Wood B. Problems associated with the presence of cyanobacteria in recreational and drinking waters. *International Journal of Environmental Health Research* 2000; 10: 203-218.
- Potes M, Costa MJ, da Silva JCB, Silva AM, Morais M. Remote sensing of water quality parameters over Alqueva Reservoir in the south of Portugal. *International Journal of Remote Sensing* 2011; 32: 3373-3388.
- Prigent C, Papa F, Aires F, Rossow WB, Matthews E. Global inundation dynamics inferred from multiple satellite observations, 1993–2000. *Journal of Geophysical Research: Atmospheres* 2007; 112: n/a-n/a.
- Qi L, Hu C, Duan H, Cannizzaro J, Ma R. A novel MERIS algorithm to derive cyanobacterial phycocyanin pigment concentrations in a eutrophic lake: Theoretical basis and practical considerations. *Remote Sensing of Environment* 2014; 154: 298-317.
- Qin B, Li W, Zhu G, Zhang Y, Wu T, Gao G. Cyanobacterial bloom management through integrated monitoring and forecasting in large shallow eutrophic Lake Taihu (China). *Journal of Hazardous Materials* 2015; 287: 356-363.
- R Development Core Team. *R: A language and environment for statistical computing*. R Foundation for Statistical Computing, Vienna, Austria, 2008.
- R Development Core Team. *R: A language and environment for statistical computing*. R Foundation for Statistical Computing, Vienna, Austria, 2010.
- R Team DC. *R: A language and environment for statistical computing*. In: *Computing RFFS*, editor, Vienna, Austria, 2016.
- Randolph K, Wilson J, Tedesco L, Li L, Pascual DL, Soyeux E. Hyperspectral remote sensing of cyanobacteria in turbid productive water using optically active pigments, chlorophyll a and phycocyanin. *Remote Sensing of Environment* 2008; 112: 4009-4019.
- Reichwaldt ES, Ghadouani A. Effects of rainfall patterns on toxic cyanobacterial blooms in a changing climate: Between simplistic scenarios and complex dynamics. *Water Research* 2012; 46: 1372-1393.
- Repavich WM, Sonzogni WC, Standridge JH, Wedepohl RE, Meisner LF. Cyanobacteria (blue-green algae) in Wisconsin waters: acute and chronic toxicity. *Water research* 1990; 24: 225-231.
- Reynolds CS. *The ecology of phytoplankton*: Cambridge University Press, 2006.

- Reynolds CS, Huszar V, Kruk C, Naselli-Flores L, Melo S. Towards a functional classification of the freshwater phytoplankton. *Journal of Plankton Research* 2002; 24: 417-428.
- Richey JE, Melack JM, Aufdenkampe AK, Ballester VM, Hess LL. Outgassing from Amazonian rivers and wetlands as a large tropical source of atmospheric CO<sub>2</sub>. *Nature* 2002; 416: 617-620.
- Ringeval B, de Noblet-Ducoudré N, Ciais P, Bousquet P, Prigent C, Papa F, et al. An attempt to quantify the impact of changes in wetland extent on methane emissions on the seasonal and interannual time scales. *Global Biogeochemical Cycles* 2010; 24: n/a-n/a.
- Rivoirard J. *Concepts and Methods of Geostatistics. Space, Structure and Randomness*. Springer, 2005, pp. 17-37.
- Roberto MC, Santana NF, Thomaz SM. Limnology in the Upper Paraná River floodplain: large-scale spatial and temporal patterns, and the influence of reservoirs. *Brazilian Journal of Biology* 2009; 69: 717-725.
- Rosa L, Sikar B, dos Santos M, Sikar E. Emissões de dióxido de carbono e de metano pelos reservatórios hidrelétricos brasileiros. Primeiro Inventário Brasileiro de Emissões Antrópicas de Gases de Efeito Estufa. Relatórios de Referência. Instituto Alberto Luiz Coimbra de Pós-Graduação e Pesquisa em Engenharia (COPPE) Ministério da Ciência e Tecnologia (MCT), Brasília, DF, 2002.
- Rosa LP, dos Santos MA, Gesteira C, Xavier AE. A model for the data extrapolation of greenhouse gas emissions in the Brazilian hydroelectric system. *Environmental Research Letters* 2016; 11: 064012.
- Rosa LP, Dos Santos MA, Matvienko B, dos Santos EO, Sikar E. Greenhouse gas emissions from hydroelectric reservoirs in tropical regions. *Climatic Change* 2004; 66: 9-21.
- Rückert GV, Giani A. Effect of nitrate and ammonium on the growth and protein concentration of *Microcystis viridis* Lemmermann (Cyanobacteria). *Brazilian Journal of Botany* 2004; 27: 325-331.
- Ruddick K, Vanhellemont Q, Dogliotti A, Nechad B, Pringle N, Van der Zande D. New opportunities and challenges for high resolution remote sensing of water colour. *Ocean Optics* 2016, Victoria, UK, 2006.
- Sahoo GB, Schladow SG. Impacts of climate change on lakes and reservoirs dynamics and restoration policies. *Sustainability Science* 2008; 3: 189-199.
- Samimi A, Zarinabadi S. Reduction of greenhouse gases emission and effect on environment. *Journal of American Science* 2012; 8: 1011-1015.

- Sandrini G, Ji X, Verspagen JMH, Tann RP, Slot PC, Luimstra VM, et al. Rapid adaptation of harmful cyanobacteria to rising CO<sub>2</sub>. *Proceedings of the National Academy of Sciences* 2016; 113: 9315-9320.
- Sant'Anna CL, Azevedo MTdP. Contribution to the knowledge of potentially toxic Cyanobacteria from Brazil. *Nova Hedwigia* 2000; 71: 359-386.
- Santos MA, Rosa LP. Global warming and hydroelectric reservoirs. COPPE/UFRJ, Electrobras, Rio de Janeiro, Brazil 2005.
- Santos MAD, Rosa LP, Matvienko B, dos Santos EO, Rocha CHEDA, Sikar E, et al. Emissões de gases de efeito estufa por reservatórios de hidrelétricas. *Oecologia Brasiliensis* 2008; 12: 12.
- Santos MAD, Rosa LP, Sikar B, Sikar E, dos Santos EO. Gross greenhouse gas fluxes from hydro-power reservoir compared to thermo-power plants. *Energy Policy* 2006; 34: 481-488.
- Saraiva AGS, Costa DF, Job FE, Lins RP. ÍNDICE DE ESTADO TRÓFICO COMO FERRAMENTA DE QUALIDADE DA ÁGUA DA LAGOA DO PARQUE SOLON DE LUCENA–PB. Bachelor, 2013.
- Schalles JF, Yacobi YZ. Remote detection and seasonal patterns of phycocyanin, carotenoid and chlorophyll pigments in eutrophic waters. *Ergebnisse Der Limnologie* 2000; 55: 153-168.
- Schröder R. Relevant parameters to define the trophic state of lakes. *Archiv fur Hydrobiologie. Stuttgart* 1991; 121: 463-472.
- Silvino RF, Barbosa FAR. Eutrophication potential of lakes: an integrated analysis of trophic state, morphometry, land occupation, and land use. *Brazilian Journal of Biology* 2015; 75: 607-615.
- Simis SG, Peters SW, Gons HJ. Remote sensing of the cyanobacterial pigment phycocyanin in turbid inland water. *Limnology and Oceanography* 2005; 50: 237-245.
- Sivonen K, Himberg K, Luukkainen R, Niemelä S, Poon G, Codd G. Preliminary characterization of neurotoxic cyanobacteria blooms and strains from Finland. *Toxicity Assessment* 1989; 4: 339-352.
- Smith VH, Schindler DW. Eutrophication science: where do we go from here? *Trends in Ecology & Evolution*; 24: 201-207.
- Smith VH, Schindler DW. Eutrophication science: where do we go from here? *Trends in Ecology & Evolution* 2009; 24: 201-207.
- Smyth TJ, Tyrrell T, Tarrant B. Time series of coccolithophore activity in the Barents Sea, from twenty years of satellite imagery. *Geophysical Research Letters* 2004; 31.
- Somerville R. *The forgiving air: understanding environmental change*: Univ of California Press, 1998.

- Soumis N, Duchemin É, Canuel R, Lucotte M. Greenhouse gas emissions from reservoirs of the western United States. *Global Biogeochemical Cycles* 2004; 18.
- Souza R, Souza E, Netto AM, Almeida AQd, Júnior GB, Silva JRI, et al. Assessment of the physical quality of a Fluvisol in the Brazilian semiarid region. *Geoderma Regional* 2017; 10: 175-182.
- Spokas K, Graff C, Morcet M, Aran C. Implications of the spatial variability of landfill emission rates on geospatial analyses. *Waste Management* 2003; 23: 599-607.
- St. Louis VL, Kelly CA, Duchemin É, Rudd JW, Rosenberg DM. Reservoir Surfaces as Sources of Greenhouse Gases to the Atmosphere: A Global Estimate: Reservoirs are sources of greenhouse gases to the atmosphere, and their surface areas have increased to the point where they should be included in global inventories of anthropogenic emissions of greenhouse gases. *AIBS Bulletin* 2000; 50: 766-775.
- Straskraba M, Tundisi JG. Guidelines of lake management-Vo9. Reservoir water quality management. 1999.
- Straskraba M, Tundisi JG. Reservoir Water Quality Management, 2013.
- Straškrabra M, Tundisi JG. Gerenciamento da qualidade da água de represas: diretrizes para gerenciamento de lagos: Oficina de Textos, 2013.
- Strömbeck N, Pierson DC. The effects of variability in the inherent optical properties on estimations of chlorophyll a by remote sensing in Swedish freshwaters. *Science of the total environment* 2001; 268: 123-137.
- Sukenik A, Hadas O, Kaplan A, Quesada A. Invasion of Nostocales (cyanobacteria) to Subtropical and Temperate Freshwater Lakes – Physiological, Regional, and Global Driving Forces. *Frontiers in Microbiology* 2012; 3: 86.
- Sun D, Hu C, Qiu Z, Shi K. Estimating phycocyanin pigment concentration in productive inland waters using Landsat measurements: a case study in Lake Dianchi. *Opt Express* 2015; 23: 3055-74.
- Susanti Y, Pratiwi H. M Estimation, S Estimation, And MM Estimation In Robust Regression. *International Journal of Pure and Applied Mathematics* 2014; 91: 349-360.
- Szeto M, Werdell PJ, Moore TS, Campbell JW. Are the world's oceans optically different? *Journal of Geophysical Research: Oceans* 2011; 116.
- Tan W, Liu P, Liu Y, Yang S, Feng S. A 30-Year Assessment of Phytoplankton Blooms in Erhai Lake Using Landsat Imagery: 1987 to 2016. *Remote Sensing* 2017; 9: 1265.
- Tavares MDRM. Estrutura da comunidade microfítoplanctônica da área de influência da UHE de Tucuruí-Pará, 2011.

- Therrien J. Revue des connaissances sur les gaz à effet de serre des milieux aquatiques—Le gaz carbonique, l'oxide nitreux et le méthane. In: Hydro-Québec RdGcGipà, editor, Québec, 2003, pp. 144.
- Therrien J. Flux de gaz à effet de serre en milieux aquatiques-Suivi 2003. Rapport de GENIVAR Groupe Conseil Inc. présenté à Hydro-Québec 2004.
- Thiemann S, Kaufmann H. Lake water quality monitoring using hyperspectral airborne data—a semiempirical multisensor and multitemporal approach for the Mecklenburg Lake District, Germany. *Remote sensing of Environment* 2002; 81: 228-237.
- Thuiller W. BIOMOD—optimizing predictions of species distributions and projecting potential future shifts under global change. *Global change biology* 2003; 9: 1353-1362.
- Timpe K, Kaplan D. The changing hydrology of a dammed Amazon. *Science Advances* 2017; 3.
- Torbick N, Corbiere M. A Multiscale Mapping Assessment of Lake Champlain Cyanobacterial Harmful Algal Blooms. 2015.
- Tranvik Lars J, Downing John A, Cotner James B, Loiselle Steven A, Striegl Robert G, Ballatore Thomas J, et al. Lakes and reservoirs as regulators of carbon cycling and climate. *Limnology and Oceanography* 2009; 54: 2298-2314.
- Tremblay A. Greenhouse gas Emissions-Fluxes and Processes: hydroelectric reservoirs and natural environments: Springer Science & Business Media, 2005.
- Tundisi, T. Matsumura-Tundisi, J. D. Arantes Junior, J.E.M. Tundisi, N.F. Manzini, Ducrot. R. The response of Carlos Botelho (Lobo, Broa) reservoir to the passage of cold fronts as reflected by physical, chemical, and biological variables. *Brazilian Journal of Biology* 2004; 64: 177-186.
- Tundisi J, Matsumura-Tundisi T, Abe D. The ecological dynamics of Barra Bonita (Tietê River, SP, Brazil) reservoir: implications for its biodiversity. *Brazilian Journal of Biology* 2008; 68: 1079-1098.
- Tundisi JG, Goldemberg J, Matsumura-Tundisi T, Saraiva ACF. How many more dams in the Amazon? *Energy Policy* 2014; 74: 703-708.
- Tundisi JG, Marco Aurélio Santos, Menezes CFS. Experience and Lessons Learned Brief - LBMI Project - Tucuruí Hydroelectric Power Plant. World Lake Database. International Lake Environment Committee Foundation (ILEC) 2006a.
- Tundisi JG, Matsumura-Tundisi T, Abe DS. Climate monitoring before and during limnological studies: a needed integration. *Brazilian Journal of Biology* 2007; 67: 795-796.

- Tundisi JG, Matsumura-Tundisi T, Calijuri MdC. Limnology and management of reservoirs in Brazil. Comparative reservoir limnology and water quality management. Springer, 1993, pp. 25-55.
- Tundisi JG, Matsumura-Tundisi T, Henry R, Rocha O, Hino K. Comparação do estado trófico de 23 reservatórios do Estado de São Paulo: eutrofização e manejo. *Limnologia e manejo de represas* 1988; 1: 165-209.
- Tundisi JG, Matsumura-Tundisi T, Rocha O. Limnologia de águas interiores: impactos, conservação e recuperação de ecossistemas aquáticos. *Águas doces no Brasil: capital ecológico, uso e conservação* 2006b; 3: 203-240.
- Tundisi JG, Tundisi TM. *Limnology*. São Paulo: CRC Press, 2012.
- Tundisi JG, Tundisi TM, Jorgensen SE. *Handbook of inland aquatic ecosystem management*: CRC Press, 2012.
- Tyler JE. The secchi disc. *Limnology and oceanography* 1968; 13.
- Tyokumbur ET, Okorie T. Studies on the distribution and abundance of plankton in Awba stream and reservoir, University of Ibadan. *Open Journal of Ecology* 2013; 03: 273-278.
- Uitz J, Claustre H, Morel A, Hooker SB. Vertical distribution of phytoplankton communities in open ocean: An assessment based on surface chlorophyll. *Journal of Geophysical Research* 2006; 111.
- USEPA. Method 365.3 Phosphorous, All Forms (Colorimetric, Ascorbic Acid, Two Reagent). Office of Research and Development. U.S. Environmental Protection Agency., Cincinnati OH 45268, 1978.
- USGS GS. *Lakes and reservoirs—Guidelines for study design and sampling. Techniques and Methods*, Reston, VA, 2018, pp. 57.
- USGS USGS. "Earth explorer". 2017, 2017.
- Utermöhl H. Zur vervollkommnung der quantitativen phytoplankton-methodik. *Mitt. int. Ver. theor. angew. Limnol.* 9, Stuttgart, Germany, 1958a, pp. 1-38.
- Utermöhl H. *Zur Vervollkommnung der Quantitativen Phytoplankton Methodik*: E. Schweizerbartsche Verlagsbuchhandlung, 1958b.
- Vachon D, Prairie YT, Cole JJ. The relationship between near-surface turbulence and gas transfer velocity in freshwater systems and its implications for floating chamber measurements of gas exchange. *Limnology and oceanography* 2010; 55: 1723-1732.
- Vanhellemont Q, Ruddick K. Turbid wakes associated with offshore wind turbines observed with Landsat 8. *Remote Sensing of Environment* 2014; 145: 105-115.
- Vanhellemont Q, Ruddick K. Advantages of high quality SWIR bands for ocean colour processing: Examples from Landsat-8. *Remote Sensing of Environment* 2015; 161: 89-106.

- Vanhellemont Q, Ruddick K. ACOLITE for Sentinel-2: Aquatic Applications of MSI imagery. Living Planet Symposium; Ouwehand, L., Ed.; ESA Communications: Noordwijk, The Netherlands. 740, 2016.
- Vargas SR. Influência da concentração de nutrientes na interação entre duas espécies fitoplanctônicas isoladas do Reservatório de Itupararanga-SP. Master degree. Universidade de São Paulo, São Paulo, 2012.
- Vermote E, Tanré D, Deuzé J, Herman M, Morcrette J, Kotchenova S. Second simulation of a satellite signal in the solar spectrum-vector (6SV). *Appl. Opt.* 2006; 45: 6762-6774.
- Verspagen JMH, Van de Waal DB, Finke JF, Visser PM, Van Donk E, Huisman J. Rising CO<sub>2</sub> Levels Will Intensify Phytoplankton Blooms in Eutrophic and Hypertrophic Lakes. *PLOS ONE* 2014; 9: e104325.
- Vieira JMP, Pinho JLS, Duarte AALS. Eutrophication vulnerability analysis: a case study. *Water Science and Technology* 1998; 37: 121-128.
- Vieira SR, Carvalho JRPd, González AP. Jack knifing for semivariogram validation. *Bragantia* 2010; 69: 97-105.
- Vieira SR, Paz Gonzalez A. Analysis of the spatial variability of crop yield and soil properties in small agricultural plots. *Bragantia* 2003; 62: 127-138.
- Vincent RK, Qin X, McKay RML, Miner J, Czajkowski K, Savino J, et al. Phycocyanin detection from LANDSAT TM data for mapping cyanobacterial blooms in Lake Erie. *Remote Sensing of Environment* 2004; 89: 381-392.
- Vollenweider RA. Scientific fundamentals of the eutrophication of lakes and flowing waters, with particular reference to nitrogen and phosphorus as factors in eutrophication. Organisation for Economic Co-operation and Development, Paris, France, 1968.
- Wagner T, Erickson LE. Sustainable Management of Eutrophic Lakes and Reservoirs. *Journal of Environmental Protection* 2017; Vol.08No.04: 28.
- Walker WW. Use of hypolimnetic oxygen depletion rate as a trophic state index for lakes. *Water Resources Research* 1979; 15: 1463-1470.
- Watanabe F, Alcântara E, Curtarelli M, Kampel M, Stech J. Landsat-based remote sensing of the colored dissolved organic matter absorption coefficient in a tropical oligotrophic reservoir. *Remote Sensing Applications: Society and Environment* 2018; 9: 82-90.
- Watanabe SF, Alcântara E, Rodrigues WT, Imai NN, Barbosa CC, Rotta HL. Estimation of Chlorophyll-a Concentration and the Trophic State of the Barra Bonita Hydroelectric Reservoir Using OLI/Landsat-8 Images. *International Journal of Environmental Research and Public Health* 2015; 12.

- Waxter MT. Analysis of Landsat Satellite Data to Monitor Water Quality Parameters in Tenmile Lake, Oregon. Master of Science (M.S.). Portland State University, Portland, Oregon, 2014.
- Wetzel RG. Limnology: lake and river ecosystems: gulf professional publishing, 2001.
- Wetzel RG, Likens GE. Composition and Biomass of Phytoplankton. In: Wetzel RG, Likens GE, editors. Limnological Analyses. Springer, New York, 2000, pp. 147-174.
- Whitmire AL, Boss E, Cowles TJ, Pegau WS. Spectral variability of the particulate backscattering ratio. *Optics Express* 2007; 15: 7019-7031.
- Woźniak M, Bradtke K, Darecki M, Krężel A. Empirical Model for Phycocyanin Concentration Estimation as an Indicator of Cyanobacterial Bloom in the Optically Complex Coastal Waters of the Baltic Sea. *Remote Sensing* 2016; 8: 212.
- Xu Y, Zhang M, Wang L, Kong L, Cai Q. Changes in water types under the regulated mode of water level in Three Gorges Reservoir, China. *Quaternary international* 2011; 244: 272-279.
- Yamamoto Y, Nakahara H. The formation and degradation of cyanobacterium *Aphanizomenon flos-aquae* blooms: the importance of pH, water temperature, and day length. *Limnology* 2005; 6: 1-6.
- Zhao Y, Wu B, Zeng Y. Spatial and temporal patterns of greenhouse gas emissions from Three Gorges Reservoir of China. *Biogeosciences* 2013; 10: 1219-1230.



---

## Summary

---

Hydropower reservoirs are man-made artificial aquatic ecosystems that present a high dynamic and complexity in space and time, with interactions between its structural (dam), physical-chemical and biological components. They are important not only for their electrical power generation, but also for other functions such as water supply (e.g. irrigation, drinking and industry water), flood control, fisheries, as ecological wetland, for leisure activities and navigation. However, their construction causes diverse impacts to terrestrial and aquatic systems. In aquatic systems they interfere with the physical and chemical conditions of the water quality due to alterations of the hydrological regime of the dammed river, and with the functioning mechanisms and succession of phytoplankton communities (Tundisi et al., 2008). Terrestrial impacts include loss of fauna and flora, dislocation of population in areas which will be flooded and increase of endemic diseases. Nevertheless, these large constructions largely affect the water environment and their impoundments regularly cause changes leading to degradation of water quality. Typical effects noticed in tropical hydropower reservoirs are eutrophication that leads to recurring algae blooms which can be harmful to human health and greenhouse emissions which is a global concern among researchers around the world due to these gases potential to contribute to global warming.

Conventionally, the study of water quality within hydroelectric reservoirs is based on systematic point sampling which however does not represent the whole system, especially in the case of large lakes. Remote sensing data have a potential to observe and study these large aquatic environments because they provide synoptic information over the whole reservoir areas, by capturing the spectral signals and their variabilities that occur and reflect from the water body.

The main objective of this thesis was to integrate geospatial information with *in situ* water quality monitoring to improve on the cost efficiency of environmental management schemes of hydropower reservoirs in the Amazon region. The main objective was achieved as a combination of four steps. The first step consist of an investigation of phytoplankton diversity and response to environmental disturbance in a sustainable reserve located within the Tucuruí hydroelectric reservoir. Knowledge about phytoplankton community structure helps in assessing the quality of a water body. However, variables related to it are not routinely surveyed in most of the water quality monitoring programs. The research was carried out in the rainy

and dry season when measurements were performed every three hours and at five different depths. A total of 40 water samples were collected to assess temporal variations of abiotic and biotic factors. Physico-chemical parameters were analysed to characterize the ecosystem and relationships between these variables and phytoplankton functional groups were statistically tested. The data were examined using analysis of variance and canonical correspondence analysis. We identified 9 functional groups in both seasons. The functional group M, which represents organisms with developed adaptations to high insolation and stable environments, had a higher relative percentage of contribution to the total biomass in the rainy season. Group P, which tends to be present in the more eutrophic lakes and is tolerant to carbon deficiency, had a higher relative percentage of contribution to the total biomass in the dry season. The results of this step indicated that the fluctuations of the water level reflected in seasonal changes of phytoplankton biomass and environmental variables. Additionally, this experiment permitted to advise on sampling strategies for monitoring phytoplankton in lakes and reservoirs.

The second step was to assess the feasibility of using medium high resolution sensors, such as Landsat-8 OLI sensor in monitoring the spatial distribution and frequency of phytoplankton blooms in the Tucuruí reservoir. Monitoring algal blooms from space is a very challenging task, which becomes particularly difficult when dealing with cyanobacteria blooms. Cyanobacteria are strategic organisms adapted to a wide variety of environmental conditions. In high concentrations, they form scum on the water surface, which is a concern for public health due to the production of toxins, as well as being a nuisance. Knowledge of the ecological role of these organisms is, therefore, essential when trying to estimate their extent from satellite-based data. In this step we present a multidisciplinary approach, based on both the ecological and the optical perspective. This approach is applied in a Brazilian Amazonian reservoir using spatial and temporal scales. We used a slope algorithm based on the red-edge bands of the OLI sensor and the slope algorithm could identify the extent of the algal bloom at both the spatial and temporal scale. Unfortunately, the performance of these algorithms is most likely affected by weather conditions and glint effects. Therefore, this study recommends that cyanobacteria or phytoplankton studies in this area ensure that their ecological functioning is carefully considered when attempting to map their occurrence using limited satellite imagery.

In step three the aim was to identify key environmental factors influencing eutrophication and associated harmful algae bloom occurrences in the Tucuruí hydropower, e.g. human influences and climate forcing (deforestation, human

settlements, aquaculture, reservoir hydrological operation cycles and management, climate variations). The eutrophication of hydroelectric reservoirs is influenced by both anthropogenic and natural factors. The trophic state of a water body is an important variable when characterizing water quality, due to nutrient inputs originating from anthropogenic sources. Few studies have examined the influence of reservoir hydrodynamics on the water quality of its limnological zones. In this context, the relationships between the hydrological cycle of an Amazon reservoir and the water quality in its limnological zones with respect to factors influencing eutrophication processes were assessed herein. Data were collected on the surface area, from 2005 to 2016, at twelve stations distributed upstream the dam. Chlorophyll-*a* (Chl-*a*), water transparency, dissolved oxygen (DO), total phosphorus, orthophosphate, total suspended solids (TSS) and turbidity were determined, as they undergo alterations during the hydrological cycle and present zonal variations. Generalized linear models were used to identify the response of limnological variables in relation to the influence of the hydrological cycle on the water quality of the longitudinal zones. The results indicated that the filling and full cycles display higher eutrophication conditions than the dry and emptying cycles, with mean phosphorus values of 30.42  $\mu\text{gL}^{-1}$  and 30.15  $\mu\text{gL}^{-1}$ . The riverine zone presented higher eutrophication conditions, with mean phosphorus values of 32.32  $\mu\text{gL}^{-1}$ , higher than the limits established in the Brazilian CONAMA 357/2005 resolution for Class 2 lentic environments ( $< 30\mu\text{gL}^{-1}$ ).

In the last step, the aim was to estimate the GHG emissions in the Tucuruí hydroelectric reservoir in temporal and spatial scales using geospatial analysis and to discuss if emissions are related to the eutrophication process due to anthropic activities or climate forcings. Hydroelectric power reservoirs are considered potential contributors to the greenhouse effect in the atmosphere through the emission of methane and carbon dioxide. In the last step, we combined *in situ* sampling and gas chromatography with geostatistical and remote sensing approaches to estimate greenhouse gas (GHG) emissions of a large hydropower reservoir. We used remote sensing data to estimate the water surface and geospatial interpolation to calculate total emissions as a function of reservoir surface area. The  $\text{CH}_4$  and  $\text{CO}_2$  gas concentrations were linearly correlated to sampling time, confirming the adequacy of the *in situ* sampling method to measure GHG diffusive fluxes from reservoir water surfaces. The combination of high purity (99.99%) ISO-norm gas standards with a gas chromatograph, enabled us to achieve low measurement detection limits of 0.87 ppm and 1.22 ppm, respectively, for  $\text{CH}_4$  (using a flame ionization or FID detector) and  $\text{CO}_2$  (using a thermal conductivity or TCD detector). Our results show that  $\text{CO}_2$  emissions are significantly (an order of  $5.10^2 - 10^3$ ) higher than those of  $\text{CH}_4$  in both

the spatial and temporal domain for this reservoir. The total diffusive GHG emissions over a year (June 2011 to May 2012) of the Tucuruí hydropower reservoir being in operation, in units of tons of carbon, added up to  $6.82 \times 10^3$  for CH<sub>4</sub> and  $1.19 \times 10^6$  for CO<sub>2</sub>. We show that *in situ* GHG sampling using small floating gas chambers and high precision gas chromatography can be combined with geospatial interpolation techniques and remote sensing data to obtain estimates of diffusive GHG emissions from large water bodies with fluctuating water surfaces such as hydropower reservoirs. We recommend that more measurements and observations on these emissions are pursued in order to support and better quantify the ongoing discussions on estimates and mitigation of GHG emissions from reservoirs in the Amazon region and elsewhere in the world.

Accordingly, with results obtained in the four step investigations conducted in this research, it is possible to conclude that the synergy between geospatial analysis and *in situ* observation is a most desirable and efficient approach to monitor the water quality of hydroelectric reservoirs.

---

## Samenvatting

---

Waterkracht centrales bestaande uit stuwdammen en reservoirs, zijn door de mens gemaakte kunstmatige aquatische ecosystemen die een hoge dynamiek en complexiteit bezitten in zowel ruimte als tijd, met interacties tussen hun structurele (dam), hydrologische, fysico-chemische en biologische componenten. Ze zijn belangrijk, niet alleen voor de elektriciteitsproductie, maar ook voor andere functies zoals waterreserves (b.v. irrigatie, drinkwater en industrieel water), overstromingscontrole, visserij, ecologisch natuurgebied, recreatie en navigatie.

De bouw van stuwdammen en reservoirs heeft echter meerdere milieueffecten op terrestrische en aquatische ecosystemen. Op aquatisch vlak hebben ze effect op de biologische, fysieke en chemische aspecten van water vanwege de veranderingen in het hydrologische regime van de afgedamde rivier. Ook de functionele mechanismen, e.g. voortplanting van phyto-, bioplankton en vis gemeenschappen ondervinden effect (Tundisi et al., 2012). Terrestrische effecten zijn onder andere verlies van flora en fauna, hersituering van bevolkingen uit de gebieden bij het stuwmeer en een mogelijke toename van endemische ziektes. Echter, deze grote bouwwerken hebben voornamelijk effect op de water ecologie en hun constructie veroorzaakt meestal een verandering die leidt tot vermindering van waterkwaliteit. Typische effecten die opgemerkt zijn in tropische waterkracht centrales zijn o.a. eutrofiëring en massale algenbloei welke nadelig kan zijn voor menselijke gezondheid, bijvoorbeeld bij blauwalgen. Een ander effect is de uitstoot van broeikasgassen die een wereldwijde zorg is bij onderzoekers vanwege het feit dat deze gassen bijdragen aan het opwarmen van de aarde.

Gewoonlijk zijn studies over waterkwaliteit in stuwmeren gebaseerd op systematische punt waarnemingen en monsternames ("*systematic point sampling*"). In vele gevallen vertegenwoordigen deze waarnemingen niet het hele systeem, en zeker niet in het geval van grote meren. Aardobservatie heeft de potentie om deze grote aquatische omgevingen te observeren omdat zij synoptische informatie over het gehele reservoir geven d.m.v. het vastleggen van spectrale signalen van straling die zich voordoet en reflecteert vanuit het waterlichaam.

Het primaire doel van deze thesis was het integreren van geospatiale of ruimtelijke informatie met *in-situ* waterkwaliteit monitoring, met als doel het verbeteren van de kosteneffectiviteit van milieubeheerssystemen van waterkracht centrales en hun

reservoirs in het Amazone gebied. Dit primaire doel werd bereikt middels een combinatie van vier stappen. De eerste stap van dit onderzoek bestond uit onderzoek naar de phytoplankton diversiteit en hun reactie op milieuverstoring in een beschermd natuurgebied, en deelgebied van het grote Tucuruí stuwmeer en reservoir. De meeste variabelen die hieraan gerelateerd zijn, worden niet routinematig onderzocht in de meeste waterkwaliteit monitoring programma's. Dit onderzoek is verricht in het regen- en droogseizoen waarbij metingen zijn gedaan iedere drie uur op vijf verschillende dieptes. In totaal werden 40 watermonsters verzameld om de tijdelijke variabiliteit ("*temporal variations*") van abiotische en biotische factoren te kunnen beoordelen. Fysisch-chemische parameters zijn geanalyseerd om het ecosysteem te kunnen karakteriseren en relaties tussen deze variabelen en phytoplankton functionele groepen werden statistisch getest. De data werd onderzocht middels analyses van variatie en canonieke correspondentie ("*canonical correspondence*") analyse. We hebben 9 verschillende functionele groepen geïdentificeerd in beide seizoenen. De functionele groep M, welke organismen voorstelt die zich hebben aangepast aan hoge isolatie en stabiele omgevingen, droeg met een hoger relatief percentage bij aan de totale biomassa in het regenseizoen. Group P, welke meer aanwezig neigt te zijn in meer eutrofe meren en welke tolerant is aan koolstof-armoede, droeg met een hoger relatief percentage bij aan de totale biomassa in het droogseizoen. Het resultaat van deze stap gaf aan dat het variëren van de waterstand effect had in seizoensgebonden veranderingen van phytoplankton biomassa en omgevingsvariabelen. Aanvullend liet dit experiment ons toe advies te geven over strategieën bij het nemen van monsters met als doel het monitoren van phytoplankton in meren en reservoirs.

De tweede stap was het beoordelen van de haalbaarheid van het gebruik van een middel hoge resolutie satelliet sensor, zoals de Landsat-8 OLI sensor voor het monitoren van de spatiale of ruimtelijke distributie en frequentie van phytoplankton bloei in het Tucuruí reservoir. Het monitoren van algenbloei vanuit de ruimte met optische sensoren is een uitdagende taak in gebieden met frequent wolkendek (zoals de Amazone), en wordt nog eens extra lastig zodra men te maken heeft met cyanobacterie of blauwalgen bloei. Cyanobacteriën zijn strategische organismen die zich hebben aangepast aan verschillende omgevingscondities. In hoge concentraties, vormen ze schuim op het wateroppervlak, wat een grote zorg is voor de volksgezondheid vanwege de productie van giftige stoffen. Tevens maken ze het water dikwijls langer onbruikbaar voor visserij, recreatie en als drinkwater. Kennis van het ecologisch functioneren van deze organismen is daarom essentieel ook voor hun detectie middels satelliet-gebaseerde data. In deze stap presenteren we een multidisciplinaire aanpak gebaseerd op zowel een ecologisch als een optisch

perspectief. Deze aanpak is toegepast op het grote Tucuruí reservoir in de Amazone. We maakten gebruik van een helling of “*slope algoritme*” gebaseerd op de rode – infrarode of “red-edge” golflengte banden van de OLI sensor. Het “slope” algoritme was in staat om het bereik van de algenbloei redelijk te bepalen op zowel spatiale en temporale schaal. Echter, de prestatie van deze algoritmes wordt sterk beïnvloed door weersomstandigheden en wateroppervlak glinsterseffecten. Daarom raden we in deze studie aan, dat cyanobacterie- of phytoplanktonstudies in dit gebied zich ervan verzekeren dat hun ecologisch functioneren nauwkeurig is mee overwogen bij het in kaart brengen van hun voorkomen wanneer gebruik wordt gemaakt van een gelimiteerd aantal satellietbeelden. Gezien het zeer frequent voorkomen van wolken, zijn niet zoveel satelliet opnames voor deze vochtige tropische gebieden voorhanden.

In stap drie was het doel, het identificeren van de belangrijkste omgevingsfactoren die invloed hebben op eutrofiëring en aanverwante schadelijke algenbloei in het Tucuruí stuwmeer, zoals menselijke invloeden en klimaat “forcing” (ontbossing, menselijke nederzettingen, aquacultuur, reservoir operaties en gerelateerde hydrologische rotaties zoals waterniveau beheer en klimaatvariaties). De eutroficatie van hydroelectrische reservoirs wordt beïnvloed door zowel antropogene als natuurlijke factoren. De “trofic” of nutrient (voedselrijkdom) status van een waterlichaam is een belangrijke variabele bij het karakteriseren van de waterkwaliteit vanwege de toevoer van voedingsstoffen vanuit antropogene bronnen. Slechts enkele studies hebben de invloed van de hydrodynamiek van reservoirs op waterkwaliteit en hun limnologische zones onderzocht. In deze context is de relatie aangekaart tussen de hydrologische cyclus van het reservoir in de Amazone en de waterkwaliteit in zijn limnologische zones m.b.t. factoren die invloed uitoefenen op eutroficatie processen. Gegevens zijn vergaard aan het oppervlak, van 2005 tot 2016 bij twaalf stations verspreid en stroomopwaarts van de dam. Chlorophyll-*a* (Chl-*a*), licht doorlaatbaarheid van water, opgeloste zuurstof, totaal en reactief (ortho) fosfaat, zwevende bestanddelen en troebelheid werden bepaald, omdat zij veranderingen ondergaan tijdens de hydrologische “operation cycle” van het stuwmeer en zij zonale variaties vertonen. Gegeneraliseerde lineaire statistische modellen zijn gebruikt bij het identificeren van de reactie van limnologische variabelen in relatie tot de invloed van de hydrologische cyclus op de waterkwaliteit, eutrofiëring in de verschillende limnische zones van het stuwmeer. De resultaten gaven aan dat gedurende het opvullen van het reservoir en bij volle watercapaciteit, hogere eutrofiëringcondities ontstonden dan tijdens de leeglopende en droge (laag water) hydrologische toestand van het stuwmeer. Ook reageerden de verschillende

longitudinale (limnische) zones verschillend t.o.v. hydrologische cyclus en eutrofiëring.

In de laatste stap was het doel om de broeikasgas of GHG (“greenhouse gas”) uitstoot in te schatten van het Tucuruí stuwmeer in de ruimte en tijd, gebruik makend van geospatiale analyse, gekoppeld aan in-situ gas monsternames en laboratorium gas chromatografie. Tevens bespraken we of de uitstoot gerelateerd was aan het eutrofiëringsproces vanwege antropische activiteiten of klimaat “forcing”. Grote waterkracht stuwmeren worden gezien als potentiële bijdragers aan het broeikas effect in de atmosfeer vanwege de uitstoot van methaan en koolstofdioxide. In de laatste stap combineerden we in-situ monsternames en gaschromatografie met geostatistische en remote sensing benaderingen om zo de broeikas effect gas (GHG) uitstoot te bepalen van het Tucuruí reservoir. We gebruikten remote sensing om de seizoen variaties in het wateroppervlak in te schatten en geospatiale interpolatie om totale uitstoot te berekenen als een functie van het reservoir oppervlak en de gasmetingen. De CH<sub>4</sub> en CO<sub>2</sub> gas concentraties waren lineair gecorreleerd met in-situ monstername-tijd, wat de geschiktheid bevestigde van de in-situ “gas chamber” monstername-methodiek om GHG diffuse fluxen te meten aan wateroppervlakken van het reservoir. De combinatie van hoge puurheid (99.99%) ISO-norm gas standaarden met een gas chromatograaf, stelde ons in staat om lage meetdetectie-limieten te behalen van 0.87 ppm en 1.22 ppm, respectievelijk, voor CH<sub>4</sub> (gebruikmakend van een vlam ionisatie of FID detector) en voor CO<sub>2</sub> (gebruikmakend van een thermische conductor- of TCD-detector). Onze resultaten tonen aan dat CO<sub>2</sub> uitstoot significant hoger is (een veelvoud  $5.10^2 - 10^3$ ) dan die van CH<sub>4</sub> in zowel het spatiale als temporale domein van dit reservoir. De totale diffuse GHG uitstoot gedurende een jaar (juni 2011 tot mei 2012) van het Tucuruí reservoir in werking, telde op tot  $6.82 \times 10^3$  ton koolstof voor CH<sub>4</sub> en  $1.19 \times 10^6$  ton koolstof voor CO<sub>2</sub>. We tonen aan dat, in situ GHG monstername middels kleine “floating gas chambers” en hoge precisie gas chromatografie, kunnen worden gecombineerd met geospatiale interpolatie-technieken en remote sensing data om te komen tot goede inschattingen m.b.t diffuse broeikasgas (GHG) uitstoot van grote waterlichamen met fluctuerende wateroppervlakken zoals waterkracht reservoirs. We raden aan dat meer metingen en observaties worden nagestreefd ten behoeve van het ondersteunen en beter onderbouwen van de doorgaande discussies over inschattingen en vermindering van GHG uitstoot van reservoirs in het Amazonegebied en elders in de wereld.

Met de resultaten behaald in de vier stappen van dit onderzoek, lijkt het mogelijk om te besluiten dat de synergie tussen geospatiale analyse en *in situ* observatie,

gekoppeld aan een multidisciplinaire aanpak, d.w.z. een combinatie van ecologie, hydrologie en aardobservatie, een nuttige en efficiënte aanpak is voor het monitoren, analyseren van de waterkwaliteit (e.g. eutrofiëring), alsook de uitstoot van broeikasgassen van grote water systemen, zoals stuwmeren en reservoirs.